

Master Thesis

Dual-Frequency Ultrasound Neuromodulation for Minimally Invasive Brain Implants

BME51010: BME Master Thesis

Dario van Wagenveld



Master Thesis

Dual-Frequency Ultrasound Neuromodulation for Minimally Invasive Brain Implants

by

Dario van Wagenveld

to obtain the degree of Master of Science

at the Delft University of Technology,

to be defended publicly on Thursday April 10, 2025 at 10:00 AM.

Student number: 4647181
Project duration: April 1, 2024 – April 10, 2025
Thesis committee: dr. ir. T. Costa, TU Delft, main supervisor
ir. S. Desmarais, TU Delft, daily supervisor
prof. dr. ir. L. Abelmann, TU Delft, external committee member

Cover: Cover image by Raman Oza
Style: TU Delft Report Style, with modifications by Daan Zwaneveld

An electronic version of this thesis is available at <http://repository.tudelft.nl/>.

Preface

This document represents my final work at TU Delft and concludes my master's studies in the Biomedical Engineering department of the Mechanical Engineering faculty. It represents a year-long project during which I learned about the use of ultrasound technology for neuromodulation applications.

This project has been very motivating throughout its duration, though challenging at times. It has allowed me to understand how to immerse myself in a new, unfamiliar topic and to dive into a question that still remains unclear. It taught me to work independently and, although still in its early stage, it has pushed me to believe in the things I do.

After finishing high school, I had the opportunity to explore different fields of study—first with a bachelor's in Aerospace Engineering, and then a master's in Biomedical Engineering. This change of fields brought me closer to what I feel is worth spending my time on. The projects I've had the chance to work on during my internship and outside of university have helped me grow in different ways as well. I had the opportunity to conduct my thesis research in the Bioelectronics Department, on the 16th floor of EWI. There, I met an incredible team of researchers who not only excel in their expertise but also show affection and humanity.

First of all, I would like to thank my supervisors, Tiago and Samuel, for their time and expertise throughout this entire year. I have learned a lot from both of you, and I've always felt that your doors were open when I needed support. I couldn't have asked for better mentors. I would also especially like to thank Diogo, Masoumeh, Ronald, Eshani, and Liwen—thank you for your time and attention, whether it was clarifying ultrasound principles, using the 3D printers, or dicing piezos.

Over the past year, I also realized that making new friends can be one of the most satisfying and unpredictable experiences. So I thank the entire 16th floor gang for your affection and the tasty foods you introduced me to.

Finally, I would like to thank all my friends from Delft, my previous and current housemates from Bagijnhof 17 and Rotterdam. I also want to thank the whole Tartufo team, who helped me create a home away from home. I am deeply grateful to my family—my parents and my brother—for their immense support and unconditional love. I want to also thank Kiki, as it is with you that I made the greatest discovery.

And finally, I want to thank Shashank. You were my big brother for far too short a time.

I keep you all in my heart. Enjoy the rest of the show.

*Dario van Wagenveld
Delft, April 2025*

Contents

Preface	i
Nomenclature	vi
1 Introduction	1
2 Motivation and Literature Research	5
2.1 Physics of Ultrasound	5
2.2 Acoustic Wave Generation	8
2.3 Beamforming	10
2.4 Ultrasound for Neuromodulation	13
2.4.1 Underlying mechanisms	14
2.4.2 Sonication parameters	15
2.4.3 Transcranial setup: tFUS	17
2.4.4 Implantable setup: μ FUS	20
2.5 Research Gap	21
3 Methodology and project outline	23
3.1 Simulation and selection	23
3.1.1 Transducer independent variables	23
3.1.2 Combined parameters	25
3.1.3 Simulation domain	26
3.1.4 Geometric Transformations	28
3.2 Optimisation	28
3.2.1 Global optimisation	29
3.2.2 Individual optimisation	31
4 Results	32
4.1 Field superposition	32
4.2 Optimisation	35
5 Discussion and Future Recommendations	41
5.1 Field superposition	41
5.2 Optimisation	42
5.3 Future Recommendations	43
6 Conclusion	45
References	47
A Appendix - Optimised Transducers Plots	53
A.1 Varying tFUS source	53
A.2 Varying μ FUS source	55
B Appendix - GA convergence	56
C Appendix - Effect of Varying tFUS parameters	57

List of Figures

1.1	Sunburst chart illustrating the studies for CNS disease conditions (inner rim) and the sonication locations (outer rim). Inner rim: AD, Alzheimer’s disease; PD, Parkinson’s disease; DOC, disorder of consciousness; MCS, minimally conscious state; GAD, generalized anxiety disorder; SUD, substance use disorder. 2nd rim: FC, frontal cortex; M1, primary motor cortex; ACC, anterior cingulate cortex; SCC, subcallosal cingulate cortex; SOZs, seizure onset zones [Adapted from Lee et al. [6]]	2
1.2	Overview of emerging neuromodulation techniques (TI: Temporal interference, NIR: Near infrared) [4]	2
1.3	Envisioned dual-frequency ultrasound neurostimulation setup	3
2.1	Fundamental schematics of acoustic wave propagation	5
2.2	Ultrasound transducer technologies [21]	9
2.3	Simple field pattern geometry of a transducer (D: source diameter, z: propagation direction, λ : wavelength) [22]	10
2.4	Traditional focusing methods ((a)-(b): Gradient-cross-sectional lens, (b) : Fresnel lens, (c) : Phased array) [Adapted from [25]]	11
2.5	Two novel beam interference methods for FUS stimulation	14
2.6	Temporal characteristics of and continuous pulsed ultrasound [Adapted from [50]]	16
2.7	The conventional experimental setup for single element transducer tFUS [61]	18
2.8	Scale of the ultrasound focus. Focal spot sizes (solid) and steering ranges (dotted line) of commonly used acoustic apertures. (A) In humans, (B) in rodents [11]	18
2.9	Implantable μ FUS systems	20
2.10	Research on dual US source setups for neuromodulation	22
2.11	Dual multi-frequency US source interference approach proposed by Riis and Kubanek [40]	22
2.12	Pattern interference radiation force setup by Kim et al. [19] using two front facing transducers	22
3.1	Research project outline	23
3.2	Schematic representation of the dual transducer setup (FL : Focal Length, f_0 : fundamental frequency, L : aperture, r : radial margin, θ : crossing angle, p_{frac} : contribution factor)	24
3.3	k-Wave simulation domain	27
3.4	Working principle of a Genetic Algorithm	30
4.1	Comparison of maximum pressure values and focal spot size	32
4.2	Maximum pressure field of the tFUS (left) and μ FUS (right) transducer fields in k-Wave	33
4.3	FoM and Focal Area as a function of p_{frac} and θ	34
4.4	FoM and Focal Area as a function of r and θ	34
4.5	Maximum pressure gain of the combined field	34
4.6	Pressure and intensity gain over time at the focal spot for the combined and the individual transducers	35
4.7	FoM and Focal Area as a function of frequency and aperture for varying tFUS parameters	35
4.8	FoM and Focal Area as a function of frequency and aperture for varying μ FUS parameters	36
4.9	Power term and maximum pressure gain for varying μ FUS parameters	36
4.10	Maximum pressure field of the optimal tFUS (left) and μ FUS (right) transducer fields in k-Wave	37
4.11	FoM and Focal Area of the combined optimal field as a function of θ and p_{frac}	37
4.12	3D plot of $\frac{1}{\sqrt{A}}$ as a function of p_{frac} and θ	38

4.13	FoM and Focal Area as a function of r and θ for the optimised transducers	38
4.14	Comparison of the pressure and intensity gain at the focal spot for the combined and the individual optimal setup	39
4.15	FoM and Focal Area as a function of frequency and aperture for varying tFUS parameters	39
4.16	FoM of the combined field	40
4.17	Max. Pressure gain and Normalised Power term as a function of frequency and aperture for varying μ FUS parameters	40
4.18	FoM and Focal Area as a function of frequency and aperture for varying μ FUS parameters	40
A.1	Focal area of the combined field for varying tFUS parameters	53
A.2	Normalised maximum pressure gain of the combined field for varying tFUS parameters	54
A.3	Normalised FoM of the combined field for varying tFUS parameters	54
A.4	Focal area of the combined field for varying μ FUS parameters	55
C.1	Fixed transducer frequency: 750 kHz, varying transducer aperture	58
C.2	Fixed Transducer Aperture: 45 mm, variable frequency	59

List of Tables

2.1	Acoustic properties of various media	7
2.2	Comparison between μ FUS and tFUS systems	21
3.1	Ranges of transducer independent variables	26
3.2	Ranges of combined parameters	26
3.3	Genetic Algorithm parameters	30
4.1	Parameters of the selected transducers	33
4.2	Parameters of the optimised transducers	36
4.3	Combined parameters of the optimised transducers	37
B.1	GA Optimization Performance and Results	56

Nomenclature

Abbreviations

Abbreviation	Definition
ARF	Acoustic Radiation Force
ASIC	Application-Specific Integrated Circuit
BBB	Blood Brain Barrier
BOLD	Blood Oxygenation Level Dependent
CNS	Central Nervous System
CSF	Cerebrospinal Fluid
DALYs	Disease Adjusted Life Years
DC	Direct Current
FWHM	Full Width at Half Maximum
FUS	Focused Ultrasound
HIFU	High Intensity Focused Ultrasound
LIFU	Low Intensity Focused Ultrasound
LIFUS	Low Intensity Focused Ultrasound Stimulation
MEMS	Microelectromechanical Systems
MEP	Motor Evoked Potential
MN	Median Nerve
MR	Magnetic Resonance
MUT	Micromachined Ultrasonic Transducers
PRF	Pulse repetition Frequency
PZT	Lead Zirconate Titanate
ROC	Radius of Curvature
rTUS	Repetitive TUS
SDT	Sonodynamic Therapy
SEP	Somatosensory Evoked Potential
tbTUS	Theta Burst TUS
tFUS	Transcranial Focused Ultrasound
TMS	Transcranial Magnetic Stimulation
TPS	Transcranial Pulsed Stimulation
TRE	Target Registration Error
TUS	Transcranial Ultrasound
US	Ultrasound
μ FUS	Microscopic Focused Ultrasound

Symbols

Symbol	Definition	Unit
A	Amplitude	[m]
A_0	Initial Amplitude	[m]
c	Speed of sound	[m/s]
d	Element Pitch	[m]
D	Diameter	[-]
DOF	Depth of Field	[m]
DC	Duty Cycle	[-]

Symbol	Definition	Unit
E_{Mech}	Mechanical Energy	[J]
E_{Elec}	Electric Energy	[J]
f	Frequency	[Hz]
F	Focal Depth	[m]
I	Intensity	[W/m ²]
I_r	Reflected Intensity	[W/m ²]
I_{SPPA}	Spatial-peak pulse average	[W/m ²]
I_{SPTA}	Spatial-peak temporal average	[W/m ²]
I_t	Transmitted Intensity	[W/m ²]
I_{ta}	Temporal Average Intensity	[W/m ²]
K_a	Bulk modulus	[N/m ²]
k_t	Coupling Coefficient	[-]
L	Aperture	[m]
MI	Mechanical Index	[-]
p	Pressure	[Pa]
P	Power	[W]
R_I	Reflection Coefficient	[-]
SD	Sonication duration	[s]
TBD	Tone Burst Duration	[s]
T	Wave Period	[s]
TI	Thermal Index	[-]
T_I	Transmission Coefficient	[-]
Z	Acoustic Impedance	[Rayl]
α	Attenuation Coefficient	[dB/m]
β	Coefficient of Non Linearity	[-]
λ	Wavelength	[m]
κ	Compressibility Coefficient	[m ² /N]
ρ	Density	[kg/m ³]
θ	Propagation Vector Angle	[rad]
θ_s	Steering Angle	[rad]

1

Introduction

The human auditory system is capable of hearing sound within a frequency range of 20 Hz to about 20kHz. Not only does this ability allow us to interact and survive in nature, but these sound waves also have beneficial effects on our health [1]. Exploiting this physical phenomenon to improve our quality of life has become a goal for many researchers. Especially the use of higher frequencies of sound, or ultrasound, has revolutionised the medical field. From real-time imaging to non-invasive ablation of cancerous tissue, ultrasound is a promising tool for many applications. More recently, the discovery of reversible effects that focused (and unfocused) ultrasound on the nervous system has sparked interest in many, leading to the concept of Low Intensity Focused Ultrasound (or LIFU) stimulation. This modulation of the neural activity in living beings generates direct effects throughout the body (e.g., suppressing tremors or inducing tingling in the fingers) and is envisioned to drive physiological changes that could potentially treat diseases.

According to Steinmetz et al. [2], in 2021 3.40 billion people were suffering from a condition which affects the nervous system, leading to 11.1 million deaths and 443 million disability-adjusted life-years (or DALYs). Some conditions responsible for the highest DALYs in that year were migraine, Parkinson's Disease, Alzheimer's Disease and other dementia and epilepsy [2]. This high number of neurological related conditions requires adequate diagnosis and treatment. Treatment for these conditions can be issued mainly in two ways: using pharmaceuticals or by means of medical devices. When considering medical devices that target regions in the central nervous system (CNS), several brain stimulations techniques are currently being used, such as deep brain stimulation (DBS), transcranial magnetic stimulation (TMS), transcranial direct current stimulation (tDCS) and focused ultrasound stimulation (FUS) [3]. Four emerging neuromodulation techniques are compared in Figure 1.3 [4]. There are several benefits of FUS compared to other techniques, the most notable ones are the greater penetration depth and the higher resolution. Although techniques involving optogenetics and invasive electrical stimulation allow for very high resolution (unrivalled resolution in the case of optogenetics), they are prone to foreign body response following implantation and do not offer the spatial coverage achieved by LIFU. Another advantage of FUS is the positive perception it holds among the general public, as reported in Atkinson-Clement, Junor, and Kaiser [5]. In this study, a survey was shared with a group of 784 people asking questions on preferences for common treatment methods such as pharmaceutical drugs, brain implants, ultrasound, magnetic, and electrical stimulations. Ultrasound stimulation emerged as the preferred technique, surpassing pharmaceuticals.

Since the first discovery of LIFU induced neuromodulation effects by Hameroff et al. [7], researchers have reached many milestones in the application of this technology in both healthy humans and clinical trials [6, 8]. The clinical trials have mainly focused on a handful of diseases which are chronic pain, disorder of consciousness (DOC), Alzheimer's disease (AD), Parkinson's disease, depression, schizophrenia, anxiety disorder, substance use disorder (SUD), epilepsy, and stroke (see Figure 1.2). Despite limited data from the technology's early stage, the results seem promising. A study by Shin, Son, and Kim [9] showed sustained reduced pain levels in chronic neuropathic pain patients after transcranial focused ultrasound (tFUS) administration to the dorsal anterior cingulate cortex (ACC). Another

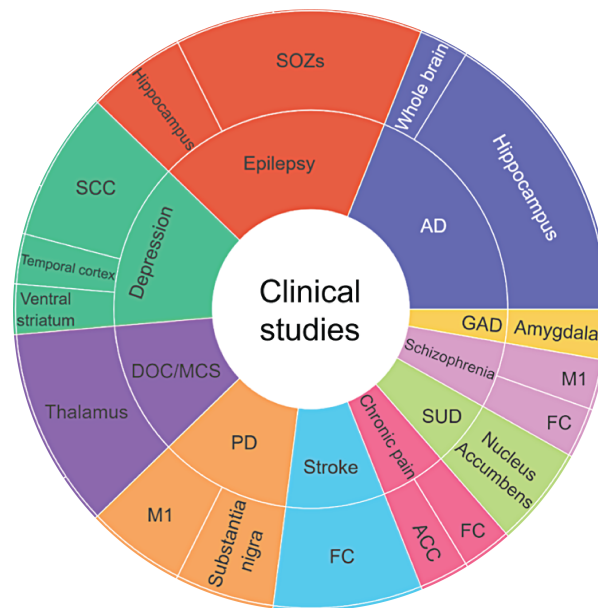


Figure 1.1: Sunburst chart illustrating the studies for CNS disease conditions (inner rim) and the sonication locations (outer rim). Inner rim: AD, Alzheimer's disease; PD, Parkinson's disease; DOC, disorder of consciousness; MCS, minimally conscious state; GAD, generalized anxiety disorder; SUD, substance use disorder. 2nd rim: FC, frontal cortex; M1, primary motor cortex; ACC, anterior cingulate cortex; SCC, subcallosal cingulate cortex; SOZs, seizure onset zones [Adapted from Lee et al. [6]]

	FUS	TI stimulation	NIR optogenetic stimulation	Nanomaterial-enabled magnetic stimulation
Energy delivery	Ultrasound	Electrical	Near-infrared	Magnetic
Invasiveness	Noninvasive	Noninvasive	Minimally invasive	Minimally invasive
Spatial resolution	~1 mm	> mm	<1 mm	<1 mm
Depth of penetration	10–15 cm or more	5 cm or more	1 cm or more	Unlimited in theory
Gene delivery	No	No	Yes	Yes
Experiment animal models	Rodents, non-human primates, human	Rodents, human	Rodents	Rodents
Stimulation mode	Fixing transducer	Fixing electrodes	Remote	Remote
Complexity level	Moderate	Moderate	Complicated	Complicated
Reversible	Yes	Yes	No	No
Cost	Moderate	Low	High	High

FUS, focused ultrasound.

Figure 1.2: Overview of emerging neuromodulation techniques (TI: Temporal interference, NIR: Near infrared) [4]

study from Shimokawa et al. [10] investigated the effect of long term TUS delivery through the bilateral temporal bones on early stage AD patients. Results showed that the progression of cognitive impairments remained unchanged for at least 1.5 years compared to the placebo group, where the conditions worsened over the same time interval. The effects that FUS stimulation has on the nervous system have been classified in two categories: online and offline effects. The first refer to differences in subject (patient) physiological state during sonication or immediately after. The divergence in neural activity (suprathreshold stimulation or subthreshold modulation [11]) can be measured directly. The second category of effects occur minutes to hours (or even days) after sonication. These reflect structural and neuroplastic changes resulting from FUS exposure. Another distinction in LIFU neuromodulation is that it can either stimulate (enhance) or inhibit (suppress) neuronal activity in targeted CNS regions. These effects depend on the brain region being targeted and the sonication parameters being used. The state of consciousness of the individual should also be taken into account as that greatly affects the outcome of US sonication as was shown in many animal studies [12].

Though showing promising results, this technology has only been applied transcranially in human trials, which requires a bulky setup and the presence of medical professionals. Currently, tFUS therapy requires patients to stay in the vicinity of a specialised facility for repeated interventions. This limits accessibility and convenience for patients. Furthermore, having US beams crossing the skull leads to

great acoustic energy losses. This limits the incoming wave to having sub-MHz frequencies, leading to reduced target resolution and unintended stimulation of other brain regions. LIFUS micro-systems have been designed to mitigate these challenges. This technology involves implanting the source in order to bypass the skull. However, this comes to the cost of a limited power supply, as the electric power unit will most probably be implanted as well.

Exploring the edge between these two setups allows for a better understanding on how they should be implemented to maximise the required effect. Furthermore, the ability to induce on demand FUS therapy by means of an implantable device allows for immediate and on demand stimulation in any situation, without the intervention of a healthcare professional. This is particularly important for patients with epilepsy, where seizures occur unpredictably, or for Parkinson's disease patients, where tremors are continuous. An implantable device will also allow for precise targeting as it bypasses the skull aberrations which permits the use of high frequency transducers. An important aspect of an implantable device is the availability of energy to power the system. To reduce the risk of infections and the burden on patients, the device should required a single surgical procedure. This leads to the entire system (including the power unit) to be implanted. Another important aspect to consider is the size of the device. Invasiveness of an implantable device scales with size, but so does the available power. By introducing a tFUS source, the power delivered to the target is shared amongst two sources. Since FUS treatments are currently delivered periodically during hospital visits, they can be paired with implantable device stimulation for more power-efficient and precise sonication. Such setup would also allow for treatments combining online and offline effects of FUS neuromodulation to be investigated.

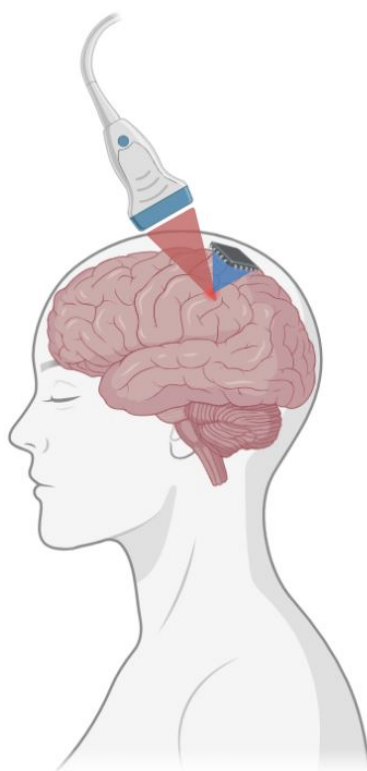


Figure 1.3: Envisioned dual-frequency ultrasound neurostimulation setup

Up to this day, there are no studies discussing the effect of combining two ultrasound sources (ie. an implantable source and a transcranial source) on the resulting pressure field. Therefore the goal of this project is to propose a first approach to analysing such setup. The research question thus becomes: How can an intersecting transcranial focused ultrasound beam and an implantable focused ultrasound (μ FUS) beam induce neuromodulation while optimising for high resolution and low power consumption for the implanted device? Following this question, two sub-questions arise:

- What is the optimal placement of tFUS sources and μ FUS sources?
- Which variables should be optimised for in order to achieve neuromodulation at minimal μ FUS power input?

In order to answer these questions, first a literature research was performed to gather the necessary knowledge regarding the technologies used in the FUS field and data needed for the project. In Chapter 2 a recap of the main findings is presented by first discussing the fundamental principles of medical ultrasound in Section 2.1. The underlying mechanisms of neuromodulation induced by ultrasound waves as well as the sonication parameters and the existing FUS setups being used are then discussed in Section 2.4. Subsequently, the project outline and the research methodologies used are presented in Chapter 3. The results gathered from the simulations and the optimisation process are presented in Chapter 4 and these are further discussed Chapter 5 alongside recommendations for future work. Finally, Chapter 6 offers concluding remarks on the study.

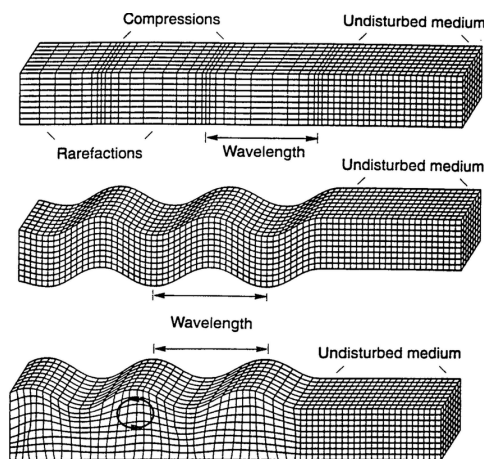
2

Motivation and Literature Research

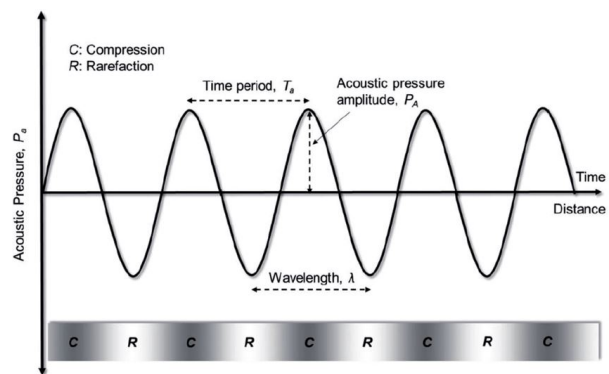
Before diving into neuromodulatory application of focused ultrasound, it is important to understand the fundamental principles of ultrasound waves. In this chapter the basic physical principles of ultrasound wave propagation, generation and focusing are presented in Section 2.1 and Section 2.2 respectively. The current theories describing the working principles of neuromodulation induced by ultrasound waves, along with the sonication parameters used in to define a FUS protocol, are discussed in Section 2.4. Finally the research gap and motivation are given in Section 2.5.

2.1. Physics of Ultrasound

Ultrasound waves are a type of acoustic (mechanical) waves that propagate through matter as pressure disturbances with frequencies higher than 20 kHz. Mechanical waves can be classified into three types, distinguished by the particle motion they induce (see Figure 2.1a): longitudinal waves, transverse waves and surface waves. Longitudinal waves carry the most amount of (stable) energy and they travel in the direction of wave propagation. This research mainly focuses on these types of waves. Transverse waves (or shear waves) travel perpendicularly to the direction of wave propagation and carry less energy compared to the previous one. In fact, they may be a result of longitudinal wave interactions [13] and are considered as a non-linear phenomenon. Finally, surface waves travel at the interface of two media and cause the particles to oscillate in a circular motion.



(a) 3 Types of mechanical waves [14]



(b) Schematic diagram of an ultrasonic wave [15]

Figure 2.1: Fundamental schematics of acoustic wave propagation

Longitudinal waves travel through matter at a speed dictated by the materials' elastic and inertial properties. More specifically, the resistance to compression and the medium density give a reasonable approximation of the speed of sound as shown in Equation (2.2).

$$\lambda = \frac{c}{f} = c \cdot T \quad (2.1) \quad c = \sqrt{\frac{K_a}{\rho}} = \sqrt{\frac{1}{\kappa \rho}} \quad (2.2)$$

where λ is the wavelength, c is the speed of sound in the medium, T is the period, K_a is the bulk modulus of the material, κ is the compressibility coefficient and ρ the density of the material.

As the wave propagates, pressure gradients emerge which oscillate in time (see Figure 2.1). The propagation of the pressure disturbance in a homogeneous and lossless medium is dictated by a set of coupled first-order partial differential equations as shown in Equation (2.3).

$$\frac{\partial \mathbf{u}}{\partial t} = -\frac{1}{\rho_0} \nabla p, \quad (\text{momentum conservation}) \quad (2.3)$$

$$\frac{\partial \rho}{\partial t} = -\rho_0 \nabla \cdot \mathbf{u}, \quad (\text{mass conservation}) \quad (2.4)$$

$$p = c_0^2 \rho. \quad (\text{pressure-density relation}) \quad (2.5)$$

where \mathbf{u} is the velocity vector, ρ_0 is the density of the medium (assuming a homogeneous medium), c_0 is the speed of sound in the medium and p the pressure field.

These equations are merged to form the well known wave equation described by the following equation:

$$\nabla^2 p - \frac{1}{c_0^2} \frac{\partial^2 p}{\partial t^2} = 0. \quad (2.6)$$

As the wave propagates through a medium, it will interfere with matter in different ways. Depending on the material, the path and the waveform, the incoming wave can undergo reflection, refraction, scattering, etc. An important phenomenon is related to the absorption of the wave by the medium. This phenomenon occurs as the mechanical energy of the wave is transferred to the medium in the form of heat as a result of viscous effects. Absorption is a phenomenon where its effect and intensity depend on the incoming wave frequency, the viscosity of the medium and the relaxation time of the medium. This phenomenon accounts for 80-90% of all energy lost by the wave.

This energy loss is quantified by looking at the amplitude attenuation of the incoming wave. When considering the attenuation of a plane wave propagating through an absorbing medium, its' amplitude becomes an exponentially decaying term given by the phenomenological model:

$$A(x) = A_0 e^{-\mu_a x} \quad (2.7) \quad \alpha = a f^b = (20 \log_{10} e) \mu_a \quad (2.8)$$

where x is the propagation direction and A_0 the initial amplitude. As stated in the previous section, the attenuation is mainly caused by absorption. The extent to which an acoustic wave is attenuated depends both on the medium properties and the frequency of the wave. The attenuation coefficient α is then defined as Equation (2.8)), where a and b are empirical values dependent on the material properties, and f is the wave frequency. Table 2.1 shows loss factor as well as other material properties for different types of tissue.

There exist different tissue models able to simulate the effects of absorption of acoustic waves, such as the classic relaxation model, the time causal model, and the Kramers-Kronig relation [16]. The effects of attenuation can be introduced using propagation operators that account for absorption and dispersion, while satisfying causality. Adding the absorption terms to the coupled first-order differential equations shown in Equation (2.3) leads to the two last equations becoming:

$$\begin{aligned} \frac{\partial \rho}{\partial t} &= -\rho_0 \nabla \cdot \mathbf{u} - \mathbf{u} \cdot \nabla \rho_0, & (\text{mass conservation}) \\ p &= c_0^2 (\rho + \mathbf{d} \cdot \nabla \rho_0 - L_o \rho), & (\text{pressure-density relation}) \end{aligned} \quad (2.9)$$

where \mathbf{d} is the acoustic particle displacement and L_o is a linear integro-differential operator. This term accounts for acoustic dispersion and absorption, ensuring causality is maintained.

Table 2.1: Acoustic properties of various media.

Medium	Sound Speed, c (m/s)	Density, ρ (g/cm ³)	Acoustic Impedance, Z (MRay)	Loss Factor (dB/cm @ 1 MHz)
Air	330	0.00125	0.0004	~1
Water	1480	1	1.48	0.002
Blood	1575	1.055	1.66	0.15
CSF*	1480	1	1.48	0.002
Brain	1550	1.03	1.60	0.8
Skin	1730	1.15	1.99	2.63
Fat	1450	0.95	1.38	0.6
Liver	1590	1.06	1.69	0.9
Kidney	1570	1.05	1.65	1
Heart	1570	1.045	1.64	2
Skull	2300	1.912	4.4	10–52 (0.2–1 MHz)

*CSF = Cerebrospinal fluid

Finally, as the intensity of the incoming wave increases, the effects of non-linear phenomena become more apparent. These occur as tissue properties (ie. density) and forces (ie. pressure) do not change in a linear fashion. Instead of having a perfectly sinusoidal signal propagating through a medium, the head-crest compresses (or the head-trough rarefies) the medium, such that the material density is altered, leading to differential velocities compressing the wave on itself. One way to account for some of these non linear effects into the coupled-first order equation is by introducing the ratio B/A [17], which originates from the Taylor series expansion that describes pressure variations in a medium as a function of density variations. This leads the coupled-first order equations to be rewritten as:

$$\begin{aligned}
 \frac{\partial \mathbf{u}}{\partial t} &= -\frac{1}{\rho_0} \nabla p, & (\text{momentum conservation}) \\
 \frac{\partial \rho}{\partial t} &= -(2\rho + \rho_0) \nabla \cdot \mathbf{u} - \mathbf{u} \cdot \nabla \rho_0, & (\text{mass conservation}) \\
 p &= c_0^2 \left(\rho + \mathbf{d} \cdot \nabla \rho_0 + \frac{B}{2A} \frac{\rho^2}{\rho_0} - L_o \rho \right) & (\text{pressure-density relation})
 \end{aligned} \tag{2.10}$$

Two important non-linear phenomena that are of particular interest when considering ultrasound neuromodulation are acoustic radiation forces and cavitation.

Acoustic Radiation Force

A non-linear phenomenon which is investigated in the realm of ultrasound neuromodulation is related to the dissipation of the acoustic wave energy through shear waves (transverse waves). This generates forces called Acoustic Radiation Forces (ARFs). According to Sarvazyan, Rudenko, and Nyborg [18], ARFs are generated by changes in the energy and momentum density of propagating waves due to absorption, scattering, or reflection from inclusions, or variations in propagation velocity across space. These forces generate an energy flow within the medium referred to as acoustic streaming. The expression of ARF is usually defined as [19]:

$$\mathbf{ARF} = \langle -\mathbf{u} \nabla \cdot (\rho \mathbf{u}) - \rho (\mathbf{u} \cdot \nabla) \mathbf{u} \rangle \tag{2.11}$$

Several assumptions can be made in order to simplify the expression. For a purely planar wave, the intensity of the radiation force at a given location can be estimated using:

$$ARF = \frac{P}{c} = \frac{2\alpha I_{ta}}{c} \tag{2.12}$$

where P is the power absorbed by the tissue, α is the absorption coefficient, I_{ta} is the temporal average intensity at that point and c the speed of sound of the medium.

Cavitation

As a high intensity acoustic wave propagates through a medium, the negative pressure can reach below the saturation pressure of this medium. This can lead to microbubble formation which expand and contract in phase with the incoming wave. The bubbles expand during the rarefaction phase and contract during the compression phase. Cavitation can both be stable or unstable (or transient), meaning that the bubble either maintain their shape and oscillate in a stable fashion or they collapse violently within a small number of cycles, reaching inner temperatures of thousands of Kelvins and very high pressures. The probability for cavitation to occur is related to the frequency of the signal, as the expanding/contracting cycle should match the oscillation frequency for optimal energy transfer.

The amount of energy carried and delivered by such waves can be described by its' acoustic intensity. This term is defined as the amount of power flowing through a given area, and is computed as:

$$\mathbf{I} = p \cdot \mathbf{u} \quad (2.13)$$

where \mathbf{u} is the particle velocity vector and p is the pressure value. The intensity at a certain location is usually given in $[W/cm^2]$.

When considering plane waves, this term can be rewritten as :

$$I = \frac{p^2}{\rho c} = \frac{p^2}{Z_0} \quad (2.14)$$

where Z_0 is the characteristic specific acoustic impedance.

2.2. Acoustic Wave Generation

Transducers are the main elements used to generate US waves. The fundamental mechanism relies on the controlled vibration of an elastic membrane at sufficiently high frequencies so as to enter the ultrasonic realm ($f_0 \geq 20$ kHz). In the medical field, US transducers can be separated into thick-film transducers and microelectromechanical systems (MEMS).

Thick film/ Piezoceramic transducers: The typical configuration of a piezoceramic (single element) transducer is shown in Figure 2.2. The main element is the piezoelectric film, which deforms when a voltage is applied across the front and back electrodes. The type of piezoelectric material used and its dimensions greatly influence the efficiency of the system. A backing layer is added such that the beam is focused in one direction and a broader bandwidth as well as a higher sensitivity can be achieved. In order to minimise wave reflection at the interface, matching layers are added to the other side of the piezoelectric element. These are designed in such way that the impedance gradually changes to the impedance of the tissue. This allows for an optimal transmission of the acoustic wave (see Equation (2.15)) from the source to the medium. The impedance value of the matching layer can be calculated by computing the geometric mean of the two adjacent layers using Equation (2.16).

$$T_I = \frac{4Z_1Z_2}{(Z_1 + Z_2)^2} \quad (2.15) \quad Z_m = \sqrt{Z_pZ_l} \quad (2.16)$$

Z_1 and Z_2 are the impedances of the incoming and receiving media respectively, Z_l and Z_p are the acoustic impedance of the loading material and piezoelectric material, respectively. Furthermore, the thickness of the layers are chosen such that the reflected wave is trapped and then re-transmitted without destructive interference ($L_p = \frac{\lambda}{2}$ and $L_m = \frac{\lambda}{4}$, where L_p is the thickness of the piezoelectric element and L_m the thickness of the matching layer). These parameters are fine-tuned in such way that the coupling coefficient is maximised [20]. An inconvenience of such transducer is its low coupling coefficient value. However, it can be improved by combining the piezoelectric material with polymers, leading to piezocomposite ultrasonic transducers. Another drawback is that it relies on thickness-mode vibration, which inherently has a high impedance.

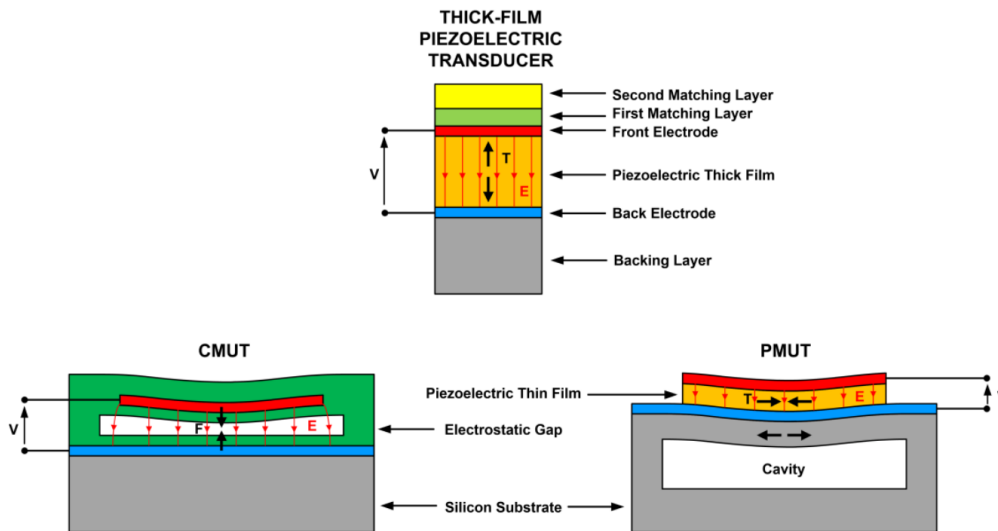


Figure 2.2: Ultrasound transducer technologies [21]

MEMS: When focusing on the medical applications of ultrasound transducers, growing interest is shown in the miniaturisation of the technology. The main reasons being the growing demand for in body us-imaging and the trend towards 3D handheld probes [21]. There are two main US MEMS transducers, or micromachined ultrasound transducers (MUTs) (see Figure 2.2).

1. **CMUTs (Capacitive Micromachined Ultrasonic Transducers)** This configuration makes use of the electrostatic force that is generated when a voltage is applied over two electrodes. The top one is coated with a passivation layer and deposited on a flexible membrane (ie. silicon), and the bottom one is adhered to the substrate. The two electrodes are separated by a vacuum gap allowing for the membrane to vibrate freely. Applying an alternating voltage makes the membrane vibrate, generating acoustic waves in the medium. A DC voltage bias is applied in order to increase effectiveness, and manipulating its value allows for different use modes (conventional, collapse and collapse-snapback) [20]. When used for sensing, the capacitance variation caused by the incoming acoustic wave is measured. It is therefore important to generate and maintain high electric fields in the gap [21]. This setup has some advantages such as greater bandwidth typically greater than 100%) and high electromechanical coupling coefficient. However, it also comes with drawbacks such as large power consumption (in part due to the DC bias applied), low ultrasonic intensity and the pulling effect.
2. **PMUTs (Piezoelectric Micromachined Ultrasonic Transducers)** These work using the same fundamental principle as traditional thick film US transducers. However, the system is made such that the curvature of the membrane changes when a voltage is applied across the electrodes. The elastic membrane will relax once the voltage is removed, creating acoustic waves in the surrounding medium. The materials commonly used for this setup are aluminium nitride (AlN) and lead zirconate titanate (PZT). It can already be noted that this design is not limited by a gap between the electrodes, which is an advantage compared to CMUTs. Furthermore, PMUTs do not require external circuit to measure the change in capacitance under external stresses which makes it more power efficient, or a voltage bias.

Transducer arrays can be created by distributing small scale single elements next to each-other. By applying differential phase on these element, electronic beam steering can be performed instead of mechanically changing the position of the single elements. An advantage of MUT membranes is that they vibrate in flexural mode, resulting in a much lower mechanical impedance. As a result, MUTs are intrinsically better acoustically matched to biological tissue and do not require the use of matching layers typically employed in traditional transducers to achieve broadband operation. Miniaturisation and low power consumption in comparison to conventional ultrasonic devices are also two key advantages of MEMS. These are key criteria when looking at implantable bioelectronic systems, as invasiveness

becomes a driving requirement.

2.3. Beamforming

As a sound wave is emitted, an interference pattern is created in the medium where the acoustic energy changes over time and space. This phenomenon is caused by diffraction [16][22]. The wave coming from a transducer can be seen as a collection of many different wavelets that will interact with each other, creating these interference patterns. When deriving the wave equations it was assumed that the wave was coming from a single source, however when considering a transducer, it is necessary to investigate the field pattern. Different simplified models are used to analyse the different regions emerging from the interferences. In simple terms, these regions are shown in Figure 2.3 given diameter D of the transducer.

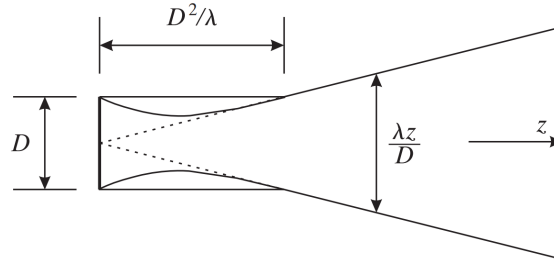


Figure 2.3: Simple field pattern geometry of a transducer (D : source diameter, z : propagation direction, λ : wavelength) [22]

- Geometric region:

$$\begin{cases} 0 \rightarrow \frac{D^2}{4\lambda} = \frac{f_0 D^2}{4c}, \text{ circular transducer} \\ 0 \rightarrow \frac{D^2}{2\lambda} = \frac{f_0 D^2}{2c}, \text{ rectangular transducer} \end{cases} \quad (2.17)$$

- Fresnel region: $0 \rightarrow \frac{D^2}{\lambda}$
- Fraunhofer region: from Fresnel region onwards. In this region, the beamwidth can be approximated by $\lambda z / D$.

When considering an array of transducers, the diameter is replaced by the aperture (L) such that:

$$L = d \cdot (\sqrt{N} - 1) \quad (2.18)$$

where N is the number of piezoelectric elements and d is the pitch between the elements. An unwanted phenomenon occurring when using transducer arrays is the creation of side lobes. This is caused by the discrete nature of these systems and the interference between the individual source waves. To avoid these effects, a pitch value smaller than $\frac{\lambda}{2}$ must be chosen [23]. The beamwidth of the main lobe is described by Equation (2.19). This approximation does not take into account the narrowing of the beam in the Fresnel region.

$$w(z) = \begin{cases} D, & z \leq \frac{D^2}{\lambda} \\ \frac{\lambda z}{D}, & z > \frac{D^2}{\lambda} \end{cases} \quad (2.19)$$

where z is the propagation direction. Though there are more detailed definitions, this simplification is still very useful for first order quantification. The lateral resolution at the focal spot is defined as the full width at half maximum (FWHM) as shown in Equation (2.21). It represents the width confined between two points where the intensity is equal to $\frac{I_{max}}{2}$ (or -6dB). The end of the geometric field is the focal spot, here the beamwidth is the smallest and of great interest as the resolution at this location is the highest. This distance is also referred to as the focal length (F). Another metric for focusing is the Depth of Field (DOF) and describes the quality of focusing. It is a measure of axial spatial resolution.

One way to define DOF for both rectangular and circular shapes is by looking at the axial distance between the locations where the width of the beam increases twofold from its narrowest point by 6 dB. The DOF is defined by Equation (2.20).

$$DOF \propto \lambda \cdot \left(\frac{F}{L}\right)^2 \quad (2.20)$$

$$FWHM \propto \lambda \cdot \frac{F}{L} \quad (2.21)$$

When considering a 3D beam, the beamshape of the central lobe can be approximated to the shape of an ellipsoid (or spheroid). The volume of such shape is defined by Equation (2.22). The difference in pressure with respect to the face of the aperture of the transducer is defined as the gain [16]. It is approximated using the equation shown in Equation (2.23).

$$V_{ol_{res}} = \frac{1}{6} \cdot \pi \cdot DOF \cdot FWHM^2 \quad (2.22) \quad G = \frac{L}{\lambda F} \quad (2.23)$$

Note that the focal length does not coincide with the location of highest pressure! The highest pressure point is found just before that point, a detailed formula is given in [24]. The diffraction formulation is used to compute a more detailed field pattern. As the source plate (transducer), vibrates in the plane of propagation it can be considered that all individual elements on this source act as dipoles.

The waveform of the acoustic wave can be manipulated in many way. This is an important aspect of medical US as it directly affects the resolution (ie. specificity), the gain and the focal depth. In order to shape this beam so as to narrow its beamwidth, allowing for better target resolution, the generated waves are focused means of different methods. The main distinction can be made on whether it involves the use of a lens or not [25].

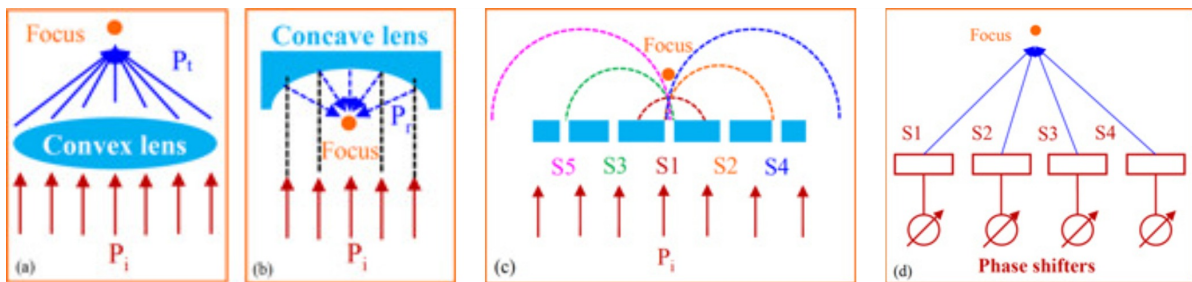


Figure 2.4: Traditional focusing methods ((a)-(b) : Gradient-cross-sectional lens, (b) : Fresnel lens, (c) : Phased array [Adapted from [25]]

Lens focusing

Traditional methods:

- **Gradient-cross-sectional lens** Just like in optics, this technique exploits the refractive properties of sound waves travelling through different media to focus the incoming waves at one particular spot. In addition to the material properties of the lens, a gradient (curvature) is present in order to refract the incoming waves at a single focus spot. Different lens designs have been proposed and concave/convex structures have been shown to focus ultrasound waves (similar to spheres). One such lens is the grooved acoustic reflection focusing lens proposed by Wang et al. [26]. The most difficult trade-off in ultrasound focusing is accuracy (or resolution) and penetration depth. In a study performed by Chen et al. [27], a double-parabolic-reflector design allowing for a pressure increase of 17 fold at the tip of the waveguide and a power increase of 213 fold was achieved. This shows the great benefit of using a lens. (See Figure 2.4 - (a) and (b))
- **Fresnel lens** Makes use of the physics of waveform diffraction. Such lens consists of a flat plate (Fresnel zone plate) with slits of different sizes where the incoming wave travels through. This leads to a set of secondary sources which will see their waves interfere in such way that constructive interference occurs at the focus point. Therefore the focal size and resolution is determined by diffraction theory (ie. Rayleigh criterion). These lenses are the most widely used of all focusing lenses and they are essential to biomedical applications [25]. (See Figure 2.4 - (c))

Novel technologies: Artificial structures

In the last decades, novel materials able to manipulate source sound beams have been developed in order to achieve high resolution imaging (by achieving negative reflective indexes in order to bypass the diffraction limit) or to filter certain wave bands. Such materials are phononic crystals and metamaterials.

- **Phononic crystals** These are a type of artificial structure conceived such that they can filter out a certain band of elastic waves frequencies. These artificial periodic structure are modulated on scales close to the wavelength of the incoming wave. The elastic and density properties of the material allow for important effects to occur such as band-gap, band edge states, and the ability to slow the velocity of sound [28]. These structures are also able to focus US waves through two working principles. First, the structure can be made such that it simulates traditional gradient cross sectional lenses with. This is achieved by introducing periodic structures with gradually changing parameters. The second working principle relies on achieving a negative refractive index. This allows for greater resolution at the focal spot, bypassing the diffraction limit [25, 29].
- **Metamaterials** Unlike phononic crystals, metamaterials do not show particular periodicity in their structure. They can focus US waves based on three types of lenses: superlens, hyperlens and metalens.
- **Metasurfaces** Acoustic metasurfaces are thin 2D materials, thinner than the wavelength of sound, with the remarkable ability to manipulate local phase shifts, modulate amplitudes or present impressive sound absorption capabilities [30]. These are based on the same principle of metamaterials, with the difference residing in the spatial dimension (2D instead of 3D). Metasurfaces are therefore planar structures, the concept is based on arrays of subwavelength units, which makes them less bulky. They can also be more easily fabricated compared to 3D metamaterials using emerging additive manufacturing techniques [31] and they are a more promising solution for small scale US focusing. Sub-wavelength resolution can be achieved through this technique [32], as well as highly tunable intensity contrast, width, and position of the beam [33]. Another advantage of this focusing technique is its ability to greatly reduce grating side-lobes found in phased-array setups [34]. This allows for more efficient energy transmission and avoid unwanted heating of surrounding tissue. Wave fields can be manipulated in many other ways by means of metasurfaces. Anomalous refraction/reflection by steering wavefront into the desired direction is the most fundamental functionality of a metasurface. Wave focusing (ie. beam focusing or point focusing) and self-bending beam are three interesting benefits of these structures. The latter (also known as self-accelerating beam) is a curved non-diffracting beam able to maintain its original path even after passing obstacles which are along the way [35]. Acoustic holography is also being explored as a technique to accurately record and reconstruct a wave field information by means of acoustic lenses [36]. Acoustic holography involves the spatial recording of the phase and amplitude characteristics of a wavefront in a way that allows it to be reconstructed through interference when exposed to a suitable acoustic source [25]. Using metasurfaces for beam manipulation also allows for multifocal applications [35].

Lens-Free focusing*Traditional methods:*

- **Curved transducer** By adding curvature to the face of the active element, the US beam will become more focused. The focal spot shifts closer to the surface of the transducer. Many commercially available transducers have this specification.
- **Phased-array** This setup makes use of an array arrangement of sources (ie. transducers) each operating with a phase delay with respect to each-other. In such way the generated wavefronts interfere constructively at a location of interest. A great advantage of arrays compared to single element transducers is their electronic beam steering and focusing capability. By changing the phase delays assigned to each transducer, the focal region can be manipulated and the beam can be steered. When considering linear arrays, the excitation time delay t_n for each element n can be calculated using:

$$\Delta t_n = (F/c)(1 - \sqrt{1 + (nd/F)^2 - 2nd \sin \theta_s / F}) \quad (2.24)$$

where θ_s is the steering angle, c the speed of sound and d the inter-element spacing. (See Figure 2.4 - (d))

- **Time reversal (TR)** This is a technique that involves the detection of a source through the recording of US waves using several transducers, time-reversal of the recorded signal and a playback of this recording using the same transducers [25]. Traditional TR requires a considerable number of receiving sensors and emission transducers. However, recent techniques involving multipath and multiple reflection characteristics in a reverberant space allow for accurate focusing using fewer sensors [25]. This technique can also be extended to complex media systems and non-linear chaotic wave systems.

Multi-source focusing

- **Multifrequency / Frequency Modulation** A less explored method resides in the modulation of a source signal (frequency modulation) or the combination of different frequency sources (multifrequency). When considering therapeutic focused ultrasound, it is shown that a multi-frequency approach is not only an efficient way of delivering energy non-invasively (eg. when performing US ablation) [37] but it also allows for increased resolution [38]. A study from Mehić et al. [39] showed that anatomical specificity of neuromodulation could be increased by using modulated ultrasound waves. Another approach proposed by Riis and Kubanek [40] allows for a 7.4 fold reduction in the focal volume when 650 Hz (central frequency) transducer arrays are used. This technique focuses on the non-uniform excitation of the transducers of a 2D array, such that they operate at different frequencies within their bandwidth. Two phased arrays facing each-other generate a continuous standing wave with increased intensity and resolution at the focal spot. It is shown that even at small bandwidth an increase in resolution is achieved.
- **Cross-beam:** Another technique explored involves the interference of ultrasound sources such that the resolution at the focal spot is increased. One method involves generating standing waves. These are created by either having two transducers facing each-other and generating their own waves which eventually will interfere, or by using one transducer and one reflective surface allowing for the reflected signal to interfere with the incident one. By creating such pattern, higher pressures can be concentrated at the (displacement) nodes. This phenomenon is widely exploited in the field of acoustic levitation. A great advantage of such setup is the possibility to generate several focal spots simultaneously, in an efficient way [41]. Another, more recent study from the same researchers has investigated the combination of standing waves and real time frequency modulation to increase the spatial resolution of the focused ultrasound beams [19] (see Figure 2.5a). The active frequency modulation allows for the focal spot to be shifted. Apart from using standing waves, another cross-beam method involves crossing several ultrasound beams onto the same location. The beams foci cross each other and allow for sub-millimetre scale resolution. In a conference paper published by Kim et al. [42] (see Figure 2.5b), a focal volume of 0.161 mm^3 was achieved by 90° crossing of two 5MHz US beams generated by curved transducers. A study from Kim et al. [43] also achieved sub-millimetre scale targeting using a novel dual-crossed transducer system with two single curved transducers. The results show that the smallest focus area was generated at a 90° crossing angle. The same concept was again used by in a study by Ilham and Kiani [44], with the use of phased arrays (32-element, 555 kHz) instead of single element transducers. It was reported that using two transducers led to a 28.4-fold reduction of the main focal zone area (A_{beam}).

2.4. Ultrasound for Neuromodulation

Neuromodulation induced by a medical device involves generating neurological responses through the transfer of energy to living cells. The effect of ultrasound application on the nervous system has gained much attention in recent years. Many successful animal trials have been conducted and the first effects of LIFU on a human brain were recorded in 2011 by Hameroff et al. [7]. Neuromodulation experiments have been performed around the same time both on the central nervous system (CNS) and on the peripheral nervous system (PNS) [12].

Being a relatively new field of research, the foundations for optimal wave parameters, stimulation locations and structured therapeutic guidelines are still being defined. In this section the working mechanisms of LIFU neuromodulation will be addressed by first understanding the underlying mechanisms in Section 2.4.1 and then by looking at the sonication parameters along with the ranges that are currently used. Finally, in Section 2.4.3 and Section 2.4.4 the existing setups used for LIFU neuromodulation

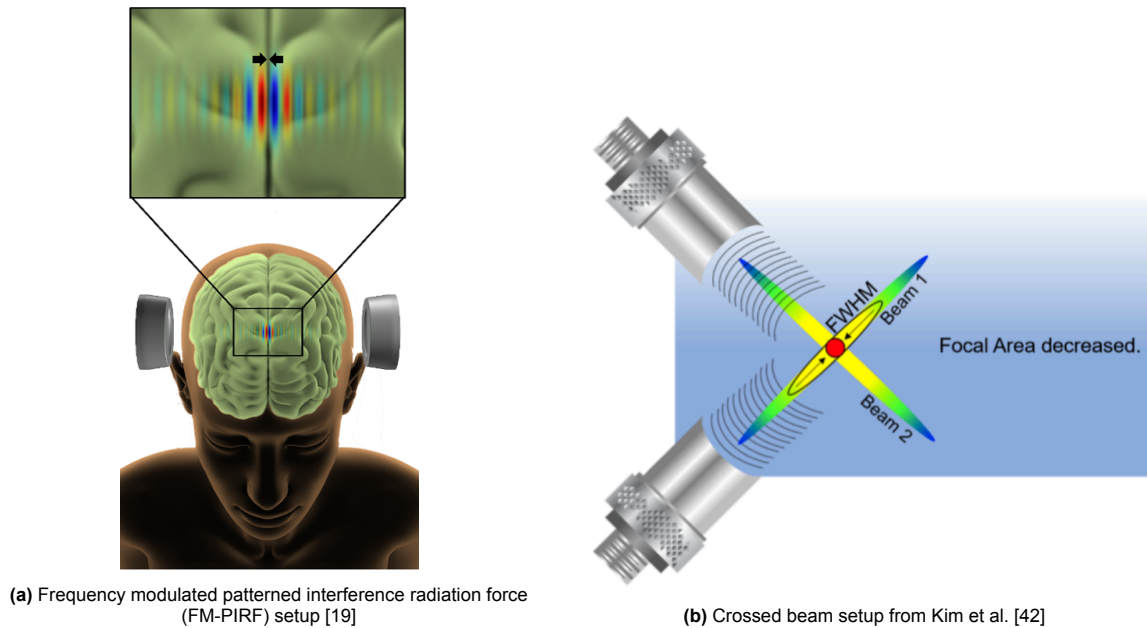


Figure 2.5: Two novel beam interference methods for FUS stimulation

will be presented as well as the emerging technologies.

2.4.1. Underlying mechanisms

In order to effectively perform neuromodulation using FUS, it is important to understand how sound waves interact with neurons, eventually leading to a modulatory activity. It is equally important to know what the waveform parameters are that allow for optimal and safe stimulation. Although the downstream effects of LIFU can be quantified and analysed, the causes for these (ie. the direct effect) are still a topic of discussion. The current most common theories are subdivided into thermal and non-thermal related, as such:

Thermal effects

As stated in Section 2.1, a fraction of the energy of an acoustic wave is absorbed by the medium as thermal energy. Though this effect is very limited at lower intensities, some studies suggest thermal effects as being the cause for LIFU neuromodulation [45]. Tissue heating at low intensities could lead to perturbation of neuronal activity levels, and temporary suppression of neural signalling [46]. It has also been noted that the effects depend on the rate of temperature change. At slow and prolonged rates, sodium channel inactivation and potassium channel activation lead to inhibition of action potential generation. However, when the temperature suddenly rises, plasma membrane capacitance changes occur leading to cell depolarisation. Additionally, variation in temperature affects ion channels and enzymatic and potential activities [47]. This theory is not popular as the temperature rise is very limited ($< 0.1^{\circ}\text{C}$) [12, 46, 48].

Non-Thermal effects

It has been shown that nerve excitation can be related to conformational changes of the cells' membrane. The well defined nerve impulse propagation from Hodgkin and Huxley [49] models the membrane as a capacitor, and subsequent studies have shown that the capacitive properties of membranes are influenced by the thickness, curvature and conformational state of the lipids [12]. Cells also present mechanosensitive ion channels on their membranes, which can have their activity be modulated as a consequence of conformation state change of the gate proteins.

- **Radiation Forces** These shear forces act on the membrane in two main ways [50]. First, mechanosensitive channels present on the cell membrane are thought to react to the direct application of ARFs (Acoustic Radiation Forces). The activation of those channels would immediately generate an action potential in the neuron. Another mechanisms would be through the conformational change

of the cell wall. It is known that neurons have different shapes based on their activity (ie. axons swell during action potential generation and propagation). A phenomenon known as electrowetting causes the membrane to change shape in order to maintain balance. FUS would work in the inverse way, changing the neural activity by affecting the local curvature. Two other phenomena being discussed focus on the effect of direct flexoelectricity (DF) and thermodynamic wave [50].

- **Stable Cavitation** Another non-linear effect thought to influence cell activity is intramembrane cavitation. Several researchers have proposed a model (NICE - intramembrane cavitation excitation) to predict action potential generation [51], which is based on the bilayer sonophore model (BLS) [52]. This model focuses on the change in membrane capacitance due to cavitation within the lipid bilayer. Though spontaneous (unstable) cavitation is not likely to happen during low intensity ultrasound (ie. diagnostic ultrasound), stable cavitation may still be present and play a role [47, 52]. Oscillation of these microbubbles might lead to pores being formed in the membrane, which would enhance the permeability and allow for gradient driven ion displacements to occur [12]. Even if sonoporation does not occur, cavitation can affect the local curvature of the cells' membrane which in turn has an effect on the excitability of that neuron [46, 12]. Furthermore, it has been discovered that the introduction of microbubbles can stimulate stable cavitation at lower power levels, leading to biological effect (such as BBBO) without inducing irreversible damage to the cell [53].

Confounding pathways

A third theory focuses on the indirect neuromodulatory effect of ultrasound through confounding pathways, particularly through the auditory pathway. During animal studies, neuronal activity were reported following tFUS of the auditory nerve, cochlear nucleus, and auditory cortex. As stated in the extensive review paper by Darmani et al. [11], studies show that that stimulation closer to the cochlea could induce more robust motor responses compared to direct stimulation of the motor cortex. Other studies have suggested that cochlear fluid plays an indirect important role in this phenomenon This raised concerns regarding the direct effect of FUS on neuromodulation. However, other research performed in different setups contradict this theory. Cultured neurons [54] as well as deafened mice [55] have been eliciting neuromodulatory effects, showing that a direct effect of FUS is indeed present. A study by Mohammadjavadi et al. [55] suggests that evoked motor responses are not a result of auditory pathway stimulation, arguing that it is the pulse envelope which indirectly affects this confounding pathway and that motor responses in deafened mice are the same as in normal hearing mice. Finally, better modelling techniques allow for the dissipation of sound waves to better be simulated. In this context, shear waves have been studied and are shown to be able to reach off target locations (ie. cochlea) and induce audible sound. Although this mechanism is not dominant, the necessary measures (ie. masking and envelope modulation) should be taken into account during experimental trials.

Although these mechanisms can be separated from each-other, there is a great possibility that FUS stimulation is a result of combined effects [12]. Furthermore, as there is an important discrepancy between the sonication parameters used for PNS and CNS FUS stimulation, the role of glial cells might play an important role in cerebral neuromodulation. These cells have shown to be sensitive to the application of FUS and their role in the brain for neuronal function and synaptic moderation is critical [56].

2.4.2. Sonication parameters

The precision, efficiency and the induced biological effects of LIFU are influenced by a set of sonication parameters. These parameters describe the sonication protocol, they are shown in Figure 2.6. When considering which waveform to use, a first distinction should be made between continuous and pulsed sonication. In fact, the ultrasound signal can be sent in a continuous fashion, without breaks, or a certain pulse repetition frequency can be applied, which interrupts the signal at every given time step. When considering LIFU, pulsed therapy is the most used one as it minimises tissue heating and requires lower thresholds for neural activation [46].

Fundamental frequency - f_0

Also referred to as the carrier wave, this parameter is fundamental when tuning for high spatial resolution. As the frequency is the inverse of the period of the wave ($f_0 = \frac{1}{T}$), the higher the frequency is, the

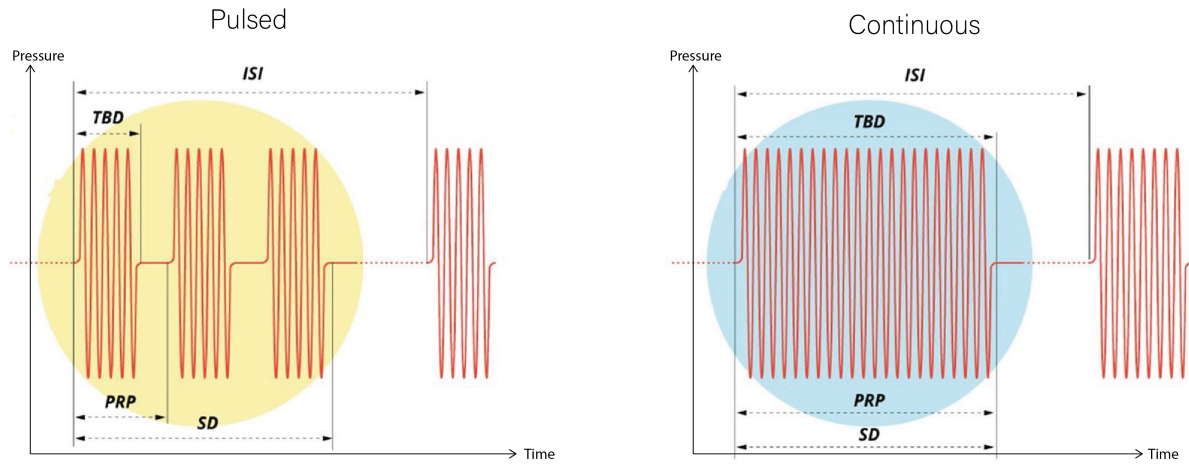


Figure 2.6: Temporal characteristics of and continuous pulsed ultrasound [Adapted from [50]]

shorter the period (wavelength). This allows for increased targeting precision which is a crucial aspect of brain stimulation in general, as increasing specificity and precise targeting is a major concern (especially when focusing on specific neurons (soma diameter: $\approx 100\mu\text{m}$)). On the other hand, ultrasound waves travelling through matter (human tissue such as skull, skin, brain, etc.) experience scattering and attenuation. As the latter is linearly related to the frequency (see Equation (2.8)), a compromise is continuously made between precision and attenuation (or focal depth). The energy lost due to attenuation is transferred to the tissues and may result in unwanted overheating effects. According to Darmani et al. [11] and Fomenko et al. [46], the optimal frequency for transcranial applications is smaller than 700 kHz, and most studies perform ultrasound stimulation with fundamental frequencies ranging from 200-650 kHz allowing for a targeting precision of 2-4 mm. It should be noted that this frequency range is limited by the attenuation and scattering effect caused by the skull and other protective layers of the brain. When it comes to implantable microsystems, these frequencies can be in the range of 2-10 MHz [57] as the skull aberration effects are avoided. This allows for significant increase in resolution.

Tone Burst Duration - TBD

Also called pulsed duration, this parameter represents the duration of fundamental frequency signal being delivered in one cycle.

Pulse repetition frequency - PRF

Avoiding irreversible heating effects on the surrounding tissues while stimulating the selected neurons is what researchers thrive for. Subdividing the sonication duration into pulses allows for a better control of these thermal effects while reaching the desired stimulating/inhibitory goals. The PRF is defined as the frequency at which the pulses (pulse duration + break) are delivered. The pulse repetition period (PRP) is the inverse hereof.

Sonication duration - SD

Sonication duration represents the sum of the PRPs delivered to the tissue during sonication. It is the interval between the start of the initial burst (pulse) to the end of the last one. The time between the start of each SD is called the interstimulus interval (ISI). The SD is determined by the TBD and the time between tone bursts (PRP) [50].

Duty cycle - DC

The duty cycle is given as a ratio, as it represents the proportion of pulse duration (at the fundamental frequency) over the pulse repetition period.

$$DC = \frac{TBD}{PRP} \quad (2.25)$$

If a continuous wave pulse is generated, the DC would be 100%. However, the pulsed paradigm is preferred as the risk of tissue (overheating) is lower as well as the stimulation threshold [46]. During pulsed stimulation, this ratio is $\pm 50\%$.

Intensity

As stated in Section 2.1, the intensity of an acoustic wave is defined as the amount of power of the wave flowing through a given area. The intensity of an US wave in a therapeutic LIFU setting is defined in two different ways:

- **Spatial-peak pulse average - I_{SPPA}**
Is defined as the average intensity of an individual pulse and is given by Equation Equation (2.26). It is a good indication of the short-term mechanical bioeffects [46].

$$I_{SPPA} = \frac{1}{TBD} \int_0^{TBD} I_{SP}(t) dt \quad (2.26)$$

- **Spatial-peak temporal average - I_{SPTA}**
This parameter describes the average intensity (or amount of energy) delivered over the entire duration of the sonication period, as given by Equation (2.27). As the smaller scale transfer of heat takes more time than the greater scale transfer of mechanical force, the I_{SPTA} is a good indication of the heating of the tissue, as this is proportional to the SD.

$$I_{SPTA} = \frac{1}{PRP} \int_0^{PRP} I_{SP}(t) dt \quad (2.27)$$

When it comes to regulation and standards, these two intensity values are used as limiting values (in the case of diagnostic ultrasound). Two other commonly used parameters, derived from the previous stated sonication parameters, are:

- **Mechanical Index - MI**
Cavitation can occur when ultrasound travels through a tissue and is an unwanted effect (if unstable) when applying. Regulatory agencies have defined a metric to estimate the probability of cavitation [58]:

$$MI = \frac{\max\{p_{negative}\}}{\sqrt{f_0}} \quad (2.28)$$

- **Thermal Index - TI**
This metric quantifies heating within the tissue. It is defined by the total power delivered (W_p) over the power necessary to heat the tissue by 1°C (W_{deg}) [12].

$$TI = \frac{W_p}{W_{deg}} \quad (2.29)$$

Numerous review papers have gathered the sonication parameters used so far in both animal studies and human trials [6, 12, 46, 59, 60] and others. Typical values are in these ranges: $f_0s = 183\text{--}5000$ kHz, $BD = 0.16\text{--}2$ ms, $PRF = 0.1\text{--}3$ kHz, $DC = 5\text{--}50\%$, $SD = 13\text{--}2000$ ms, and $ISI = 1\text{--}90$ s [61]. Regarding the required pressure levels for neuromodulation, these can vary from hundreds kPa to a few MPa. This depends on the target and sonication pattern [12, 61]. LIFU studies on humans have used intensity values in the ranging between $1.5\text{--}17.5$ W/cm^2 . Limits to some of these parameters are dictated by different regulatory bodies [62], however this is limited to diagnostic US applications.

Now that the definition of sonication parameters and their typical values have been defined, the existing tFUS and μ FUS setups will be discussed.

2.4.3. Transcranial setup: tFUS

So far, the effects of LIFU neuromodulation have been studied using a transcranial setup. The US waves are generated outside of the patients' body and focused on the inside. The advantage of this setup is that it is completely non-invasive. There is no surgical procedure that needs to be performed.

Devices and Setup

The main components found in a tUS neuromodulation setup are shown in Figure 2.7. A function generator creates a sinusoidal function which oscillates at the wanted fundamental frequency f_0 . This signal is partitioned (or pulsed) by means of a second function generator, passing an amount of oscillations equal to the TBD at a frequency dictated by the PRF. A power amplifier is then used to amplify the sinusoidal pulsed signal before applying it to the transducer. The ultrasound parameters are chosen such that the intensity, depth and resolution match the intended ones.

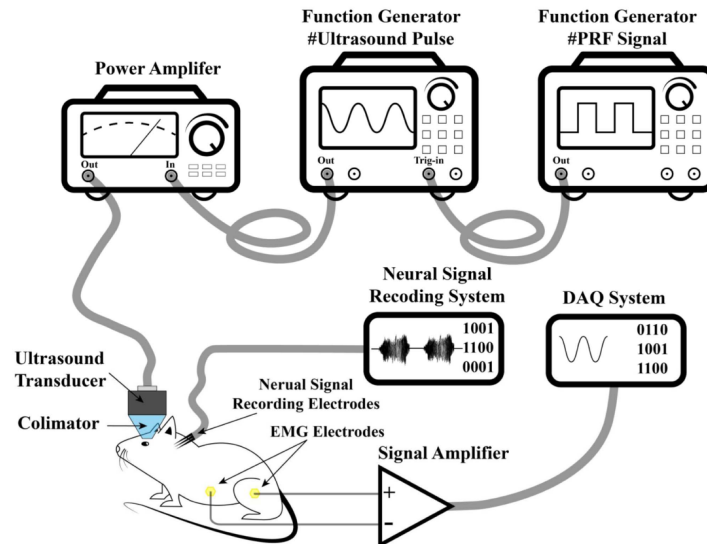


Figure 2.7: The conventional experimental setup for single element transducer tFUS [61]

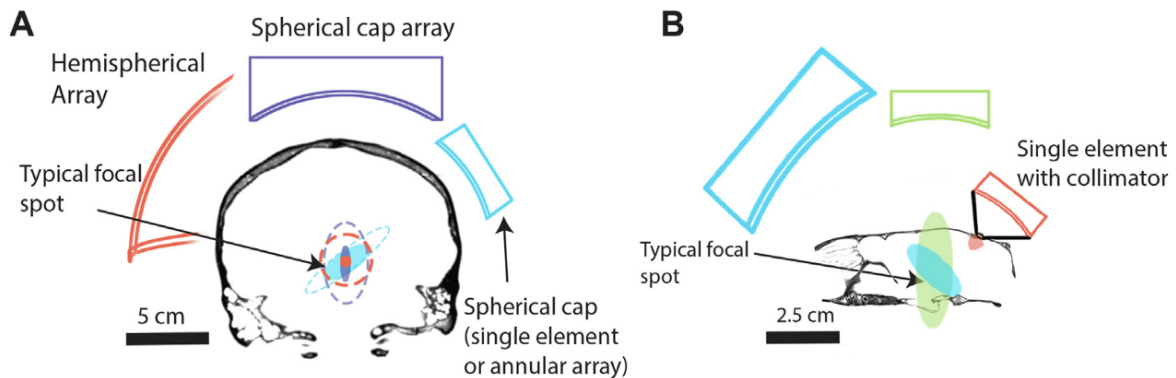


Figure 2.8: Scale of the ultrasound focus. Focal spot sizes (solid) and steering ranges (dotted line) of commonly used acoustic apertures. (A) In humans, (B) in rodents [11]

During experimental trials, different transducer setups have been used. As the goal is to generate a small focus area/volume, and as aperture is proportional to the resolution, substantial setups such as hemispherical arrays have been used for tFUS (see Figure 2.8). These setups are bulky, require whole head shaving and the use of a frame to suspend the head in a water bath [11]. If an array setup is used, the adequate phase delay is computed for each transducer to focus the beam. A detailed table stating the different tFUS devices used in human trials is presented in Sarica et al. [8].

Real-time tracking of the true focus point is crucial. In order to track the beam focus, different targeting techniques have been used including image-guided neuronavigation, MR-guided navigation, ARF MRI, the use of custom-built headsets/helmets and others. A detailed list of all tracking methods used during human and clinical trial is presented in Lee et al. [6]. The most preferred techniques (which do not require a live MR-setup) are the image-guided neuronavigation systems. Often, optical tracking is

used as a navigation technique. It consists in placing markers on both the subject head and the active device, and then imaging them. These reflective markers on the transducer device are used to track its position in physical space using an infrared camera. The same is performed for the subjects head. As the markers can be seen in CT/MRI images, neuroimages are acquired and a rigid transform is computed, mapping the reflective markers to the image space. In this way the position of the transducer (and the previously computed focus) can be overlaid on top of the anatomical image [63]. The error between the computed focus and the real focus is called the target registration error (TRE) and has been shown to be as small as 2 mm or less [64].

Sonication Protocols

Different sonication protocols have been used so far, ranging from random (even unfocused) stimulation to patterns matching the natural brain rhythms. As tFUS is an emerging technology, inspiration is taken from other non invasive brain stimulation (NIBS) techniques. These protocols dictate parameter values that should be used and/or locations that should be targeted.

- **Theta burst TUS (tbTUS):** this protocol takes its name from the hippocampal theta rhythm related to learning and memory processes [63]. It corresponds to an 80 second train of 20 millisecond bursts of ultrasound (0.5 MHz) repeated at 5Hz (PRF).
- **Repetitive TUS (rTUS):** rTUS involves the delivery of ultrasound pulses in a repetitive, continuous pattern. The frequency of these pulses can vary depending on the protocol but does not follow a specific rhythmic pattern. This is the most commonly used protocol.
- **Transcranial pulsed stimulation (TPS):** In contrast to rTUS, TPS uses single ultrashort pulses ($\sim 3 \mu\text{s}$) repeated at very low frequencies (1-5 Hz) with a similar sonication time of several minutes [65].

These protocols can have a great impact on the efficiency of sonication. In fact, when comparing the targeting of primary motor cortex (M1) using both tbTUS and rTUS with comparable parameter values, the SD was 80s for the first and 15 minutes for the second, for the same long-lasting offline MEP (motor evoked potentials) amplitude increment [8].

Limitations

- **Skull effects:** One important limitation of this setup is the attenuation caused by the skull. As the skull has a heterogeneous structure (spongy, non-isotropic properties, etc.), the impedance mismatch is important and the aberration effects are significant. High frequencies cannot be used in this setup and researchers have concluded that the optimal value for the fundamental frequency is below 700 kHz [8, 46]. This sets a limit to the resolution that can be achieved. An extensive experimental research performed by Chen et al. [66] showed that the transmission efficiency decreases exponentially, while the -6 Db beamwidth decreases logarithmically with the increase of ultrasound frequency. Furthermore, the scattering induced by the skull leads to offsets which stimulate unintended regions, making it more difficult to clearly link the stimulation protocol to the measured effect. This also adds complexity when comparing the outcome of different studies as these effects are case specific. The scattering is also thought to play a major role in undesired auditory cortex activation due to the mechanical conduction through the skull (see Section 2.4.1). The internal heterogeneity and shape of the skull has led researchers to investigate the ideal placement of the transducers given the skull shape such that the transmission is optimised. In a study by Park, Pahk, and Kim [67], a computationally inexpensive method of placement of the tFUS transducers was created based on the average reflection coefficient (ARC). The coefficient is calculated for different transducer locations. An interesting placement location would be around the temporal area and the bregma, as these have the smallest thickness [68].
- **Bulky setup:** Current tFUS setups require substantial setups which are costly and difficult to handle. Most studies so far have made use of single-element transducers which need precise placement. The individual is asked to remain as static as possible in order to ensure proper alignment after the calibration process. This is a major source of uncertainty and may lead to increased TRE. This limitation is also of great importance during animal studies. As the subject needs to be immobilised, anaesthesia is usually administered. However, it has been reported that the use of narcotics has a great impact on the effectiveness of tFUS administration [46]. This limits

the use of tFUS as a therapeutic application. Furthermore, this setup cannot be used for patients needing direct, unpredictable intervention (ie. seizure detection and mitigation). Finally, the need for a dedicated professional, medical devices and space limits the use of such interventions to high income settings.

2.4.4. Implantable setup: μ FUS

In order to overcome the limitations faced by conventional tFUS, wearable machines are being developed. As a final goal is to reach specific neuron populations (or even single neuron) size resolution, US waves at MHz frequencies need to be generated. Having an implantable device beyond the skull barrier allows this. Single-element transducers have been redesigned to be used in vivo (as wearable devices) and these have been successfully tested in living mice. But there are limitations to their use such as the inability to change the stimulation target, their large form factor and the need for cutting edge power amplifiers [23]. In order to overcome this issue, phased arrays can be used. These microsystems consist of two main components: the transmit beamformer and high-voltage (HV) drivers. The low voltage level signal from the beamformer is supplied to the HV drivers which in turn drive each transducer from the array with the necessary voltage pulses. These components can be implemented using different approaches as described in Javid, Ilham, and Kiani [61]. When using discrete components, the costs tend to be lower and more readily available, however the device becomes more bulky, which is a drawback when it comes to miniaturisation. Implementing the components on an application-specific integrated circuit (ASIC) allows for a more compact transmitter design, this also leads to reduced interconnect complexity and reduced parasitic effects (see Figure 2.9b).

In a paper published by Ilham and Kiani [44], a comprehensive study is performed on characteristics of millimetre-sized transducers. Particular attention is given to the spatial resolution and the power efficiency of the device, as these parameters are limiting for the type of setup and application. It is shown that even for μ FUS, it is desirable to have acoustically matched focused transducers with high quality factor which leads to higher resolution and better power efficiency. Several designs were recently developed and they are shown in [44]. Two miniaturized phased arrays setups were designed by Seok et al. [69] and Rivandi and Costa [23].

A fully implantable system was developed by Seok et al. [70] (see Figure 2.9a).

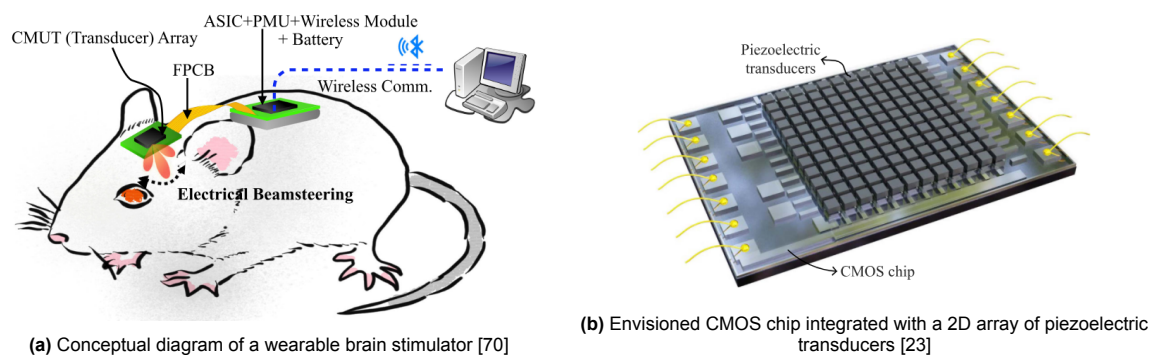


Figure 2.9: Implantable μ FUS systems

Limitations

- **Miniaturisation** Reducing the invasiveness of the device can be achieved by reducing the size of it. Implementing the components on an ASIC allows for compact designs to be made having an area of a few squared centimetres. Furthermore, using emerging MUT technology also allows for a more compact design. This technology is also MRI compatible, which is important for diagnostic guidance [71]. However, minimizing the size can also limit the functionalities of the device, such as the use of broadband transducers or complex sonication patterns to be implemented.
- **Limited power** Having a fully implanted neurostimulation device requires the entire system, and therefore the power system to be implanted as well. The energy necessary to power the device and fulfil the required stimulation therapy should be readily available. The energy available is thus limited, which requires the device to be as power efficient as possible.

- **Biocompatibility** As the device would be implanted, a driving requirement is related to biocompatibility. When looking at the transducers, PMUT/PZT transducers require hermetic encapsulation as they contain lead, which in turn greatly affects their power-efficiency. Using a CMUT allows to overcome this issue, but the high voltage bias would increase the power consumption [71].

2.5. Research Gap

When considering LIFU for neuromodulation, there are still ongoing discussions on the actual underlying mechanisms. Mechanical forces (ARFs) induced (indirectly) by the US wave is thought to activate the mechanosensitive channels of the cells and to generate action potentials due to the conformational change of the membrane. Cavitation is also thought to be a cause, although the frequencies and intensities used are relatively low. Thermal effects and confounding pathways (ie. auditory tract) are causes that may play a role, but their effects are considered to be minimal. The reason neuromodulation occur can probably be explained through a combination of these causes. The incident waveform can be adapted by changing the sonication parameters, in order to achieve the intended intensities, at the intended location. Typical values currently used are in these ranges: $f_0 = 183\text{--}5000$ kHz, $BD = 0.16\text{--}2$ ms, $PRF = 0.1\text{--}3$ kHz, $DC = 5\text{--}50\%$, $SD = 13\text{--}2000$ ms, and $ISI = 1\text{--}90$ s. FUS neuromodulation has mainly been administered in a transcranial fashion. This setup has its benefits such as being fully non-invasive, however being restricted to a complex system (ie. machines, professional clinicians, isolated environment, etc.) does not allow for flexible and on-the-spot treatment. The aberrations induced by the skull are significant and cannot be avoided in such setup. The development of implantable microsystems (μ FUS) overcomes the limitations set by tFUS. These cm-sized concepts could revolutionised LIFU neuromodulation by being implanted on the surface of the brain. There are some drawback to this setup as well, such as limited available power, the need for a biocompatible system and the reduction in features linked to the miniaturisation of the device. The two setups which have been presented, tFUS and μ FUS both have their advantage and drawbacks (see table below).

Table 2.2: Comparison between μ FUS and tFUS systems

	f_0	Resolution	Power availability	Sized constrain	On demand stimulation	Bio-compatible
μ FUS	MHz	High	Limited	cm-scale	Yes	Yes
tFUS	Sub-MHz	Low	Unlimited	None	No	No

Being able to combine these two technologies would allow for the drawbacks of one to be compensated by the benefits of the other. Investigating on the effects of crossing high frequency beams generated by implantable (MHz) transducers with low frequency beams generated by transducers outside of the body could lead to increased resolution and greater power efficiency. Cross-beam studies were performed using two identical US sources and these have shown great results for both sub-MHz (555 Hz) and 5MHz sources, reaching focal volumes up to 0.14 mm^3 [44]. As multiple sources are used, standing waves as well as frequency modulation could be introduced to narrow the focus volume even further [19, 40]. This would also allow for the power consumption to be distributed over the sources, as well as increased ARFs intensities, which are thought to be major players for neuromodulation. The increased resolution from such a combined setup would mainly be a result of bypassing the skull with the implantable micro-system, while its power consumption can be reduced by having an external source focused on the same target area.

The studies performed by Kim et al. [42], Kim et al. [43] and Ilham and Kiani [44] do investigate the effects of interfering beams from two different transducers. However, the transducers being investigated have identical characteristics. Although an important change in focal area and intensity is seen at the focal spot, information is lacking regarding the effects of changing the fundamental parameters of the sources such as the aperture and the fundamental frequency on these metrics. The interference has either solely focused identical single element transducers (Figure 2.10a) or use two identical phased arrays (Figure 2.10b).

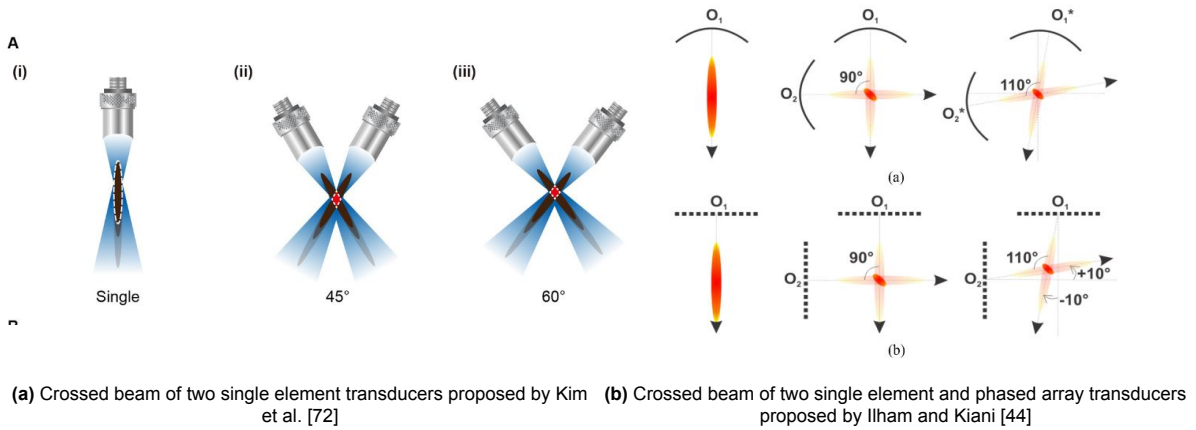


Figure 2.10: Research on dual US source setups for neuromodulation

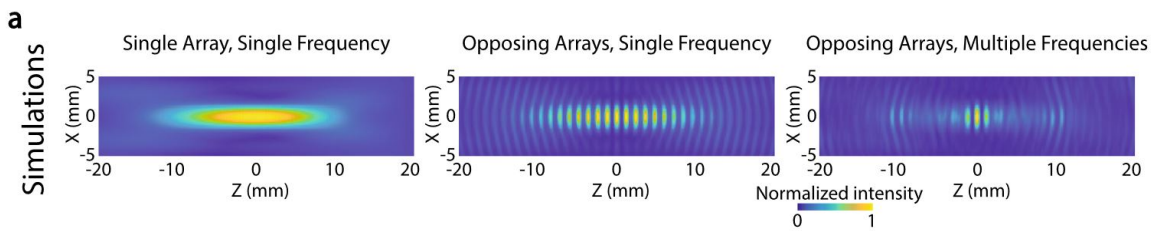


Figure 2.11: Dual multi-frequency US source interference approach proposed by Riis and Kubanek [40]

The effects caused by changes in US wave frequency have somewhat been investigated in the papers by Riis and Kubanek [40] and Kim et al. [19]. The concept of frequency modulation and pattern interference radiation force (PIRF), have shown to substantially decrease size of the focal volume. In these setups, standing waves are generated by the transducers facing each-other. In order to focus these standing wave on a specific region and avoid this phenomenon from happening elsewhere, a frequency modulated wave pattern is delivered, instead of a continuous wave. This setup however focuses on the creation of standing waves and sets the angle at which the two beams cross to 180° . Another important aspect is that the setups focus on transcranial applications, where the available power and the size of the transducer are not limiting. Therefore the power efficiency of (at least one of) the transducers is not taken into account. Methods for analysing the effects of changing the driving parameters in a dual transducer setup need to be defined. In the following chapter, the methodologies used during this project to answer the research question are presented.

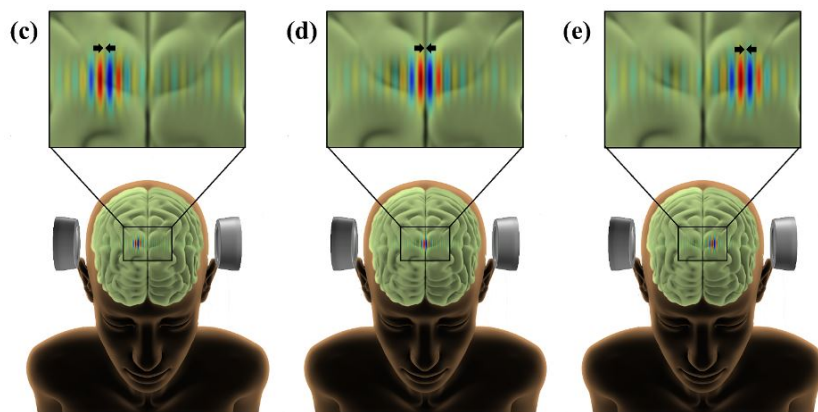


Figure 2.12: Pattern interference radiation force setup by Kim et al. [19] using two front facing transducers

3

Methodology and project outline

In order to answer the research question posed, a methodology for the project is proposed. A timeline of the research process is depicted in Figure 3.1. The first step consists in defining the parameters that will be investigated, as well as the simulation protocol. From this, a dataset of pressure fields is generated. The steps taken to generate a dataset of pressure fields are described in Section 3.1. Following this, the geometric transformations performed to merge the data sets will be shown in Section 3.1.4. An optimisation process is then implemented in Section 3.2 to determine the optimal placement and the optimal individual characteristics for a set of transducers.

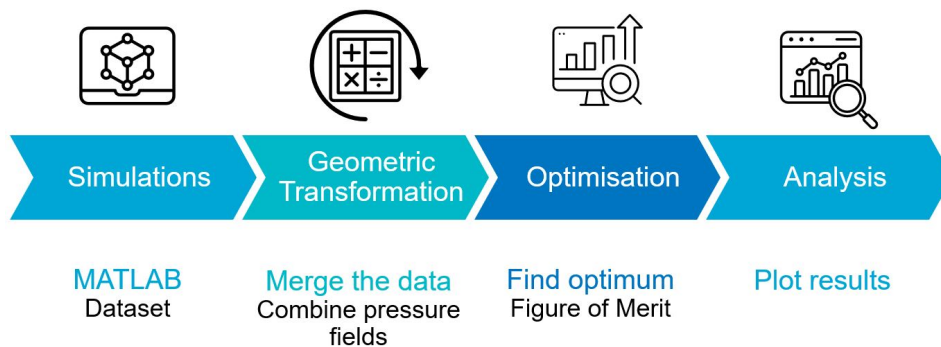


Figure 3.1: Research project outline

3.1. Simulation and selection

A set of independent variables needs to be defined and the metrics for analysis need to be chosen to investigate the cause and effect relationship in a dual source setup. For simplicity purposes, the transducers are modelled as single element curved transducers in this project. The results following this assumption are valid for an ultrasound phased-array setup as the focus will be on the interfering pattern of the generated pressure field.

These parameters can be divided into two categories: transducer independent variables and combined parameters. A schematic representation of the setup with the independent variables is shown in Figure 3.2.

3.1.1. Transducer independent variables

The first category relates to the fundamental parameters of the individual transducers which directly affect the US waveform they generate. As the goal of this project is to better understand the interaction between a tFUS source and a μ FUS source, the current technological boundaries and limitations should be taken into account, while creating an interesting search domain while keeping in mind the assigned

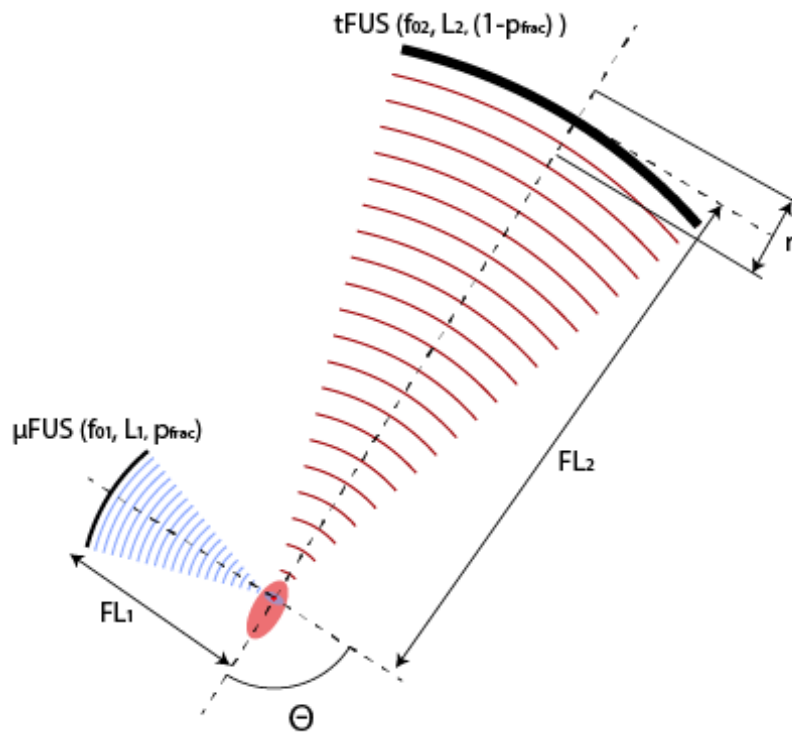


Figure 3.2: Schematic representation of the dual transducer setup (FL : Focal Length, f_0 : fundamental frequency, L : aperture, r : radial margin, θ : crossing angle, p_{frac} : contribution factor)

role of both transducers. These parameters chosen for both sources, the defined ranges and the motivation behind them are shown below.

The parameters for the μ FUS source are:

- **Fundamental frequency: 1 - 6 MHz**

Increasing the resolution of the focal area is a key aspect of neuromodulation. This is the main motivation for bypassing the skull and studying the effect of using implantable devices. In this case, higher fundamental frequencies can be used compared to tFUS setups. In order to maximise the spatial resolution (Equation (2.20), Equation (2.21)), while keeping a reasonable range to reduce computational cost, an upper limit of 6MHz is chosen. Increasing this value would allow for higher resolutions to be achieved, however the tissue absorption would become more significant and the focal depth would decrease. The lower limit has been set to 1 MHz, allowing for a reasonably small focal area to be generated, while aiming for a greater focal depth.

- **Aperture: 10 - 40 mm**

When considering an implantable device, power efficiency and invasiveness are two key aspects that have to be optimized for. The size of the implanted device should be minimal such as to minimise the foreign body response (FOR), and the power efficiency should be maximised as the device should have the longest possible operating life, and therefore minimum power consumption. Minimising the aperture allows for this. However, FWHM is inversely proportional to the aperture and the DOF is inversely proportional to the square of the aperture. Therefore, a greater aperture will increase the resolution.

The parameters for the tFUS source are:

- **Fundamental frequency: 350 - 750 kHz**

The tFUS source is confronted with the skull, which greatly interferes with and absorbs the incoming US waves. As this effect is directly related to the frequency of the incoming wave, an upper limit is set to 750 kHz. In a study published by Chen et al. [66], the tFUS transmission efficiency through a human skull has shown to be minimal at frequencies < 750 kHz. To ensure

higher transmission efficiency and avoid unnecessary (and dangerous) tissue heating, this value has been chosen as an upper limit. The lower limit is dictated by the increase in beam width as the frequency is decreased. Although the main purpose of this transducer is to deliver a pressure baseline where the μ FUS will focus upon, the focal area should be kept at a minimum, which is why a lower bound of 350 kHz is chosen.

- **Aperture : 15 - 65 mm**

The tFUS source is not strongly limited by size nor power consumption as it external to the body. Therefore the range of aperture is mainly based on existing technologies [44, 61]. This transducer will be located further away from the focal spot than the implanted source. As aperture is proportional to focal depth, a greater aperture allows for greater penetration depth, which is crucial in this case. Though the size of the device is not limiting, the patient using this device should experience a minimum level of discomfort. Therefore the maximum aperture has been limited to 65 mm.

Another important parameter when it comes to simulating single element transducers is related to the focusing of the beams. As stated in Section 2.2, US beams can be focused in different ways. When simulating, the easiest approach is to add a radius of curvature (ROC) to the surface of the transducer. The ROC has been parametrised by using a approximate formula derived by Huang and Ding [73] to be a function of focal distance, medium absorption and transducer aperture (see Equation (3.1)). As the f-number is given by these two terms, the degree of focusing is dictated by this factor. For both transducers the f-number ranges from 2 to 4.

$$\gamma_p = \frac{\beta}{1 + \frac{2\beta^2(1+\alpha_T\beta)}{1+2\beta \left[1 + \left(\frac{1}{2} + \frac{1}{2(1+\frac{\alpha_T\beta}{2})} \right) \alpha_T\beta \right]}} \quad (3.1)$$

where γ_p is the fractional focal length, $\beta = A/z_0$ is the normalized geometric focal length (or focal strength), A is the geometric focal point (or the ROC), z_0 is the natural focus of the transducer, $\alpha_T = \alpha \cdot z_0$ where α is the attenuation coefficient as defined by Equation (2.8). Applying this formula allows for the parametric and precise positioning of the transducers during the simulations.

3.1.2. Combined parameters

The combined parameters are an additional set of variable that are expected to affect the pressure field when two ultrasound sources are used. These are related to the relative position and contribution of each transducer, and these are listed below:

- **Crossing Angle - θ : 0 - 2π rad**

The crossing angle spans the entire range of angles. This allows for the exploration of all possible orientations relative to the two transducers. Although a symmetric pattern is expected between the two hemispheres ($0 \rightarrow \pi$ and $\pi \rightarrow 2\pi$), θ is chosen to span the entire circle so as to verify the subsequent geometric transformations.

- **Radial Margin - r : 0 - ± 5 cm**

This term has been introduced to allow for fine tuning of the superposition of the fields at the focal spot. As the tFUS source is external, this term adds a margin to the radial distance of this transducer with respect to the expected focal spot given by Equation (3.1). This term therefore allows for a wider search space during the optimisation process, and for better understanding of what the effects could be of a misaligned transducer in this setup.

- **Contribution factor - p_{frac} : 0 - 1**

The amplitude of the initial US wave generated by the transducers should be taken into account when superposing the two fields. The pressure distribution is dictated by the initial pressure (which is proportional to the amplitude of the signal) and in turn affects the resolution of the focal spot (as dictated by Equations (2.20) to (2.22)). In order to reduced the number of variables, this contribution factor is a measure of the amplitude of the μ FUS transducer signal with respect to the external one. Therefore, when considering an initial wave amplitude of A , the contribution factor will multiply the μ FUS transducer amplitude by p_{frac} and the tFUS by $(1 - p_{frac})$.

The values for both the individual and the combined parameters are summarised in Table 3.1 and Table 3.2 below.

Table 3.1: Ranges of transducer independent variables

Transducers	Aperture (mm)	Frequency (MHz)	f-number (-)
μ FUS	10 : 40 (7 steps)	1 : 6 (6 steps)	2 : 4 (5 steps)
tFUS	15 : 65 (6 steps)	0.35 : 0.75 (5 steps)	2 : 4 (5 steps)

Table 3.2: Ranges of combined parameters

Parameters	Range	Units
Crossing angle	0 : 2π	(rad)
Contribution factor	0 : 1	(-)
Radial Margin	-5 : 5	(cm)

The total number of combinations given the individual transducer parameters is therefore: $7 \times 6 \times 5 \times 6 \times 5 \times 5 = 31500$. This is not taking into account the combined parameters which will greatly increase this number. It can already be noted that a full analysis, where the entire setup is simulated, will be computationally expensive, memory intensive and time consuming. This issue will be addressed in the next subsection.

3.1.3. Simulation domain

There are different approaches available when simulating ultrasound wave propagation. These approaches are reflected in the different types of simulation software that are available. The existing models can be classified in three categories:

1. *Semi analytical models:* Ray tracing and Transfer function methods are usually used as such methods to solve the wave equation.
2. *Numerical models:* Finite differences and k-space models are the most used ones to numerically solve the wave equation in a (t)FUS setup. A widely used MATLAB toolbox is called k-Wave [74]. The forward simulations are based on a k-space pseudo-spectral time domain solution to coupled first-order acoustic equations.
3. *Hybrid models:* In the case of tFUS, the greatest limitation to use analytical methods is the heterogeneity of the skull. The problem could be divided into using numerical solvers for the wave-skull interactions, and analytical solvers before and after that stage, considering those media to be homogeneous [75].

For this application, k-Wave was chosen as a simulation software. The choice was made based on several reasons. First of all, as the intention is to simulate US propagation through heterogeneous medium (skull, brain), a software where different media could be simulated was needed. The k-Wave toolbox allows for medium properties (speed of sound and density) to be defined at each grid point in the computation domain. This toolbox also allows absorption and (some) non-linear phenomena to be taken into account. The medium absorption and dispersion properties are taken into account by means of the Kramers-Kronig (K-K) relations. The non-linear effects are simulated by introducing a new term in the pressure-density relation, which represent the second order terms of the Taylor expansion of the equation of state. Furthermore, the ability to model both 2D and 3D is of interest as the first setup allows for faster computation of the main characteristics of a pressure field and the second allows for the focal volume to be computed more accurately. Finally, as k-Wave is widely used in research, especially in the literature which is of interest to this project, it allows for direct comparison to be performed with

previous studies and therefore, easily troubleshoot any possible errors.

The goal of this step is to generate a dataset of interfering pressure fields produced by two transducers, such that the influence of the different design parameters on the resulting pressure distribution can be studied. This problem can be addressed in two main ways. The two transducers can be simulated simultaneously, such that k-Wave outputs the resulting pressure and velocity fields directly. This would be the most accurate simulation method as the influence of one source directly affects the pressure field of the other. Furthermore, this allows for the non linear terms to be computed. However, this would come to the expense of great computational costs (memory intensive and computationally expensive) as stated earlier. For instance, when looking at Figure 3.3, the computation time would on average take 7 minutes for one set of parameters, using a spatial a resolution (or grid size) of $\frac{\lambda_{\mu FUS}}{3}$. Given the 31500 parameter combinations that have been defined, this would take around 3675 hours to run, which is cumbersome for a statistical study. In order to overcome this cost, the two transducers are simulated individually and in a second term, their pressure fields are linearly superposed.

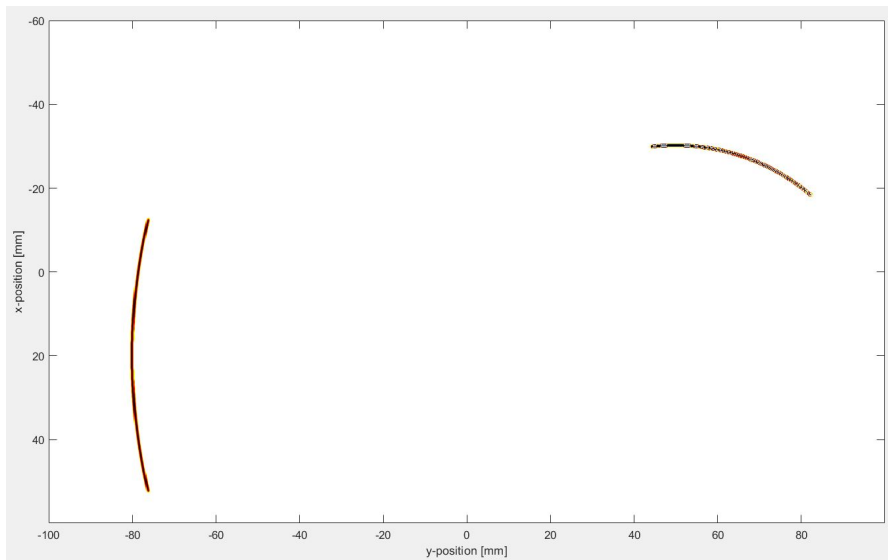


Figure 3.3: k-Wave simulation domain

When doing so the average computation time for a μ FUS transducer field is 4 minutes, while for a tFUS setup it represents a few seconds. Also, the combined parameters don't have to be taken into account at this stage, as the individual pressure fields will be superposed through geometric transformations in a second stage. Therefore, this method greatly reduces computation time and allows for easy data manipulation. In fact, using this method allows for any combined pressure field to be generated without having to rely on simulations or a memory intensive dataset of all possible fields superpositions. However, this entails that the computed pressure field is purely linear (there is no non-linear effects taken into account).

In order to generate the data sets for both transducers, a Matlab [76] function was implemented where the inputs are the individual parameters (as stated earlier) and the outputs are the maximum pressure field, the pressure field at each time step and the non-staggered velocity field. For each simulation, the computational grid is defined as $N_x \times N_y$ where $N_x = 2 * FL$ and $N_y = 1.5 * L$. This allows for the expected focal spot to coincide with the centre of the grid. The spatial resolution is defined as $\frac{\lambda}{3}$. This ensures the Nyquist criterion of 2 grid points per wavelength is satisfied, while keeping the computational burden and memory usage to a minimum.

As the intention of this project is to validate simulated results with experimental data, the medium properties have been set to those of water as given in Kinsler et al. [77] where $\text{medium.alphacoeff} = 0.00217$ and $\text{medium.alphapower} = 2$. The density and speed of sound in the medium are 1000 kg/m^3 and 1500 m/s respectively. As non-linearities are not taken into account during the simulations, the

non-linear coefficient $BonA$ is omitted. A simple sinusoidal signal is defined at each source point on the transducer mask as shown in Equation (3.2):

$$x(t) = A \sin(2\pi f_0 t) \quad (3.2)$$

where A is the amplitude and f_0 the oscillation frequency. An effect of omitting non linearities is that the magnitude of the pressure field is directly proportional to the initial amplitude, therefore an amplitude of 1 is used in the simulation. The sensor has been defined as the entire simulation domain for the tFUS simulations; as the total required memory for all the simulations would only be 672 Mb. However, as the spatial resolution of the μ FUS is higher (and therefore also the memory usage as well), a smaller sensor mask was defined of dimensions $0.4 \cdot N_x \times 0.4 \cdot N_y$. The time step used during the simulations is defined by Equation (3.3).

$$\Delta t = \frac{CFL \Delta x}{c_{max}} \quad (3.3)$$

where CFL is the Courant-Friedrichs Lewy number, which is defined as the ratio of the distance a wave traverses in a single time step to the spacing of the grid ($CFL \equiv c_0 \Delta t / \Delta x$), Δx is the grid spacing and c_{max} is the maximum speed of sound in the domain. The CFL is a useful non dimensional parameter that is related to temporal stability. This parameter is kept at a default value of 0.3, which gives a good compromise between accuracy and computational efficiency [78]. This time step was adapted in such way that the period of the pressure field at the focal spot is an integer multiple of the time step of the simulation. This allows for a single period of the pressure field data to be stored and repeated.

These inputs are the fed into the `kspaceFirstOrder2D` function of `kWave`. The simulations were run and stored on the supercomputer of TU Delft, DelftBlue [79].

3.1.4. Geometric Transformations

Once the dataset has been generated, the individual fields need to be superposed such that a combined field can be generated and analysed. A function has been defined in MATLAB, which takes the data of the μ FUS and tFUS source as well as the combined parameters θ , p_{frac} and r .

To increase the computation speed and reduce the memory usage, an area of 2 by 2 cm^2 centred around the focal point is selected from both fields. For the tFUS source, the selected square is shifted by r from the centre. This reflects the change in radial distance of the tFUS source. The spatial resolution of both fields is matched by interpolating the tFUS data using the Image Processing Toolbox function `imresize3` using nearest-neighbour interpolation. This interpolation is the most accurate for spatial interpolation as it retains the integrity of the original pressure field while changing the resolution. In order to introduce the crossing angle θ to the field, the tFUS matrix is rotated using the `imrotate3` function using nearest-neighbour interpolation as well. After rescaling the matrices, the temporal resolution needs to be matched and the fields need to be synchronised. When looking at the oscillating pressure value at a single point in the pressure field, the superposition of the two original signals is seen. If the root mean square value of the combined field needs to be computed, the common period needs to be determined as well. As the two original signals are simple sinusoids and thus, periodic, the common period is computed by finding the least common multiple. The two individual fields are repeated until the common period is reached. Finally, the temporal resolution of the two fields is matched by again applying `imresize3` using cubic interpolation. The two signals are combined after scaling, with the μ FUS field multiplied by p_{frac} and the tFUS field by $1 - p_{frac}$.

After the combined pressure field is generated, the metrics of interest are computed. The root mean square pressure field is computed using the built in `rms` function in the time dimension over one period. The focal area is computed by taking all the grid points having a pressure value such that $p > 0.71 \cdot p_{max}$ [44].

3.2. Optimisation

After generating and analysing the fields, it is of interest to find the optimal parameter combination to maximise a defined figure of merit. To do so, an optimisation process is setup. In this project, two

optimisation procedures are defined and used. This enables a comparison of results between different optimisation methods. Thus, if the outcome of both methods leads to the same results, these can be considered as more robust. The two optimisation methods will be referred to as global optimisation and individual optimisation.

3.2.1. Global optimisation

Global optimisation consists in finding the maximum of a function on a given domain. In contrast to local optimisation, global optimisation seeks to find the set of parameters that lead to the greatest value over the entire domain and not remain stuck in a localised optimum. An optimisation process is often stated as a minimisation problem, for the sake of clarity the objective function is defined for maximisation. This does not affect the outcome, as maximising this function is equal to minimising its inverse.

First of all, the function for which the maximum needs to be found, or the objective function, has to be defined. To do so, a figure of merit is chosen and given in Equation (3.4):

$$FOM = \frac{(1 - p_{frac}) \cdot p_{max_{tot}} \cdot p_{max_{\mu FUS}} \cdot FL_{\mu FUS}}{L_{\mu FUS} \cdot \sqrt{A_p}} \quad (3.4)$$

where $p_{max_{tot}}$ is the maximum pressure value of the combined field, $FL_{\mu FUS}$ is the focal length of the μFUS transducer, $p_{max_{\mu FUS}}$ is the maximum pressure value of the field generated by the μFUS source only, $L_{\mu FUS}$ is the aperture of the μFUS source and A_p is the focal area of the combined field.

Looking back at the goal of the project, there are two main objectives to work towards:

1. Maximising the resolution of the focal area
2. Maximising the power efficiency of the μFUS source

Maximising the resolution of the focal area results in minimising focal area itself. Therefore the term $\sqrt{A_p}$ is included in the denominator. A term related to the power efficiency of the μFUS transducer based on the available dependent variables is given by $\frac{p_{max_{\mu FUS}}}{L_{\mu FUS}}$. This has been adapted from the FoM derived by Ilham, Kashani, and Kiani [80] for US phased arrays. As k-Wave models the transducer as single pressure sources based on the grid size, the aperture and the initial pressure, increasing the aperture would lead to an increase in input power. Furthermore, as the square of the maximum pressure generated by a US source is proportional to the input power, this term ensures that the total input power remains constant for different sets of parameters.

Another term that has to be maximised is the maximum pressure delivered by the combined transducers, and is therefore included in the nominator as $p_{max_{tot}}$. The ability to reach target deep within the brain is another challenge that needs to be designed for. As the minimum distance between the source and the focal spot is dictated by the μFUS source, its focal length is also added to the numerator as $FL_{\mu FUS}$. Finally, the contribution factor is added to the nominator as $(1 - p_{frac})$ such that the function does not go towards infinity in the case where $p_{frac} = 0$.

This function takes as input all the individual and combined parameters as defined earlier; and has the form:

$$f(f_{0_{\mu FUS}}, f_{0_{tFUS}}, L_{\mu FUS}, L_{tFUS}, r, p_{frac}, \theta) = FOM \quad (3.5)$$

Looking at the input variables, the problem at stake is a mixed-integer optimisation problem. There are a number of mixed-integer optimisation algorithms that have been developed based different fundamental working mechanisms (deterministic, heuristic). In this case, Genetic Algorithm Optimisation, an evolutionary population based algorithm, has been chosen. This type of algorithm can handle integers naturally, it explores many solutions simultaneously which helps to avoid local optima and it doesn't rely on derivatives of the objective function. The latter is an important factor as the function used includes several cumbersome geometric transformations. A schematic representation of the working principles of such algorithm is shown in Figure 3.4.

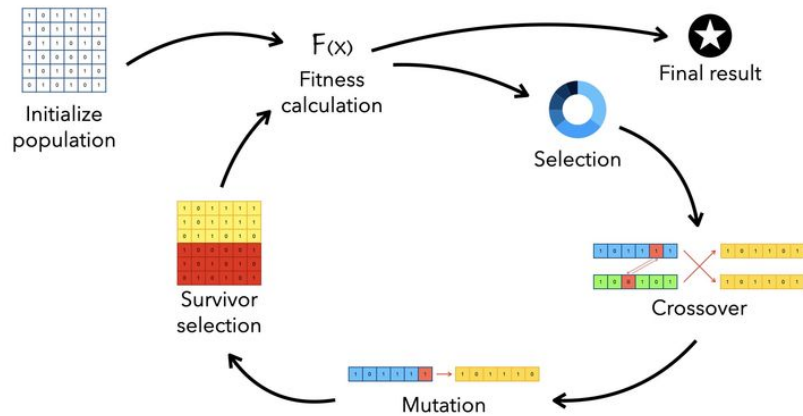


Figure 3.4: Working principle of a Genetic Algorithm

This stochastic optimisation algorithm can easily be implemented in MATLAB. Genetic algorithms (GA) work by generating a random initial population (where a "population" represents a group of individuals, each having a set of input variables) and computes the fitness values of each member of this population. Based on these scores, the algorithm selects a subset of individuals, called "parents", that will carry their genome to the subsequent generation. A smaller section of this subset will remain unchanged in the subsequent generation, this group is called "elite". The rest of the "parents" undergo either "mutation" or "crossover" based on the GA input parameters. The first implies that random changes are made to the members of the parent population, while the other combines the parameters values amongst the selected parents to form a child. This process is repeated until the tolerance defined by the user is met or the maximum number of iterations has been reached. The algorithm then stops and outputs the solution it has converged to.

The GA is tuned by modifying the the values of these parameters. In order to ensure convergence of the algorithm and to optimise the computation time and memory usage, a sensitivity analysis must be performed on these parameters. A range is chosen for the maximum population size, the maximum number of generations and the tolerance as shown in Table 3.3.

Table 3.3: Genetic Algorithm parameters

Parameters	Values
Population size	50, 100, 200
Maximum Generations	50, 100, 200
Tolerance	1e-4, 1e-2
Elite count	$0.05 \times \text{Population size}$

A greater population size allows for a greater search space to be explored. This minimises the risk of remaining stuck in a local minimum which the subsequent generations can hardly escape. However, this requires considerably more computational power and memory usage as the number of candidates at each generation is substantial. On the other hand, having a small population size limits the exploration capabilities of the algorithm, but the efficiency is greatly improved.

The stopping conditions for the algorithm are dictated by the maximum number of generations and/or the tolerance. The first parameter relates to the maximum number of iterations the algorithm will perform. The greater this term is, the more opportunities the algorithm has to generate new individuals and explore in detail the domain it has converged to. But again, this comes to the cost of computational power and longer times. The tolerance defines the maximum allowable relative change in fitness

function over a set number of generations. This allows to define a limit to the precision the algorithm has to reach, avoiding unnecessary computations which do not bring significant improvement to the output. The greater this value, the earlier an optimisation run will stall. Finally, the elite count relates to the number of individuals that will automatically survive to the next generation, without undergoing mutation or crossover. These individuals have the best fitness value.

The functions and options used for the selection, mutation and crossover of the individuals are kept to the default.

3.2.2. Individual optimisation

A second optimisation procedure has been defined to find the best combination of transducers and combined parameters to maximise the objective of this project, which is achieve high resolution and low μ FUS input power. Instead of relying on a global optimisation method that generates solutions using the entire set of available parameters, this method individually select the best transducers based on a FoM specific to its purpose.

- μ FUS Source Selection

As this source will generate higher frequency signals, it will inherently have a higher resolution at the focal spot. Furthermore, it has to be optimised for power efficiency as well. A selection is performed on the μ FUS data set using the following FoM:

$$FoM_{\mu FUS} = \frac{FL_{\mu FUS} \cdot p_{max_{\mu FUS}}}{L_{\mu FUS} \cdot \sqrt{A_{p_{\mu FUS}}}} \quad (3.6)$$

- tFUS Source Selection

As stated earlier, the external source is not limited to the power usage, there for the term $\frac{p_{max_{tFUS}}}{L_{tFUS}}$ is not crucial in this case. This source is expected to deliver power on a greater area such that the μ FUS source can focus on this area to add the necessary change in pressure to generate a high resolution focal spot with higher pressure values (by exploiting this pressure "baseline" provided by the tFUS source). In this case the pressure term $p_{max_{tFUS}}^2$ is squared. In such way a greater weight is given to this parameter as the objective is to provide greater pressure gain with this transducer. The FoM for this transducer is defined as:

$$FoM_{tFUS} = \frac{FL_{tFUS} \cdot p_{max_{tFUS}}^2}{\sqrt{A_{p_{tFUS}}}} \quad (3.7)$$

4

Results

In Chapter 3 the methods used to investigate the effect of combining a set of transducers with independent characteristics were defined. In the following chapter the results of the simulations, the geometric transformations and the optimisation processes are shown. First, the superposition of two pressure fields generated by two transducers, one from the μ FUS data set and the other from the tFUS data set, is analysed in Section 4.1. Then the superposition of the fields that resulted from the GA optimisation will be shown in Section 4.2.

4.1. Field superposition

The first results to analyse are the differences between direct simulations in a two-transducers setup, and the geometric transformations (i.e. superposition of individual fields) defined in the previous section. A comparison between the maximum pressure values and the size of the focal spots for the two methods is shown in Figure 4.1. The frequencies of the transducers used in the simulation are 750 kHz and 2 MHz for the tFUS and the μ FUS source respectively. The difference in pressure values remain close to 0 in the area in close proximity of the focal area. The highest value reaches 7% and is located further from the focal spot (i.e. the centre grid).

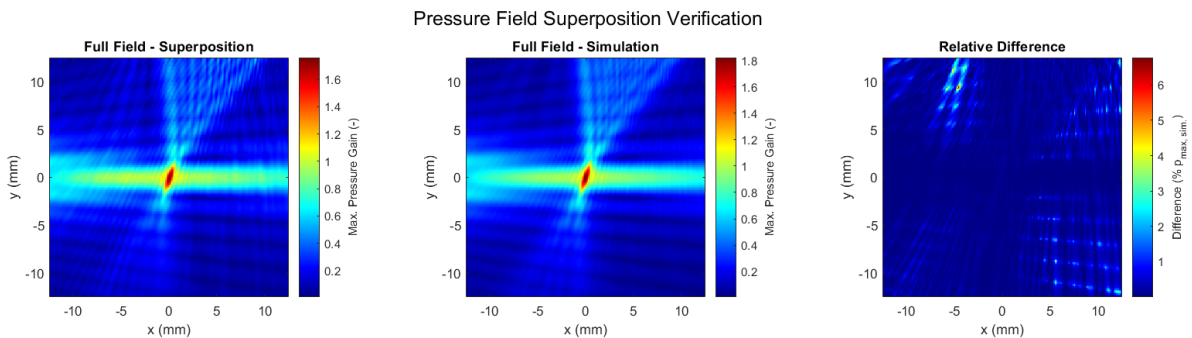
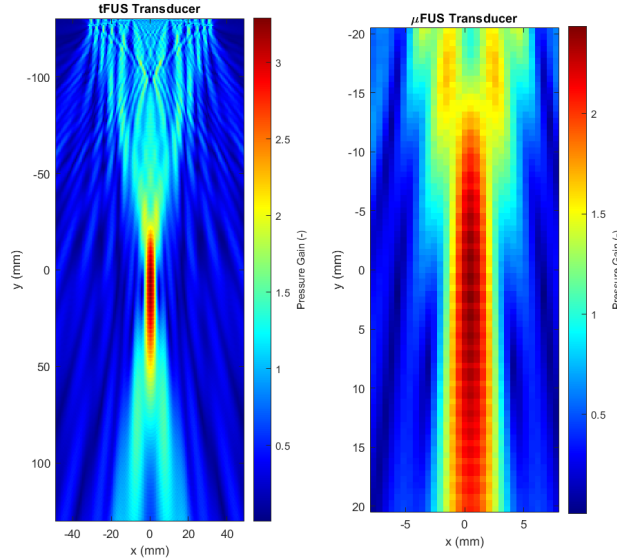


Figure 4.1: Comparison of maximum pressure values and focal spot size

In order to better understand the interaction between the fields and the effect of changing the combined parameters on the figure of merit derived in Section 3.2, two transducers (from the two different sets) having comparable focal areas have been selected for analysis. This choice was made in order to avoid dominance on the results from one of the transducers in such way to have a better visualisation of wave interference. The parameters of each transducer is shown in Table 4.1 and a plot of the pressure field they generate is shown in Figure 4.2.

Table 4.1: Parameters of the selected transducers

Transducer	Frequency (kHz)	Aperture (m)	Focal Length (m)
μ FUS	1e3	2.5e-2	5e-2
tFUS	750	6.5e-2	13e-2

**Figure 4.2:** Maximum pressure field of the tFUS (left) and μ FUS (right) transducer fields in k-Wave

The fields are then superposed and the figure of merit as well as the focal area are plotted as a 3D figure with the crossing angle θ on the x-axis and the contribution factor p_{frac} on the y-axis as shown in Figure 4.3. The radial margin is fixed to $r = 0$ (m). In Figure 4.3a, there are two regions of maximum FoM centred around $\theta = (2n + 1) \cdot \frac{\pi}{2}$ (rad) and $p_{frac} \simeq 0.57$. The FoM parabolically reaches 0 as the p_{frac} reaches 1 or 0. In Figure 4.3b, as the contribution takes the maximum/minimum value, the focal area remains constant for varying θ . The minimum focal area is reached at values of $p_{frac} = 0.57$. For both plots in Figure 4.3, there is an abrupt change in value at $\theta = \pi$. The other parameter to be taken into account is the radial margin. This factor was introduced to fine tune the location of the tFUS transducer such that the FoM is maximised. When looking at Figure 4.4, the optimal value for r is close to zero. The focal area reaches a maximum for $\theta = \pi$ and minimum r values ($r = 0.05$ (m)). This metric is minimised for $\theta = (2n + 1) \cdot \frac{\pi}{2}$ (rad). The maximum pressure gain experienced in the superposed pressure field is shown in Figure 4.5. This metric changes parabolically with r , reaching a maximum value around $r = 0$ (m). Changing the crossing angle has little influence on the gain.

An interesting aspect to analyse is the pressure and intensity fluctuations at the focal spot (ie. the centre grid) of the combined field and compare these results to the fields generated by the individual transducers. The differences between the individual setups are presented in Figure 4.6a and Figure 4.6b. In Figure 4.6a, the continuous tendencies of the original sine-waves interfere to create a periodic but pulsed pressure field. The maximum pressure gain value reaches 1.5 for the tFUS signal, 1.3 for the μ FUS signal and 2.7 for the combined field. This represents a 2 fold increase in pressure gain at the focal spot with respect to the μ FUS source. The pulsating tendency is even more apparent when looking at the intensity gain values in Figure 4.6b. As $I \propto p^2$ (Equation (2.14)), the difference in intensity values is more significant between the setups. The maximum intensity gain value for the tFUS field reaches 2.2, for the μ FUS field 1.7, and for the combined field there is a 2.3 fold increase compared to the maximum value of the individual fields, reaching a value of 7.3 .

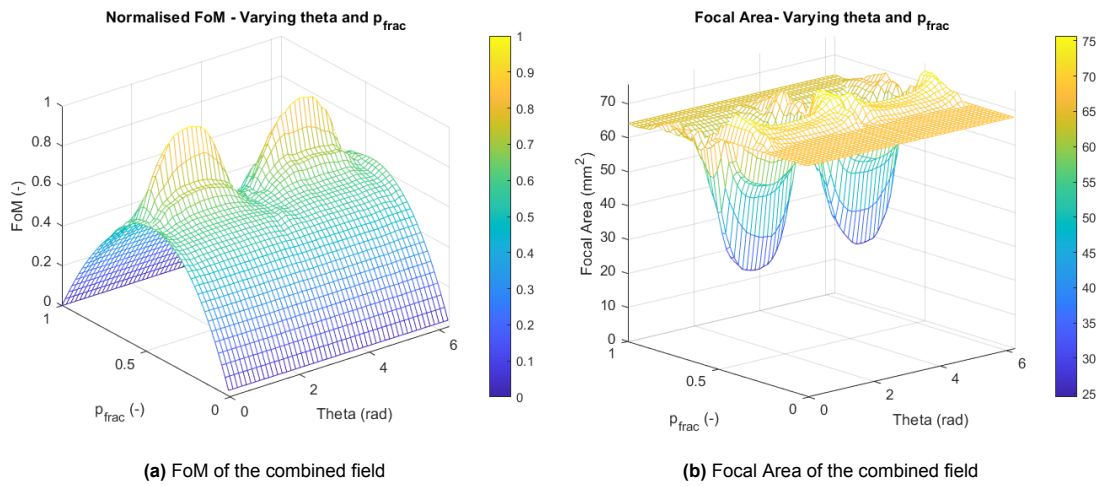


Figure 4.3: FoM and Focal Area as a function of p_{frac} and θ

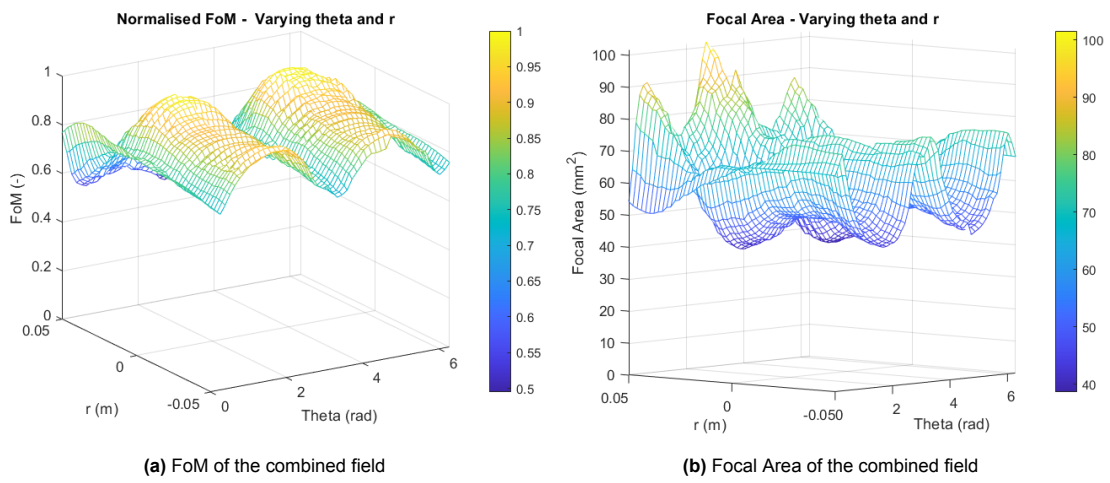


Figure 4.4: FoM and Focal Area as a function of r and θ

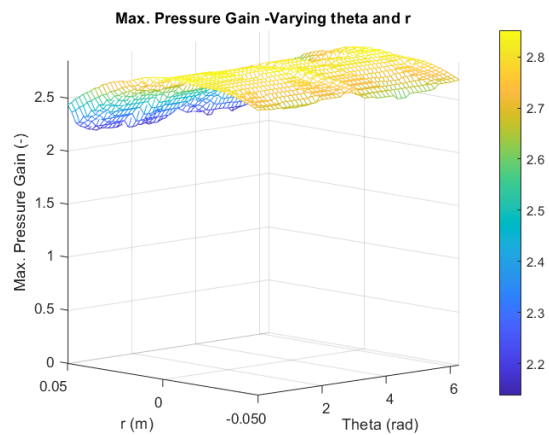


Figure 4.5: Maximum pressure gain of the combined field

In order to understand the influence of the transducer independent variables, 3D column charts are created with f_0 (frequency) and L (aperture) on the x- and y- axis respectively. In both plots Figure 4.7 and Figure 4.9, the one of the two transducers is fixed, while the independent variables of the other are

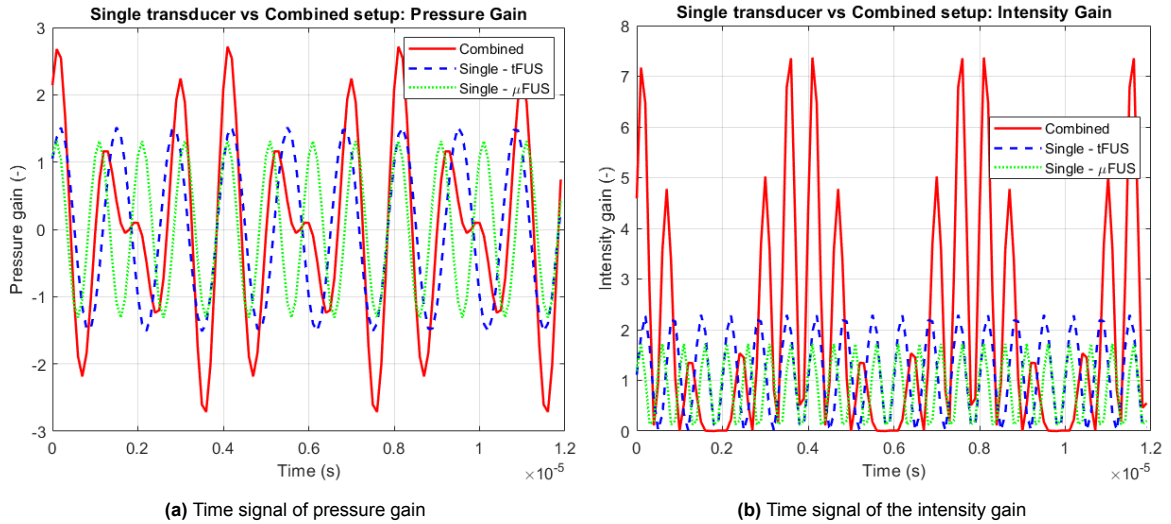


Figure 4.6: Pressure and intensity gain over time at the focal spot for the combined and the individual transducers

changed. For both cases, increasing the frequency and the aperture leads to an overall decrease of the focal area (Figures 4.7b and 4.9b). When varying the μ FUS parameters, the differences in focal area are more significant at the lowest frequency (1 MHz). In this case decreasing the aperture size increases the focal area. The changes in focal area are still noticeable as the μ FUS source frequency increases, but the effect of changing aperture becomes less apparent at high frequencies. The minimum focal area ($A = 2.3 \text{ mm}^2$) is reached at a μ FUS aperture of 35 mm and a frequency of 750 kHz. The inverse trend is seen in the normalised FoM plots. The FoM for both cases (Figures 4.7a and 4.8a) shows an increase in FoM with increasing aperture and frequency. In Figure 4.7a the maximum value is reached when $L_{tFUS} = 55 \text{ mm}$ and $f_{tFUS} = 0.75 \text{ MHz}$, while in Figure 4.8a, the maximum is reached at the highest frequency and aperture values. The term related to the power efficiency of the μ FUS transducer given by $\frac{P_{max}}{L}$ (see Section 3.2) is plotted in Figure 4.9a. It shows that decreasing the aperture and increasing the frequency decreases this power term of the transducer. The optimal value is found at highest frequency ($f_{\mu FUS} = 6 \text{ MHz}$) and the smallest aperture ($L_{\mu FUS} = 10 \text{ mm}$).

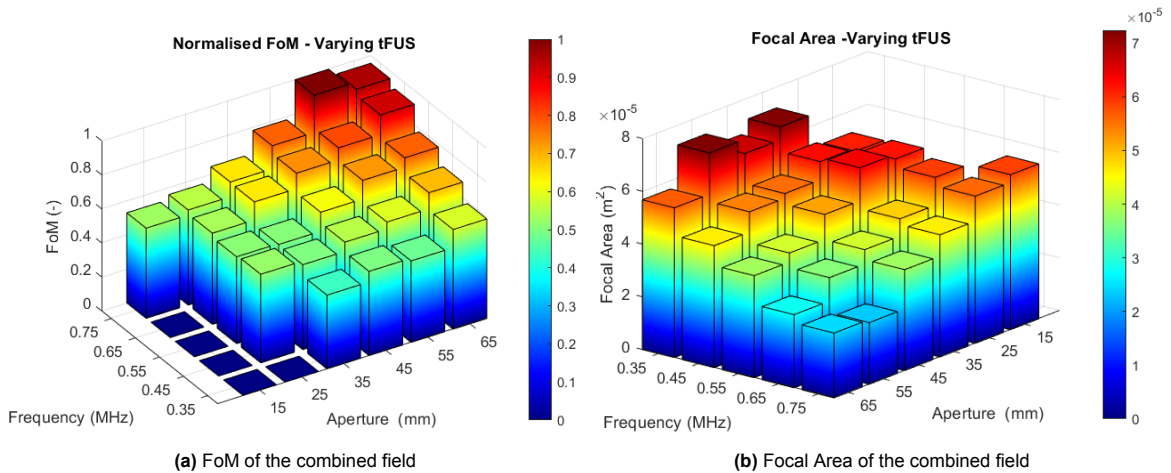


Figure 4.7: FoM and Focal Area as a function of frequency and aperture for varying tFUS parameters

4.2. Optimisation

After running the genetic algorithm, the individual parameters and the combined parameters that give the optimal FoM values are gathered. The transducer independent variables coincided with the values gathered from the second optimisation method. Therefore only one set of transducers is shown in this

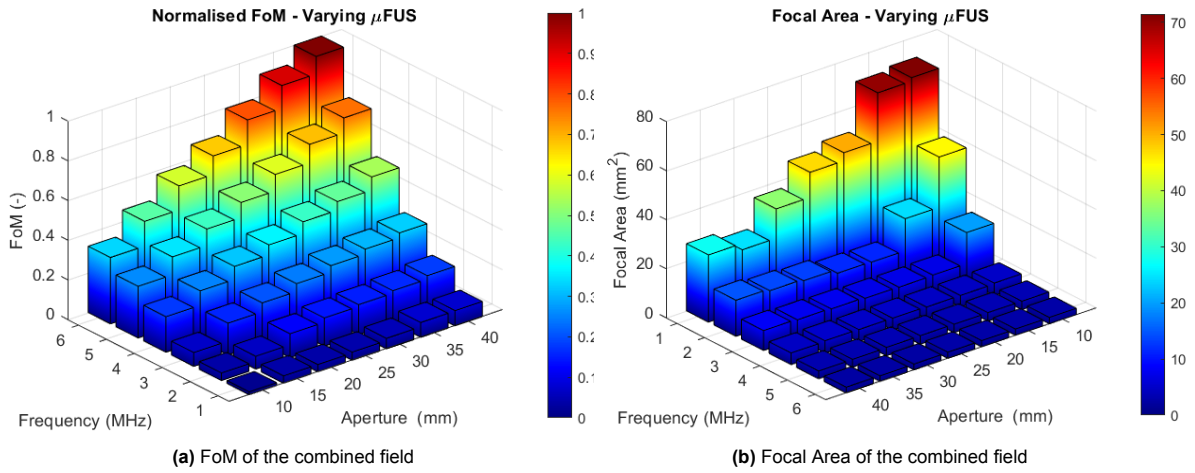


Figure 4.8: FoM and Focal Area as a function of frequency and aperture for varying μ FUS parameters

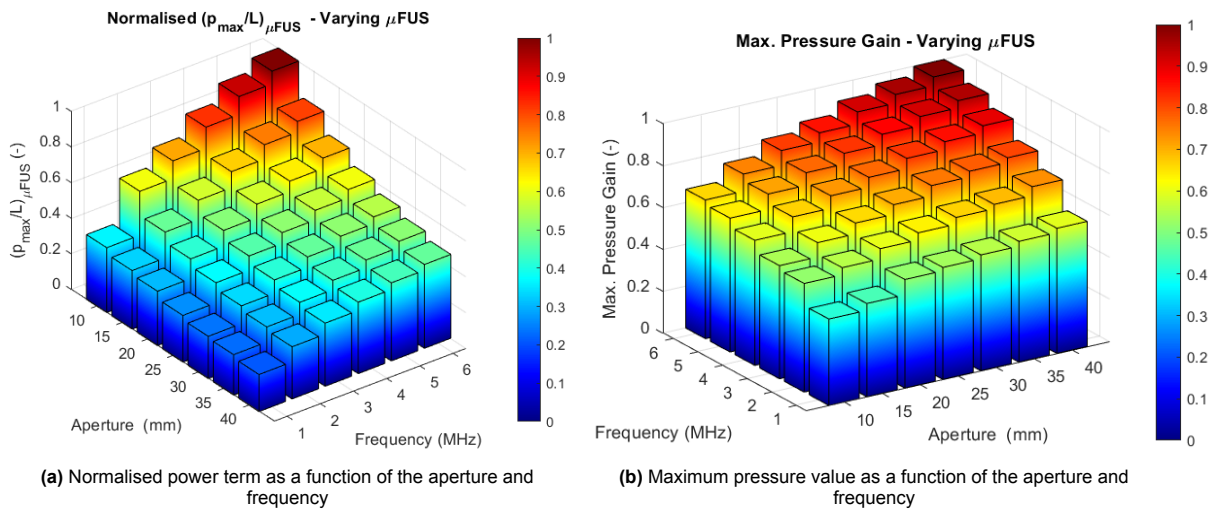


Figure 4.9: Power term and maximum pressure gain for varying μ FUS parameters

section. The parameters values are shown in Table 4.2 and Table 4.3. A sensibility analysis on those values has been performed by generating results for the different parameters shown in Table 3.3. The results and plots in Appendix B show that the same results are found for different sets of GA parameters. A plot of the individual pressure fields generated by the two transducers is shown in Figure 4.10, using the maximum pressure field (ie. the field showing the maximum pressure value registered at each grid point).

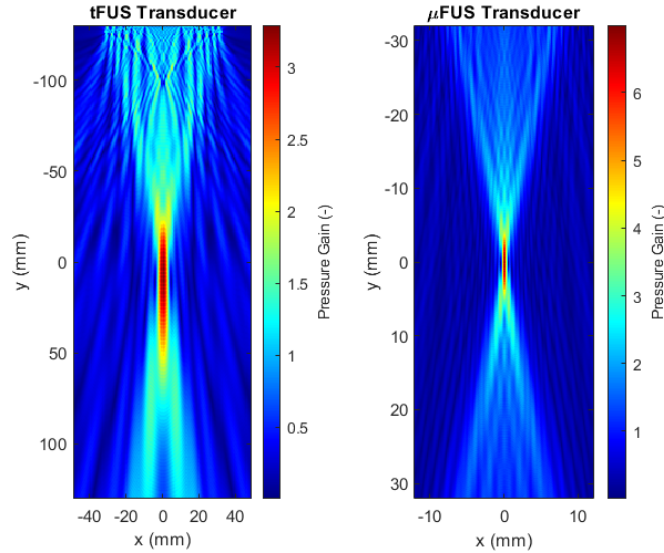
Table 4.2: Parameters of the optimised transducers

Transducer	Frequency (kHz)	Aperture (m)	Focal Length (m)
μ FUS	6e3	4e-2	8e-2
tFUS	750	6.5e-2	13e-2

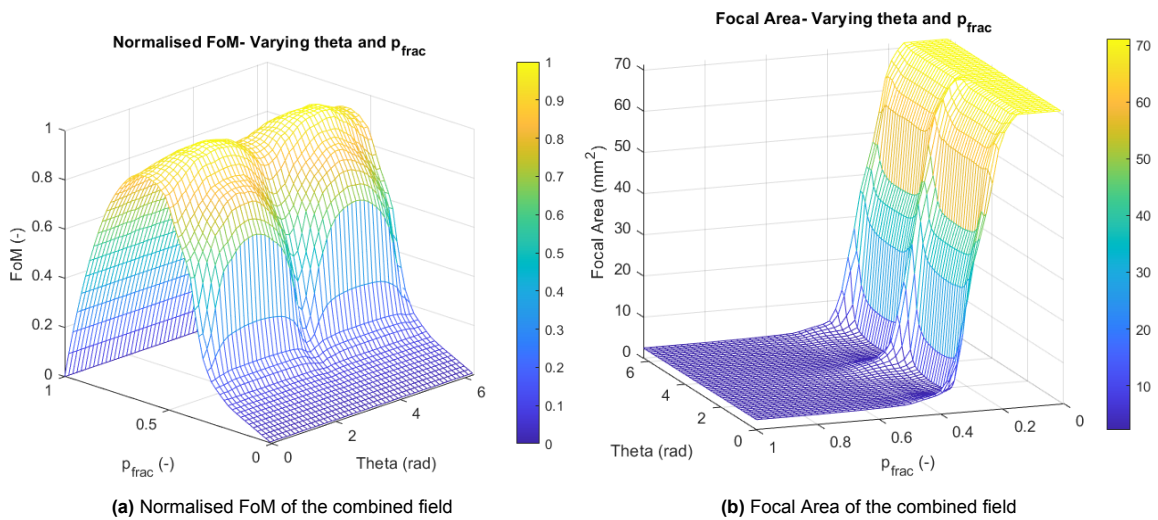
After superposing these two fields, the FoM and the size of the resulting focal area are computed. The results are shown in Figure 4.11 and Figure 4.13. Figure 4.11a shows the FoM as a function of p_{frac} and θ in Figure 4.11a. There is symmetry about the x, z plane at $\theta \simeq \pi$ (rad) and the maximum value lays around $p_{frac} \simeq 0.6$. When considering the focal area of the combined fields, two distinct regions emerge. For values of $0.4 \leq p_{frac} \leq 1$, the focal area remains constant at $2.5mm^2$. For values of

Table 4.3: Combined parameters of the optimised transducers

Parameters	p_{frac} (-)	θ (deg)	r (m)
Values	6.12e-01	106.8	4.96e-03

**Figure 4.10:** Maximum pressure field of the optimal tFUS (left) and μ FUS (right) transducer fields in k-Wave

this contribution factor in the range $0 \leq p_{frac} \leq 0.13$, the focal area remains relatively constant at $71.11mm^2$. In the region between these two, a sudden transition emerges. The influence of changing the crossing angle is visible in this transition zone where $0.13 \leq p_{frac} \leq 0.4$. Plotting the normalised values of $1/\sqrt{A}$ in Figure 4.12 shows that there is a minimum at $p_{frac} = 0.51$ and $\theta \simeq 1.4$ (rad) where the focal area reaches $2.24mm^2$. The minimum values of the focal area are found at $\theta = (2n + 1) \cdot \frac{\pi}{2}$ and the maximum values at $\theta = n \cdot \pi$. The effect of varying the radial margin on the FoM and the focal area is shown in Figure 4.13. The value of p_{frac} for these plots is kept at 6.12e-01. The minimum focal area and maximum FoM values are found at $\theta = (2n + 1) \cdot \frac{\pi}{2}$. The focal area and FoM remain within the 95% of the optimal value when $\theta = (2n + 1) \cdot \frac{\pi}{2} \pm 0.35$ (rad) and $r \leq 0.01$ (m).

**(a)** Normalised FoM of the combined field**(b)** Focal Area of the combined field**Figure 4.11:** FoM and Focal Area of the combined optimal field as a function of θ and p_{frac}

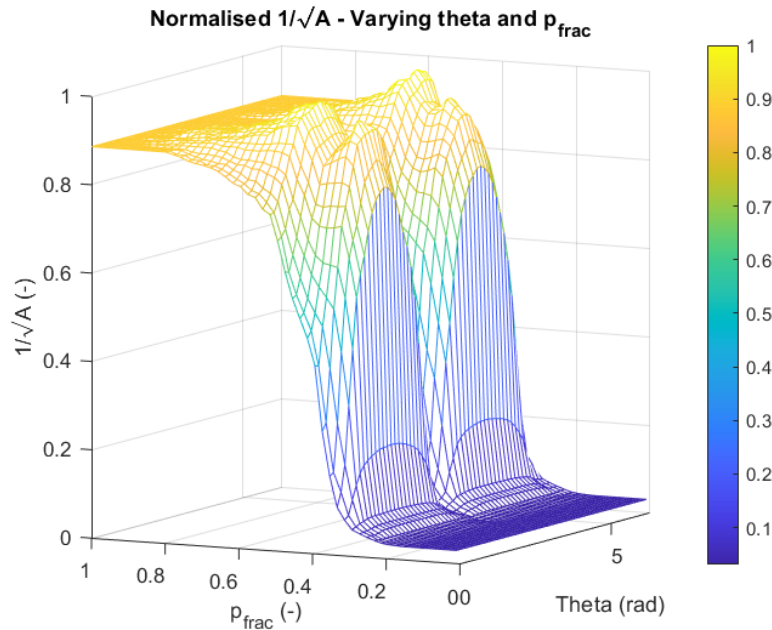


Figure 4.12: 3D plot of $\frac{1}{\sqrt{A}}$ as a function of p_{frac} and θ , where A is the p_{rms} focal area,

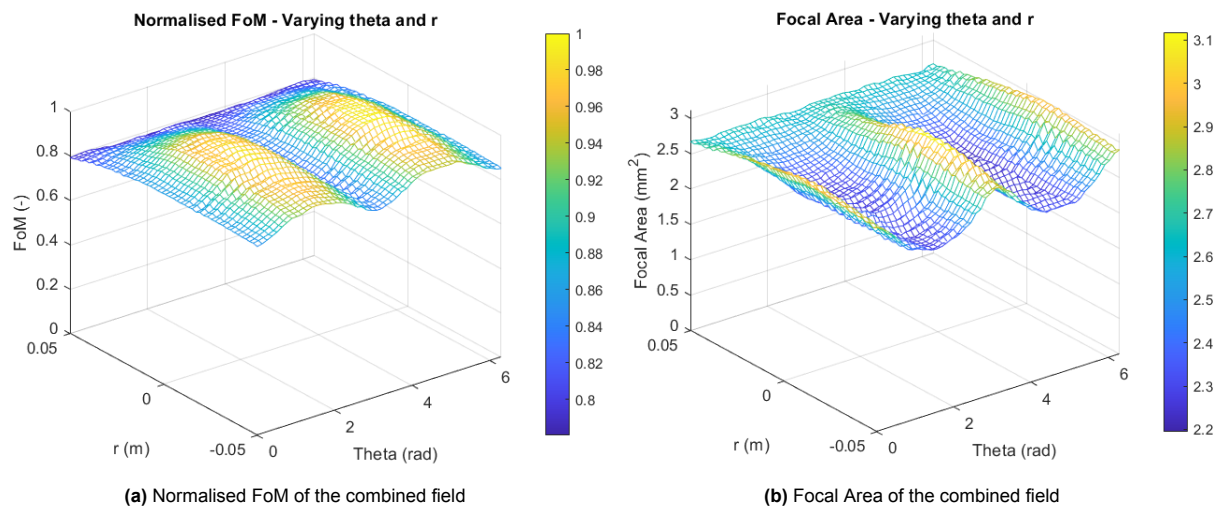


Figure 4.13: FoM and Focal Area as a function of r and θ for the optimised transducers

The pressure and intensity gain values over time at the focal spot are shown in Figure 4.14a and Figure 4.14b respectively. The same temporal tendencies as for the previous setup (Figure 4.6a and Figure 4.6b) can be seen. The pressure gain values for the μ FUS transducer oscillate between ± 4.2 , for the tFUS transducer this value is ± 1.2 . When combining the transducers, the maximum pressure gain reaches 5.4 which is a 28.5% increase compared to the single μ FUS setup. The intensity gain of the individual μ FUS field oscillates and reaches a maximum of 18.2, while the tFUS intensity reaches a maximum gain of 1.4. The combined field intensity value oscillates and reaches a maximum at 29.6. This is more than 60% increase compared to the individual (μ FUS) maximum intensity gain value.

The effect of varying the frequency and the aperture of the two transducers individually is plotted in the following box-plots. When varying the tFUS parameters, the focal area decreases as the aperture and the frequency increase as is shown in Figure 4.15b. The maximum pressure gain reaches is maximised as the aperture and the frequency of the tFUS source are maximised as well, as is shown in Figure 4.15a. There is a 20% increase in maximum pressure between the lowest and the optimal

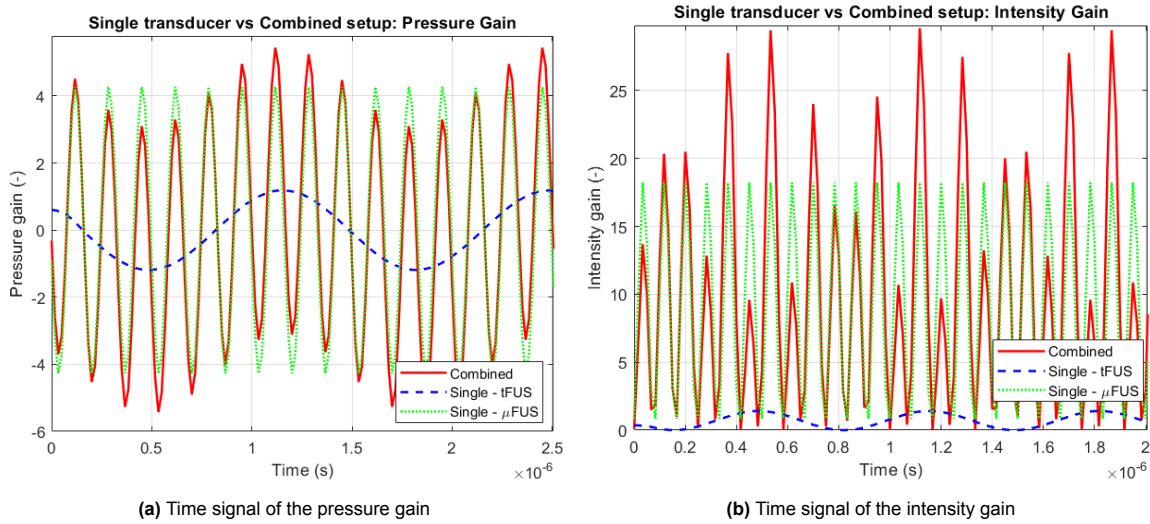


Figure 4.14: Comparison of the pressure and intensity gain at the focal spot for the combined and the individual optimal setup

value. The FoM follows these same tendencies as shown in Figure 4.16. The same results are plotted for varying μ FUS parameters. The maximum RMS pressure gain reaches a maximum as the aperture and the frequency of the μ FUS source are maximised (Figure 4.17a). The power term, defined by $p_{max_{\mu FUS}}/L_{\mu FUS}$, is plotted in Figure 4.17b. This value tends to increase with increasing frequency and is inversely proportional to the aperture. The maximum value is found at the smallest aperture ($L_{\mu FUS} = 10$ mm) and the highest frequency ($f_{\mu FUS} = 6$ MHz). As shown in Figure 4.18b, at low frequencies ($f_{\mu FUS} = 1$ -3 MHz) the focal area increases as the frequency and the aperture decrease, reaching a maximum at $f_{\mu FUS} = 1$ MHz and $L_{\mu FUS} = 10$ mm. At higher frequencies, the changes in focal area become less apparent as the aperture changes, but still decreases as the frequency increases Figure 4.18b. The FoM increases with increasing μ FUS source frequency and aperture as shown in Figure 4.18a. A zoomed version of the plots is given in Appendix A.

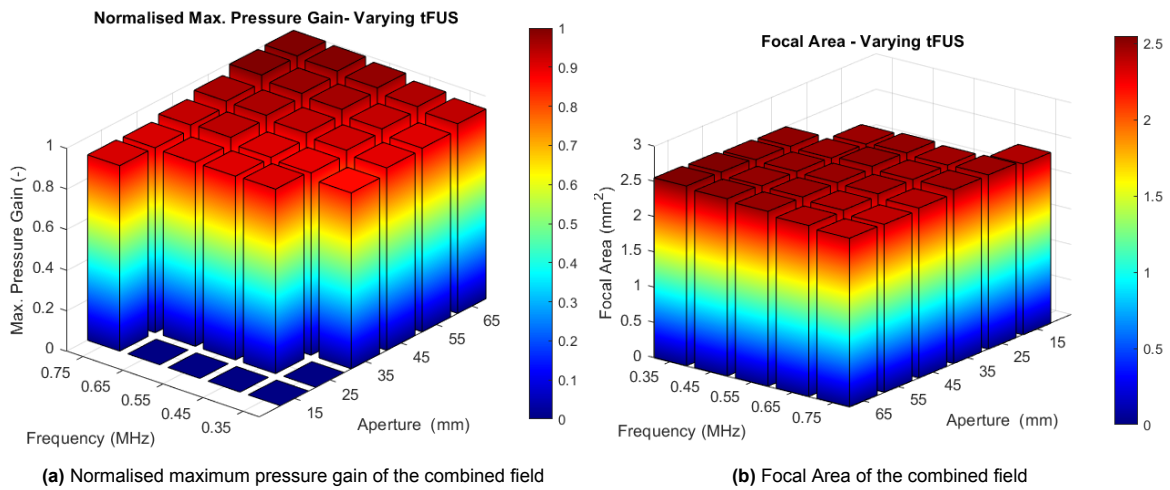


Figure 4.15: FoM and Focal Area as a function of frequency and aperture for varying tFUS parameters

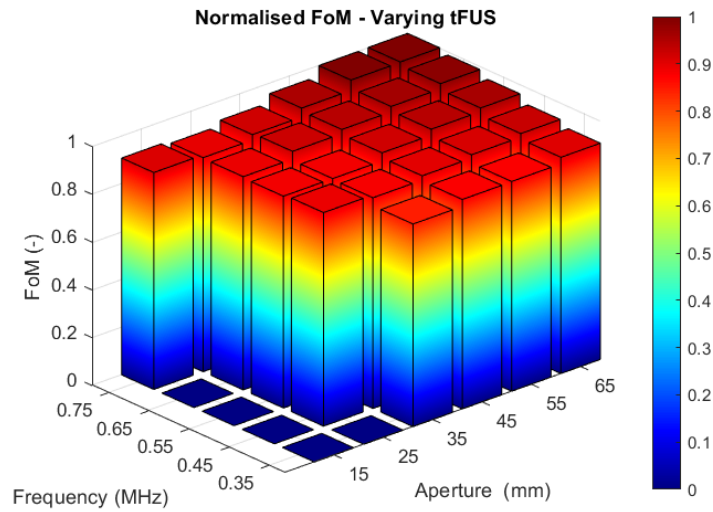
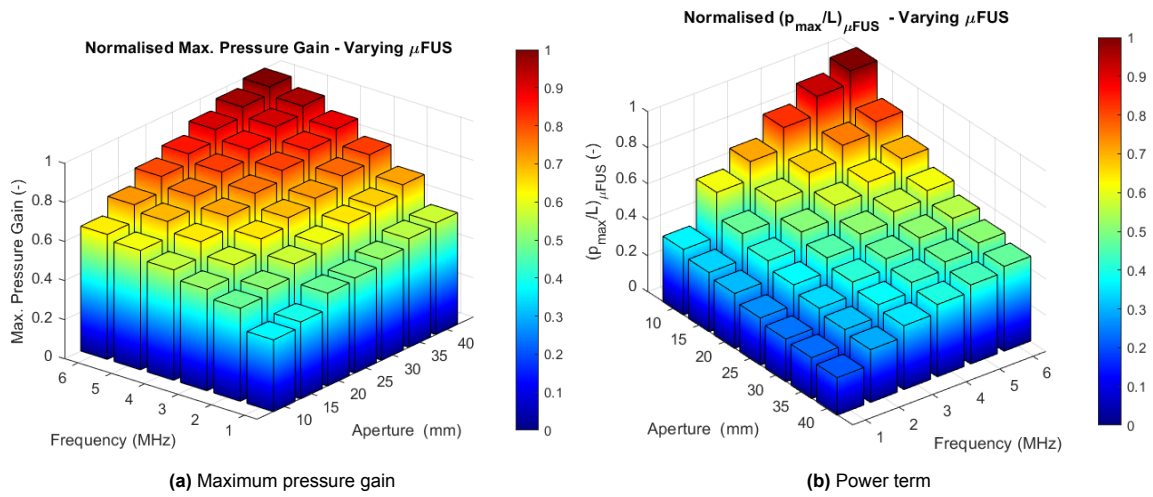


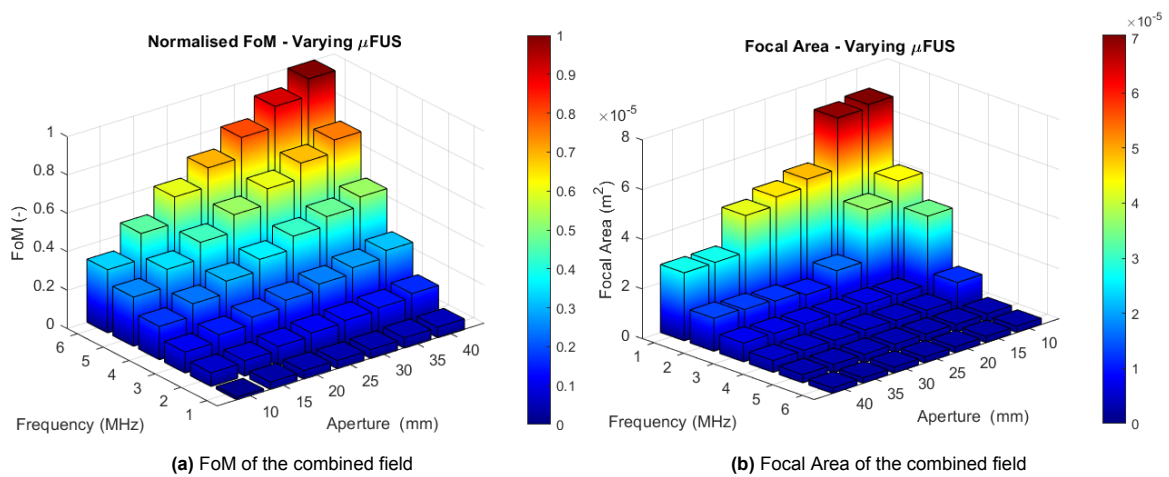
Figure 4.16: FoM of the combined field



(a) Maximum pressure gain

(b) Power term

Figure 4.17: Max. Pressure gain and Normalised Power term as a function of frequency and aperture for varying μ FUS parameters



(a) FoM of the combined field

(b) Focal Area of the combined field

Figure 4.18: FoM and Focal Area as a function of frequency and aperture for varying μ FUS parameters

5

Discussion and Future Recommendations

The objective of this study was to investigate to which extent combining two ultrasound sources with different fundamental parameters affects the metrics of interest when considering focused ultrasound neuromodulation. In order to compare the results and allow for an optimisation method to be implemented, a figure of merit was created by merging the focal area, power consumption of the implanted transducer, the maximum pressure delivered at the focal spot and the focal length. During this research project, a dataset of pressure fields was generated using a linear ultrasound simulation model for two single element curved transducers having different apertures, fundamental frequencies and f-numbers. After performing geometric transformations on the 2D time varying pressure field matrices, different dual transducer setups involving different contribution factors and relative positions were evaluated for the metrics of interest and the figure of merit. Two optimisation methods were proposed to find the transducers combination which would maximise the figure of merit.

5.1. Field superposition

The field superposition method implemented in this project has allowed for significant reduction in computation time. The amount of simulations performed was 360 (210 for the μ FUS and 150 for the tFUS), compared to the 31500 needed for a single set of combined parameters. The results of the superposition and geometric transformations have been verified and showed negligible differences in results (Figure 4.1). The linear simulation domain, the relatively low frequencies and the homogeneous medium allow is a benefit for using this method.

In Section 4.1, the superposition of two transducers having comparable individual focal spots shows that the figure of merit is maximised at values of $\theta \simeq (2n + 1) \cdot \frac{\pi}{2}$ rad and $p_{frac} \simeq 0.5$. When considering the size of the focal area for these values of θ and p_{frac} , as shown in Figure 4.3b, this metric is minimised. These results are consistent with other studies investigating crossed beam interactions [61, 81, 82]. A value of p_{frac} close to 50% means that the two sources need to evenly contribute to the final pressure field in order to minimise the focal area and optimise the figure of merit. If these crossing conditions are met, the size of the focal area decreases by more than 50%. In this study, the term relating to the power consumption of the implantable transducer is given by $\frac{P_{max\mu FUS}}{L_{\mu FUS}}$. Therefore the nominator (the maximum pressure value) is the only factor affecting the power consumption of the μ FUS transducer, which is proportional to p_{frac} . A lower value of p_{frac} relates to a lower power delivered by the μ FUS source. A lower value of p_{frac} is therefore favourable. Given the FoM used, the power delivered by this source can be reduced by 50% when $\theta \simeq (2n + 1) \cdot \pi/2$ rad and $p_{frac} \simeq 0.5$.

As the radial margin changes, the optimum r value is found to be close to 0. This shows that the predicted focal spot does coincide with the centre grid, and that this condition is preferred for a dual transducer setup. This allows for the areas of maximum pressure to superpose efficiently, leading to

a decreased focal area (Figure 4.4b) and hence a higher FoM (Figure 4.5). This condition is also preferred when considering the maximum pressure gain, as shown in Figure 4.3a. Since the frequencies of the two transducers are relatively similar (750 kHz and 1 MHz), their time signal interference creates pulsing patterns that can enhance pressure levels at the focal point. This naturally occurring interference pulse can be leveraged for neuromodulation, where pulsating sonication patterns are commonly used to ensure both safety and efficacy in therapeutic applications (see Section 2.4.2). When the fields interfere constructively, there is a 2 fold increase in pressure gain, and 2.3 fold increase in the maximum intensity gain value at the focal spot. A substantial intensity increase can be generated when combining these two sources which is beneficial for ultrasound neuromodulation as a greater amount of energy can be delivered to the target.

Finally, changing the frequency and the aperture of the individual transducers has an important effect on the metrics of interest as shown by the box-plots in Figure 4.7, Figure 4.9 and Figure 4.9a. Overall, increasing the aperture of the tFUS transducer leads to a smaller focal area. This is a result of relative contribution of the transducers to the pressure field (see Appendix C). As the magnitude of the pressure field delivered by the tFUS transducer increases, the pressure gain delivered by the two fields reach similar levels which in turn affects the focal area. The pressure delivered by the two sources has to be in the same range of values to see a beneficial effect (a reduction) on the focal area of the combined field. Increasing the frequency of the tFUS transducer leads to a smaller focal area of the individual field. This reduces the focal area of the combined field as well.

Changing the μ FUS parameters has a greater impact on the focal area, compared to changing the tFUS parameters. This is reflected by the greater change in normalised FoM (Figure 4.8a) and focal area values (Figure 4.9b). The overall effect of changing the μ FUS parameters is similar to those of changing the tFUS parameters. When plotting the term $\frac{p_{max\mu FUS}}{L_{\mu FUS}}$ for varying aperture and frequency, the optimal value is reached at the highest frequency (6 MHz) and the smallest aperture (10 mm). As the aperture is increased, more input power is needed to drive the active element. As the frequency is increased, the gain increases (as shown by Equation (2.23)) and therefore $p_{max\mu FUS}$ increases as-well.

5.2. Optimisation

When running the genetic algorithm using the FoM defined in Section 3.2 as objective function, the same output is generated for different tuning parameters (see Appendix B). The output of the GA is stable for the types of transducers needed to maximise the FoM. The combined parameters θ and r vary slightly, however. The small discrepancies in θ can be related to the symmetry about $\theta = (2n+1) \cdot \frac{\pi}{2}$ (rad) (see Figure 4.3b). As the interference pattern is complex and greatly depends on the coordinates and orientation of the sources, there are different combinations of θ and r that can give competing results. These results show that even GA tuning parameters that minimise the computation cost give similar results compared to the more expensive parameters, while considerably reducing the computation time (2.6 fold decrease in computation time).

The second optimisation method involved the selection of individual transducers based on a FoM specific to each source. The optimal transducers emerging from this selection are identical to those that resulted from the genetic algorithm. This first selection required considerably less resources than the previous approach (a few seconds compared to 10 minutes for the GA). The optimal combined parameters are then found by finding the maximum of the global FoM (which is the one used directly in the GA) against these parameters.

Obtaining identical results from both optimisation methods validates that, for the FoMs defined in this project, selecting two sources based on their individual performance results in a optimal dual source setup.

The focal area of the optimal combined fields (Figure 4.11b) shows two distinct flat regions, each dominated by the individual transducers. For values of $0.4 \leq p_{frac} \leq 1$, the focal area is purely dictated by the focal area of the μ FUS transducer. While for values of $0 \leq p_{frac} \leq 0.13$, the focal area is purely dictated by the focal area of the tFUS transducer. There is no clear overlap zone where the minimum focal area is found as it was the case in Figure 4.3b, and the influence of the crossing angle is only

visible in the transition zone. By plotting $1/\sqrt{A}$, there a small decrease in the focal area at $p_{frac} \simeq 0.6$ (Figure 4.12). The effect of the crossing angle follows the same tendencies as for the non-optimal setup (ie. $\max \theta \simeq (2n + 1) \cdot \pi/2$). These results show that, even if the transducers have very distinct focal area sizes and fundamental frequencies, the combined focal area will still decrease if the contribution factor and the crossing angle are properly selected. Given the FoM used, the acoustic pressure delivered can be reduced by $\simeq 40\%$ when $\theta \simeq (2n + 1) \cdot \pi/2$ rad and , as $p \propto P_{in}^2$, the power input reduces by 76 %.

Changing the radial margin of the tFUS source (Figure 4.13) shows that the optimal r value is close to zero, meaning that the predicted focal spots coincides with the centre grid. The stretch of higher FoM (and lower focal area) values along the negative r values show that the focal length of the tFUS transducer can be increased without significantly affecting the focal area or the FoM. Another interesting aspect of these plots is their oscillatory behaviour (especially the FoM). As the parameters in the FoM calculation are found based on the p_{rms} values, the changes in r and θ reflect these oscillatory patterns.

The temporal changes at the focal spot show other benefits of using a dual frequency setup (Figures 4.14a and 4.14b). The higher frequency pressure signal acts as a carrier for the lower frequency one. The maximum pressure gain and intensity gain are increased by $\simeq 30\%$ and $\simeq 60\%$ respectively. As the frequencies of the two sources are more distinct than in the previous setting, the pattern is less pulsed. This also leads to the pulsing pattern of the combined signal to be mainly dictated by the tFUS transducer frequency.

Changing the frequency and aperture of the tFUS source while keeping the optimal combined parameters (r, θ and p_{frac}) does not greatly affect the size of the focal area, although higher frequencies and greater apertures reduce the size. The size of the focal area is mainly dictated by the μ FUS transducer, therefore changing the parameters of the other transducer has a small effect. The maximum pressure of the combined field however, experiences a maximum increases of 20%. As the aperture of the tFUS transducer is less limiting than the implanted source, increasing this parameter is beneficial for this application.

As the fundamental parameters of the μ FUS source are changed, their effect on the relevant metrics are more significant. Increasing the aperture and the frequency reduces the focal area and increases the maximum pressure gain. The difference in pressure gain becomes more significant as the maximum increase reaches 60%.

5.3. Future Recommendations

The current project can be interpreted as an initial approach to analysing the effects of changing the value of fundamental parameters when combining two ultrasound sources. However, it is recommended to invest in further research to better understand the interference patterns created by the two sources as well, the effects that different media have on wave propagation and how to overcome directivity issues caused by the dual source setup.

First of all, it is recommended to investigate different sets of FoMs. These are highly tunable metrics that depend on the parameters of interest as well as the user defining them. Investigating the effects of different FoMs and/or different weights assigned to them allows for a better understanding of their effects on the outcome.

Secondly, it is recommended to perform the simulations in a 3D domain in order to analyse the focal volume, not only the focal area. The software used in this project (k-Wave) allows for this. Secondly, the results of these simulations should be validate by means of an experiment. One option is by fabricating single element transducers (or phased arrays that have the same beam-forming properties) and measuring the resulting pressure fields in a water tank using a hydrophone [19]. Since the setup involves two transducers, the hydrophone will not be directly facing the sources, which can influence the measured pressure fluctuations due to directionality. To assess this directionality effect, it is recommended to conduct multiple measurement sets with the hydrophone oriented in different directions.

Furthermore, the simulations should be performed using biological medium properties. As biological tissue has different material properties (ie. acoustic impedance) and is heterogeneous, it will greatly affect the sound propagation. The presence of the skull is an important limiting factor to the US wave

propagation coming from the tFUS source [66]. The simulation package used in this project (k-Wave) allows for heterogeneous medium properties to be added to the simulation domain. These can be imported as Hounsfield units, from which the speed of sound is computed during the simulations. There are numerous human CT scan databases online, one of which is the Human Visible Project Human [83] where male and female CT scan data can be retrieved. The data can be processed using Slicer [84] before importing it to k-Wave.

Finally, it is recommended to perform the simulations (and the validation using experiments) using phased arrays instead of single element sources. As the final setup will most probably involve phased arrays, this should be included in the simulation model. Introducing active steering from phased arrays also allows for the focal length of the transducers to be added as a metric to the analysis. The effect of steering can then be quantified and the interference pattern created by two phased array sources can be compared to the single elements setup.

6

Conclusion

As neurological diseases continue to be a major global concern [2], the need for innovative therapeutic approaches and technologies to treat them remains a top priority. Neuromodulation using ultrasound is an innovative modality that shows promising results in both human and clinical trials [11]. The protocols involved in such therapy require bulky apparatus, specialised clinicians and repeated (sometimes lengthy) hospital visits. Researchers are currently investigating on the miniaturisation of this technology to create implantable devices capable of autonomously targetting very precise locations in the CNS. This would allow unpredictable events (ie. epileptic seizures) to be suppressed in real time. However, as the device is expected to be fully implanted, the available power for sonication is limited. Combining these two modalities (transcranial and microscopic FUS) would allow a patient to be monitored by a medical specialist during hospital visits where offline effects can be induced using two sources allowing for high pressure, and precise targetting. At the same time, low pressure online effects (ie. seizure/tremor suppression) can be administered without requiring clinician intervention. It is therefore essential to understand the effect of combining two such sources on the final pressure field, as well as the power efficiency of the implanted transducer.

For this research project, a literature review of current ultrasound neuromodulation technologies was performed. This allowed for a deeper understanding of the physics of ultrasound, the generation and focusing of ultrasound beams as well as the technologies and sonication parameters used in FUS neuromodulation therapy. Simulations using a specialised US software (MATLAB k-Wave) were conducted to create a dataset of pressure fields for different single element transducer parameters (frequency, aperture, f-number). Geometric transformations were performed on these matrices to superpose the pressure fields, allowing for a time efficient and extensive analysis of the effects of changing fundamental parameters on the metrics of interest (focal area, pressure gain, FoM). Two optimisation methods were then proposed to determine the optimal parameters for the transducers, as well as their relative position, based on a figure of merit which accounts for the metrics of interest (small focal area, efficient implantable US source, etc).

Linear analysis through geometric transformations and superposition of pressure field data allows for a computationally efficient analysis of dual-frequency ultrasound transducer setups. The results have also shown that combining two sources can have an important impact on the resulting pressure field, and that both individual transducer parameters and combined parameters greatly influence the results. When combining two sources with comparable focal areas due to their fundamental parameters being relatively similar, the change in focal area (between the individual and the combined setup) becomes significant. The size can decrease up to 50 % when the contribution of the two sources is similar ($p_{frac} \simeq 50\%$) and the crossing angle is such that $\theta \simeq (2n + 1) \cdot \pi/2$. When the fundamental frequencies are close to each-other, a pulsating pattern is generated at the focal spot along with a significant increase in maximum pressure and intensity (2 and 3.4 fold increase, respectively). As the transducers differ in fundamental parameters, the pulsating pattern becomes more continuous and the lower frequency signal acts as a carrier wave for the higher frequency wave. The same values for p_{frac} and θ as stated earlier yield the smallest focal area and highest FoM. Furthermore, it was shown that

two distinct optimisation methods led to the same results. The result from these methods were two transducers having the highest possible frequency and aperture. This leads to the smallest focal area ($2.5 \text{ (mm}^2\text{)}$) and highest maximum pressure at the focal spot. While still allowing for a 40% increase in power efficiency compared to the lowest values, this metric is not fully optimised, as the aperture (and thus the power required) is the largest.

This research shows that there are significant benefits to using dual-frequency transducer setups for focused ultrasound neuromodulation purposes. The focal area, as well as the power consumption of an implantable transducer can greatly be decreased if the right parameters are chosen. Further research into this domain is required to quantify the effect of biological tissue absorption, non-linearities and the impact of using phased arrays instead of single element transducers. Furthermore, these results need to be validated with an experimental setup.

References

- [1] Alfredo Raglio et al. “Effects of music and music therapy on mood in neurological patients”. In: *World journal of psychiatry* 5.1 (Jan. 2015), pp. 68–68. DOI: <https://doi.org/10.5498/wjp.v5.i1.68>. URL: <https://www.ncbi.nlm.nih.gov/pmc/articles/PMC4369551/>.
- [2] Jaimie D Steinmetz et al. “Global, regional, and national burden of disorders affecting the nervous system, 1990–2021: a systematic analysis for the Global Burden of Disease Study 2021”. In: *The Lancet Neurology* 23.4 (2021), pp. 344–381. DOI: [https://doi.org/10.1016/S1474-4422\(24\)00038-3](https://doi.org/10.1016/S1474-4422(24)00038-3). URL: [https://www.thelancet.com/journals/laneur/article/PIIS1474-4422\(24\)00038-3/fulltext](https://www.thelancet.com/journals/laneur/article/PIIS1474-4422(24)00038-3/fulltext).
- [3] Benjamin Davidson et al. “Neuromodulation techniques – From non-invasive brain stimulation to deep brain stimulation”. In: *Neurotherapeutics* 21.3 (Feb. 2024), e00330–e00330. DOI: <https://doi.org/10.1016/j.neurot.2024.e00330>. URL: <https://www.sciencedirect.com/science/article/pii/S1878747924000163>.
- [4] Xiaodong Liu et al. “Review of Noninvasive or Minimally Invasive Deep Brain Stimulation”. In: *Frontiers in Behavioral Neuroscience* 15 (2022). DOI: 10.3389/fnbeh.2021.820017.
- [5] Cyril Atkinson-Clement, Andrea Junor, and Marcus Kaiser. “Neuromodulation perception by the general public”. In: *Scientific Reports* 15.1 (Feb. 2025). DOI: <https://doi.org/10.1038/s41598-025-89437-8>. URL: <https://www.nature.com/articles/s41598-025-89437-8#Sec11>.
- [6] Kyuheon Lee et al. “A review of functional neuromodulation in humans using low-intensity transcranial focused ultrasound”. In: *Biomedical engineering letters* 14.3 (Mar. 2024), pp. 407–438. DOI: <https://doi.org/10.1007/s13534-024-00369-0>. URL: <https://link.springer.com/article/10.1007/s13534-024-00369-0#citeas>.
- [7] Stuart Hameroff et al. “Transcranial Ultrasound (TUS) Effects on Mental States: A Pilot Study”. In: *Brain Stimulation* 6.3 (May 2013), pp. 409–415. DOI: 10.1016/j.brs.2012.05.002.
- [8] Can Sarica et al. “Human Studies of Transcranial Ultrasound neuromodulation: A systematic review of effectiveness and safety”. In: *Brain Stimulation* 15.3 (May 2022), pp. 737–746. DOI: 10.1016/j.brs.2022.05.002.
- [9] Dong Hoon Shin, Seong Son, and Eun Young Kim. “Low-Energy Transcranial Navigation-Guided Focused Ultrasound for Neuropathic Pain: An Exploratory Study”. In: *Brain Sciences* 13.10 (Oct. 2023), pp. 1433–1433. DOI: <https://doi.org/10.3390/brainsci13101433>. URL: <https://www.mdpi.com/2076-3425/13/10/1433>.
- [10] Hiroaki Shimokawa et al. “A Pilot Study of Whole-Brain Low-Intensity Pulsed Ultrasound Therapy for Early Stage of Alzheimer’s Disease (LIPUS-AD): A Randomized, Double-Blind, Placebo-Controlled Trial”. In: *The Tohoku Journal of Experimental Medicine* 258.3 (Jan. 2022), pp. 167–175. DOI: <https://doi.org/10.1620/tjem.2022.j078>. URL: https://www.jstage.jst.go.jp/article/tjem/258/3/258_2022.J078/_article.
- [11] Ghazaleh Darmani et al. “Non-invasive transcranial ultrasound stimulation for neuromodulation”. In: *Clinical Neurophysiology* 135 (Mar. 2022), pp. 51–73. DOI: <https://doi.org/10.1016/j.clinph.2021.12.010>. URL: <https://www.sciencedirect.com/science/article/pii/S1388245721008920?pes=vor>.
- [12] Joseph Blackmore et al. “Ultrasound Neuromodulation: A Review of Results, Mechanisms and Safety”. In: *Ultrasound in Medicine I&B; Biology* 45.7 (July 2019), pp. 1509–1536. DOI: 10.1016/j.ultrasmedbio.2018.12.015.
- [13] URL: <https://www.nde-ed.org/Physics/Sound/index.xhtml>.
- [14] Philip Kearey, Michael Brooks, and Ian Hill. *An introduction to geophysical exploration*. Jan. 2009.

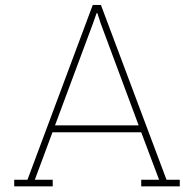
- [15] John P Lorimer and Timothy J Mason. “Sonochemistry. Part 1—The physical aspects”. In: *Chemical Society Reviews* 16.0 (Jan. 1987), pp. 239–274. DOI: <https://doi.org/10.1039/cs9871600239>. URL: <https://pubs.rsc.org/en/content/articlelanding/1987/cs/cs9871600239>.
- [16] Thomas L Szabo. “Diagnostic Ultrasound Imaging: Inside Out”. In: *Elsevier eBooks* (Jan. 2014). DOI: <https://doi.org/10.1016/c2011-0-07261-7>. URL: <https://www.sciencedirect.com/book/9780123964878/diagnostic-ultrasound-imaging-inside-out>.
- [17] Mark F. Hamilton and David T. Blackstock, eds. *Nonlinear Acoustics*. Cham: Springer Nature, 2024. ISBN: 978-3-031-58963-8. DOI: 10.1007/978-3-031-58963-8. URL: <https://library.oapen.org/handle/20.500.12657/96136>.
- [18] Armen P. Sarvazyan, Oleg V. Rudenko, and Wesley L. Nyborg. “Biomedical Applications of Radiation Force of Ultrasound: Historical Roots and Physical Basis”. In: *Ultrasound in Medicine I& Biology* 36.9 (Sept. 2010), pp. 1379–1394. DOI: 10.1016/j.ultrasmedbio.2010.05.015.
- [19] Young Hun Kim et al. “High-spatial-resolution transcranial focused ultrasound neuromodulation using frequency-modulated pattern interference radiation force”. In: *Ultrasonics* 140 (May 2024), p. 107298. DOI: 10.1016/j.ultras.2024.107298.
- [20] Joontaek Jung et al. “Review of piezoelectric micromachined ultrasonic transducers and their applications”. In: *Journal of Micromechanics and Microengineering* 27.11 (Sept. 2017), p. 113001. DOI: 10.1088/1361-6439/aa851b.
- [21] Nenad Mihajlovic. *A European MEMS Ultrasound Benchmark Scientific White Paper*. Tech. rep. Health.E Lighthouse, Nov. 2021, p. 44. URL: <https://www.s2e2.fr/wp-content/uploads/2022/03/CMUT-PMUT-Benchmark-Technical-Whitepaper.pdf>.
- [22] S.W. Rienstra and A. Hirschberg. *An introduction to acoustics*. English. Extended and revised edition of IWDE 92-06. Technische Universiteit Eindhoven, 2004.
- [23] Hassan Rivandi and Tiago L. Costa. “A 2D Ultrasound Phased-Array Transmitter ASIC for High-Frequency US Stimulation and Powering”. In: *IEEE Transactions on Biomedical Circuits and Systems* 17.4 (Aug. 2023), pp. 701–712. DOI: 10.1109/tbcas.2023.3288891.
- [24] Albert Goldstein. “Steady state spherically focused, circular aperture beam patterns”. In: *Ultrasound in Medicine I& Biology* 32.10 (Oct. 2006), pp. 1441–1458. DOI: 10.1016/j.ultrasmedbio.2006.06.013.
- [25] Fuyin Ma et al. “Acoustic focusing and imaging via phononic crystal and acoustic metamaterials”. In: *Journal of Applied Physics* 131.1 (2022). DOI: 10.1063/5.0074503.
- [26] Aixia Wang et al. “Broadband aberration-free focusing reflector for acoustic waves”. In: *Physics Letters A* 381.42 (Nov. 2017), pp. 3599–3603. DOI: 10.1016/j.physleta.2017.08.038.
- [27] Kang Chen et al. “Acoustic focusing to the waveguides utilizing double parabolic reflectors”. In: *Applied Physics Letters* 114.7 (Feb. 2019). DOI: 10.1063/1.5086086.
- [28] Ming-Hui Lu, Liang Feng, and Yan-Feng Chen. “Phononic crystals and acoustic metamaterials”. In: *Materials today* 12.12 (Dec. 2009), pp. 34–42. DOI: [https://doi.org/10.1016/s1369-7021\(09\)70315-3](https://doi.org/10.1016/s1369-7021(09)70315-3). URL: <https://www.sciencedirect.com/science/article/pii/S1369702109703153>.
- [29] Reza Abasi, Loïc Markley, and George V. Eleftheriades. “Experimental verification of subwavelength acoustic focusing using a near-field array of closely spaced elements”. In: *The Journal of the Acoustical Society of America* 130.6 (Nov. 2011), EL405–EL409. DOI: <https://doi.org/10.1121/1.3662029>. URL: <https://pubs.aip.org/asa/jasa/article/130/6/EL405/905034/Experimental-verification-of-subwavelength>.
- [30] B. Assouar et al. “Acoustic metasurfaces”. In: *Nature reviews. Materials* 3.12 (Oct. 2018), pp. 460–472. DOI: <https://doi.org/10.1038/s41578-018-0061-4>. URL: <https://www.nature.com/articles/s41578-018-0061-4>.
- [31] Syed S Bukhari, J.C. Vardaxoglou, and William Whittow. “A Metasurfaces Review: Definitions and Applications”. In: *Applied sciences* 9.13 (July 2019), pp. 2727–2727. DOI: <https://doi.org/10.3390/app9132727>. URL: <https://www.mdpi.com/2076-3417/9/13/2727>.

- [32] Jian-ping Xia et al. “Broadband Tunable Acoustic Asymmetric Focusing Lens from Dual-Layer Metasurfaces”. In: *Physical review applied* 10.1 (July 2018). DOI: <https://doi.org/10.1103/physrevapplied.10.014016>. URL: <https://journals.aps.org/prapplied/abstract/10.1103/PhysRevApplied.10.014016>.
- [33] Xue Jiang et al. “Ultrasonic sharp autofocusing with acoustic metasurface”. In: *Physical review B/Physical review. B* 102.6 (Aug. 2020). DOI: <https://doi.org/10.1103/physrevb.102.064308>. URL: <https://journals.aps.org/prb/abstract/10.1103/PhysRevB.102.064308>.
- [34] Yaxi Shen et al. “Active Acoustic Metasurface: Complete Elimination of Grating Lobes for High-Quality Ultrasound Focusing and Controllable Steering”. In: *Physical review applied* 11.3 (Mar. 2019). DOI: <https://doi.org/10.1103/physrevapplied.11.034009>. URL: <https://journals.aps.org/prapplied/abstract/10.1103/PhysRevApplied.11.034009>.
- [35] Ali Chen et al. “Design of Acoustic/Elastic Phase Gradient Metasurfaces: Principles, Functional Elements, Tunability, and Coding”. In: *Applied mechanics reviews* 74.2 (Mar. 2022). DOI: <https://doi.org/10.1115/1.4054629>. URL: <https://asmedigitalcollection.asme.org/appliedmechanicsreviews/article/74/2/020801/1141168/Design-of-Acoustic-Elastic-Phase-Gradient>.
- [36] Sergio Jiménez-Gambín et al. “Holograms to Focus Arbitrary Ultrasonic Fields through the Skull”. In: *Physical Review Applied* 12.1 (2019). DOI: [10.1103/physrevapplied.12.014016](https://doi.org/10.1103/physrevapplied.12.014016).
- [37] Dingjie Suo et al. “Numerical investigation of the inertial cavitation threshold under multi-frequency ultrasound”. In: *Ultrasonics Sonochemistry* 41 (Mar. 2018), pp. 419–426. DOI: [10.1016/j.ultsonch.2017.10.004](https://doi.org/10.1016/j.ultsonch.2017.10.004).
- [38] Dong Zhang et al. “Multi-frequency therapeutic ultrasound: A review”. In: *Ultrasonics sonochemistry* 100 (Nov. 2023), pp. 106608–106608. DOI: <https://doi.org/10.1016/j.ultsonch.2023.106608>. URL: <https://www.sciencedirect.com/science/article/pii/S1350417723003206?via%3Dihub>.
- [39] Edin Mehić et al. “Increased Anatomical Specificity of Neuromodulation via Modulated Focused Ultrasound”. In: *PloS one* 9.2 (Feb. 2014), e86939–e86939. DOI: <https://doi.org/10.1371/journal.pone.0086939>. URL: <https://journals.plos.org/plosone/article?id=10.1371/journal.pone.0086939>.
- [40] Thomas Riis and Jan Kubanek. “Multifrequency-based sharpening of focal volume”. In: *Scientific reports* 12.1 (Dec. 2022). DOI: <https://doi.org/10.1038/s41598-022-25886-9>. URL: <https://pubmed.ncbi.nlm.nih.gov/36543884/#:~:text=The%20method%20superimposes%20beams%20of,else%2C%20thus%20sharpening%20the%20focus..>
- [41] Young Hun Kim et al. “Patterned Interference Radiation Force for Transcranial Neuromodulation”. In: *Ultrasound in medicine & biology* 48.3 (Mar. 2022), pp. 497–511. DOI: <https://doi.org/10.1016/j.ultrasmedbio.2021.11.006>. URL: <https://www.sciencedirect.com/science/article/pii/S0301562921004853>.
- [42] Seongyeon Kim et al. “Improved Target Specificity of Transcranial Focused Ultrasound Stimulation (TFUS) using Double-Crossed Ultrasound Transducers”. In: *2018 40th Annual International Conference of the IEEE Engineering in Medicine and Biology Society (EMBC)*. 2018, pp. 2679–2682. DOI: [10.1109/EMBC.2018.8512812](https://doi.org/10.1109/EMBC.2018.8512812).
- [43] Seongyeon Kim et al. “Transcranial focused ultrasound stimulation with high spatial resolution”. In: *Brain stimulation* 14.2 (Mar. 2021), pp. 290–300. DOI: <https://doi.org/10.1016/j.brs.2021.01.002>. URL: <https://pubmed.ncbi.nlm.nih.gov/33450428/>.
- [44] Sheikh Jawad Ilham and Mehdi Kiani. “Towards High-Resolution Ultrasound Neuromodulation With Crossed-Beam Phased Arrays”. In: *IEEE transactions on biomedical circuits and systems* 17.3 (June 2023), pp. 534–546. DOI: <https://doi.org/10.1109/tbcas.2023.3285724>. URL: <https://pubmed.ncbi.nlm.nih.gov/37310841/>.
- [45] Morgan N. Collins, Wynn Legon, and Karen A. Mesce. “The Inhibitory Thermal Effects of Focused Ultrasound on an Identified, Single Motoneuron”. In: *eneuro* 8.2 (Mar. 2021), ENEURO.0514–20.2021. DOI: <https://doi.org/10.1523/eneuro.0514-20.2021>. URL: <https://pmc.ncbi.nlm.nih.gov/articles/PMC8174046/>.

- [46] Anton Fomenko et al. “Low-intensity ultrasound neuromodulation: An overview of mechanisms and emerging human applications”. In: *Brain Stimulation* 11.6 (Nov. 2018), pp. 1209–1217. DOI: 10.1016/j.brs.2018.08.013.
- [47] David P Darrow. “Focused Ultrasound for Neuromodulation”. In: *Neurotherapeutics* 16.1 (Jan. 2019), pp. 88–99. DOI: 10.1007/s13311-018-00691-3.
- [48] Hongchae Baek, Ki Joo Pakk, and Hyungmin Kim. “A review of low-intensity focused ultrasound for neuromodulation”. In: *Biomedical engineering letters* 7.2 (Jan. 2017), pp. 135–142. DOI: <https://doi.org/10.1007/s13534-016-0007-y>. URL: <https://link.springer.com/article/10.1007/s13534-016-0007-y>.
- [49] A. L. Hodgkin and A. F. Huxley. “A quantitative description of membrane current and its application to conduction and excitation in nerve”. In: *The Journal of Physiology* 117.4 (Aug. 1952), pp. 500–544. DOI: 10.1113/jphysiol.1952.sp004764.
- [50] John Dell’Italia et al. “Current State of Potential Mechanisms Supporting Low Intensity Focused Ultrasound for Neuromodulation”. In: *Frontiers in human neuroscience* 16 (Apr. 2022). DOI: <https://doi.org/10.3389/fnhum.2022.872639>. URL: <https://www.frontiersin.org/articles/10.3389/fnhum.2022.872639/full>.
- [51] Michael Plaksin, Eitan Kimmel, and Shy Shoham. “Cell-Type-Selective Effects of Intramembrane Cavitation as a Unifying Theoretical Framework for Ultrasonic Neuromodulation”. In: *eneuro* 3.3 (May 2016), ENEURO.0136–15.2016. DOI: 10.1523/eneuro.0136-15.2016.
- [52] Boris Krasovitski et al. “Intramembrane cavitation as a unifying mechanism for ultrasound-induced bioeffects”. In: *Proceedings of the National Academy of Sciences* 108.8 (Feb. 2011), pp. 3258–3263. DOI: 10.1073/pnas.1015771108.
- [53] Ying Meng, Kullervo Hynynen, and Nir Lipsman. “Applications of focused ultrasound in the brain: from thermoablation to drug delivery”. In: *Nature Reviews Neurology* 17.1 (Oct. 2020), pp. 7–22. DOI: 10.1038/s41582-020-00418-z.
- [54] Sangjin Yoo et al. “Focused ultrasound excites cortical neurons via mechanosensitive calcium accumulation and ion channel amplification”. In: *Nature Communications* 13.1 (Jan. 2022). DOI: 10.1038/s41467-022-28040-1.
- [55] Morteza Mohammadjavadi et al. “Elimination of peripheral auditory pathway activation does not affect motor responses from ultrasound neuromodulation”. In: *Brain Stimulation* 12.4 (July 2019), pp. 901–910. DOI: 10.1016/j.brs.2019.03.005.
- [56] Eric A. Newman and Kathleen R. Zahs. “Modulation of Neuronal Activity by Glial Cells in the Retina”. In: *The Journal of Neuroscience* 18.11 (June 1998), pp. 4022–4028. DOI: <https://doi.org/10.1523/jneurosci.18-11-04022.1998>.
- [57] Hesam Sadeghi Gougheri et al. “A Comprehensive Study of Ultrasound Transducer Characteristics in Microscopic Ultrasound Neuromodulation”. In: *IEEE Transactions on Biomedical Circuits and Systems* 13.5 (Oct. 2019), pp. 835–847. DOI: <https://doi.org/10.1109/tbcas.2019.2922027>. URL: <https://pubmed.ncbi.nlm.nih.gov/31199268/>.
- [58] Omer Naor, Steve L Krupa, and Shy Shoham. “Ultrasonic neuromodulation”. In: *Journal of Neural Engineering* 13.3 (May 2016), pp. 031003–031003. DOI: <https://doi.org/10.1088/1741-2560/13/3/031003>.
- [59] Tingting Zhang et al. “Transcranial Focused Ultrasound Neuromodulation: A Review of the Excitatory and Inhibitory Effects on Brain Activity in Human and Animals”. In: *Frontiers in Human Neuroscience* 15 (Sept. 2021). DOI: 10.3389/fnhum.2021.749162.
- [60] Penny Ping Qin et al. “The effectiveness and safety of low-intensity transcranial ultrasound stimulation: A systematic review of human and animal studies”. In: *Neuroscience I& Biobehavioral Reviews* 156 (Jan. 2024), p. 105501. DOI: 10.1016/j.neubiorev.2023.105501.
- [61] Ardavan Javid, Sheikh Ilham, and Mehdi Kiani. “A Review of Ultrasound Neuromodulation Technologies”. In: *IEEE Transactions on Biomedical Circuits and Systems* 17.5 (2023), pp. 1084–1096. DOI: 10.1109/tbcas.2023.3299750.

- [62] ITTRUST. *ITTRUST - Working group: Safety - Bioeffects*. https://itrusst.com/wg_safety_bioeffects.html. Accessed: 2025-03-04.
- [63] Ke Zeng et al. "Induction of Human Motor Cortex Plasticity by Theta Burst Transcranial Ultrasound Stimulation". In: *Annals of Neurology* 91.2 (Jan. 2022), pp. 238–252. DOI: 10.1002/ana.26294.
- [64] Robert F. Labadie, Bryan M. Davis, and J. Michael Fitzpatrick. "Image-guided surgery: what is the accuracy?" In: *Current Opinion in Otolaryngology I&; Head and Neck Surgery* 13.1 (Feb. 2005), pp. 27–31. DOI: 10.1097/00020840-200502000-00008.
- [65] Dennis Q. Truong et al. "Comparison of Transcranial Focused Ultrasound and Transcranial Pulse Stimulation for Neuromodulation: A Computational Study". In: *Neuromodulation: Technology at the Neural Interface* 25.4 (2022), pp. 606–613. DOI: 10.1016/j.neurom.2021.12.012.
- [66] Mengyue Chen et al. "Numerical and experimental evaluation of low intensity transcranial focused ultrasound wave propagation using human skulls for brain neuromodulation". In: *Medical Physics* 50.1 (Nov. 2022), pp. 38–49. DOI: 10.1002/mp.16090.
- [67] Tae Young Park, Ki Joo Pahk, and Hyungmin Kim. "Method to optimize the placement of a single-element transducer for transcranial focused ultrasound". In: *Computer Methods and Programs in Biomedicine* 179 (Oct. 2019), p. 104982. DOI: 10.1016/j.cmpb.2019.104982.
- [68] Dimopoulos. "Skull morphology and its neurosurgical implications in the Hippocratic era". In: *Neurosurgical focus* 23.1 (2014). DOI: <https://doi.org/10.3171/foc.2007.23.1.10>. URL: <https://pubmed.ncbi.nlm.nih.gov/17961053/>.
- [69] Chunkyun Seok et al. "A Wearable Ultrasonic Neurostimulator—Part II: A 2D CMUT Phased Array System With a Flip-Chip Bonded ASIC". In: *IEEE Transactions on Biomedical Circuits and Systems* 15.4 (Aug. 2021), pp. 705–718. DOI: 10.1109/tbcas.2021.3105064.
- [70] Chunkyun Seok et al. "A Wearable Ultrasonic Neurostimulator - Part I: A 1D CMUT Phased Array System for Chronic Implantation in Small Animals". In: *IEEE Transactions on Biomedical Circuits and Systems* 15.4 (Aug. 2021), pp. 692–704. DOI: 10.1109/tbcas.2021.3100458.
- [71] Elisabetta Moisello et al. "PMUT and CMUT Devices for Biomedical Applications: A Review". In: *IEEE Access* 12 (Jan. 2024), pp. 18640–18657. DOI: 10.1109/access.2024.3359906.
- [72] Seongyeon Kim et al. "Transcranial focused ultrasound stimulation with high spatial resolution." eng. In: *Brain stimulation* 14.2 (Apr. 2021). Place: United States, pp. 290–300. ISSN: 1876-4754. DOI: 10.1016/j.brs.2021.01.002.
- [73] Jin H. Huang and Desheng Ding. "A simple approximate formula for the physical focal length of spherically focused transducers". In: *IEEE Transactions on Ultrasonics, Ferroelectrics, and Frequency Control* 56.12 (2009), pp. 2764–2768. DOI: 10.1109/TUFFC.2009.1368.
- [74] Bradley E. Treeby and B. T. Cox. "k-Wave: MATLAB toolbox for the simulation and reconstruction of photoacoustic wave fields". In: *Journal of Biomedical Optics* 15.2 (Jan. 2010), p. 021314. DOI: 10.1117/1.3360308.
- [75] Célestine Angla et al. "Transcranial ultrasound simulations: A review". In: *Medical Physics* 50.2 (Sept. 2022), pp. 1051–1072. DOI: 10.1002/mp.15955.
- [76] *MATLAB version 9.3.0.713579 (R2017b)*. The Mathworks, Inc. Natick, Massachusetts, 2017.
- [77] Lawrence E. Kinsler et al. *Fundamentals of Acoustics*. 4th. John Wiley & Sons, 2000. URL: https://api_library.lqdtu.edu.vn/media/FundamentalsOfAcoustics.pdf.
- [78] Bradley E. Treeby and Ben T. Cox. *k-Wave User Manual Version 1.1*. Department of Medical Physics and Biomedical Engineering, University College London. 2017. URL: http://www.k-wave.org/manual/k-wave_user_manual_1.1.pdf.
- [79] Delft High Performance Computing Centre (DHPC). *DelftBlue Supercomputer (Phase 2)*. <https://www.tudelft.nl/dhpc/ark:/44463/DelftBluePhase2>. 2024.
- [80] Sheikh Jawad Ilham, Zeinab Kashani, and Mehdi Kiani. "Design and Optimization of Ultrasound Phased Arrays for Large-Scale Ultrasound Neuromodulation". In: *IEEE Transactions on Biomedical Circuits and Systems* 15.6 (Dec. 2021), pp. 1454–1466. DOI: <https://doi.org/10.1109/tbcas.2021.3133133>. URL: <https://pubmed.ncbi.nlm.nih.gov/34874867/>.

- [81] Seongyeon Kim et al. "Improved Target Specificity of Transcranial Focused Ultrasound Stimulation (TFUS) using Double-Crossed Ultrasound Transducers". In: (2018), pp. 2679–2682. DOI: 10.1109/EMBC.2018.8512812.
- [82] Kasra Naftchi-Ardebili et al. "Focal Volume, Acoustic Radiation Force, and Strain in Two-Transducer Regimes". In: *IEEE Transactions on Ultrasonics Ferroelectrics and Frequency Control* (Jan. 2024), pp. 1–1. DOI: <https://doi.org/10.1109/tuffc.2024.3456048>. URL: <https://pubmed.ncbi.nlm.nih.gov/39240744/>.
- [83] M.J. Ackerman. "The Visible Human Project". In: *Proceedings of the IEEE* 86.3 (Mar. 1998), pp. 504–511. DOI: <https://doi.org/10.1109/5.662875>. URL: <https://ieeexplore.ieee.org/document/662875>.
- [84] 2025. URL: <https://www.slicer.org/>.



Appendix - Optimised Transducers Plots

Here are zoomed in versions of the box plots for the optimised transducers setup.

A.1. Varying tFUS source

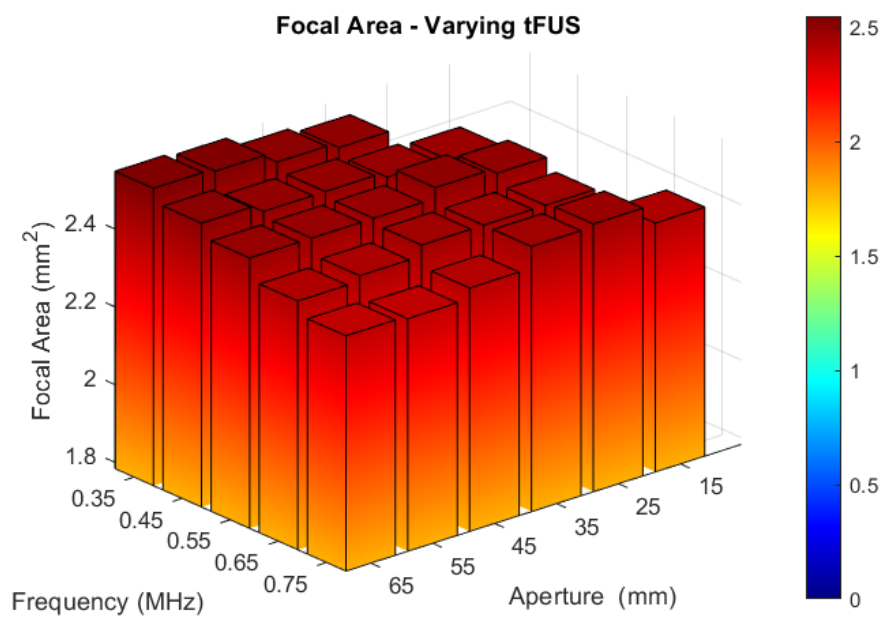


Figure A.1: Focal area of the combined field for varying tFUS parameters

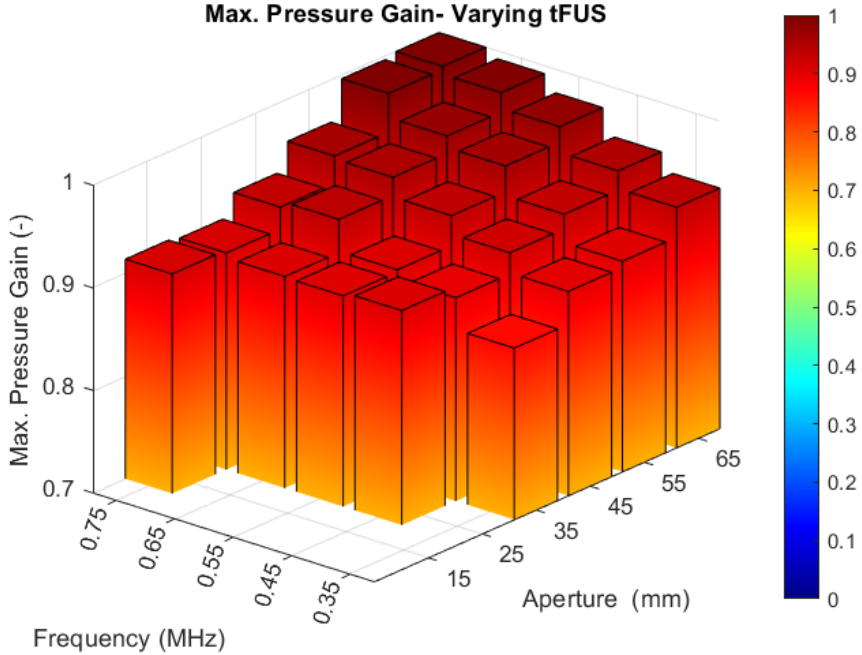


Figure A.2: Normalised maximum pressure gain of the combined field for varying tFUS parameters

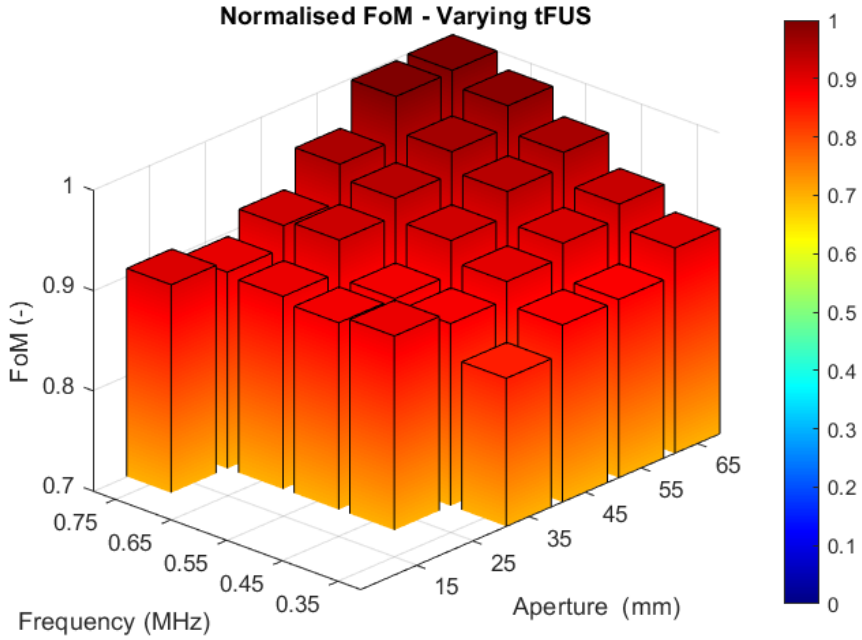


Figure A.3: Normalised FoM of the combined field for varying tFUS parameters

A.2. Varying μ FUS source

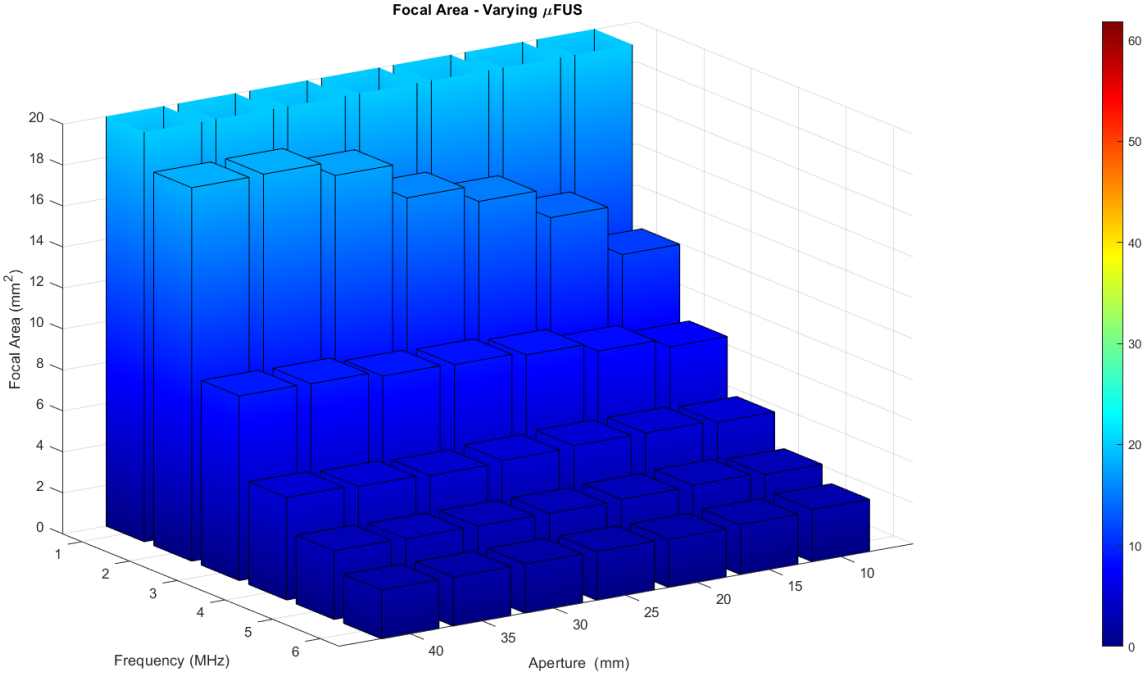


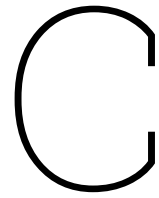
Figure A.4: Focal area of the combined field for varying μ FUS parameters

B

Appendix - GA convergence

Table B.1: GA Optimization Performance and Results

Population Size	Max Generations	Tolerance	Best Solution [f_{01} , f_{02} , L_1 , L_2 , θ , r , p_{frac}]	Elapsed Time (s)
50	50	1.00e-02	[6,5,7,6,1.44,5.00e-03,0.611]	949
50	50	1.00e-04	[6,5,7,6,1.33,2.38e-02,0.612]	917
50	100	1.00e-02	[6,5,7,6,1.97,1.71e-02,0.611]	982
50	100	1.00e-04	[6,5,7,6,1.77,5.60e-03,0.610]	829
50	200	1.00e-02	[6,5,7,6,1.29,2.40e-03,0.611]	710
50	200	1.00e-04	[6,5,7,6,1.68,1.90e-03,0.610]	643
100	50	1.00e-02	[6,5,7,6,1.68,2.10e-03,0.610]	1.24e+03
100	50	1.00e-04	[6,5,7,6,1.92,9.03e-03,0.610]	1.23e+03
100	100	1.00e-02	[6,5,7,6,1.60,1.80e-03,0.610]	1.18e+03
100	100	1.00e-04	[6,5,7,6,1.60,1.80e-03,0.610]	1.17e+03
100	200	1.00e-02	[6,5,7,6,1.75,7.10e-03,0.610]	1.35e+03
100	200	1.00e-04	[6,5,7,6,1.58,1.80e-03,0.610]	2.25e+03
200	50	1.00e-02	[6,5,7,6,1.29,2.00e-03,0.610]	2.31e+03
200	50	1.00e-04	[6,5,7,6,1.29,2.00e-03,0.610]	2.24e+03
200	100	1.00e-02	[6,5,7,6,1.77,1.90e-03,0.626]	2.22e+03
200	100	1.00e-04	[6,5,7,6,1.75,2.30e-03,0.610]	2.21e+03
200	200	1.00e-02	[6,5,7,6,1.46,2.00e-03,0.610]	2.47e+03



Appendix - Effect of Varying tFUS parameters

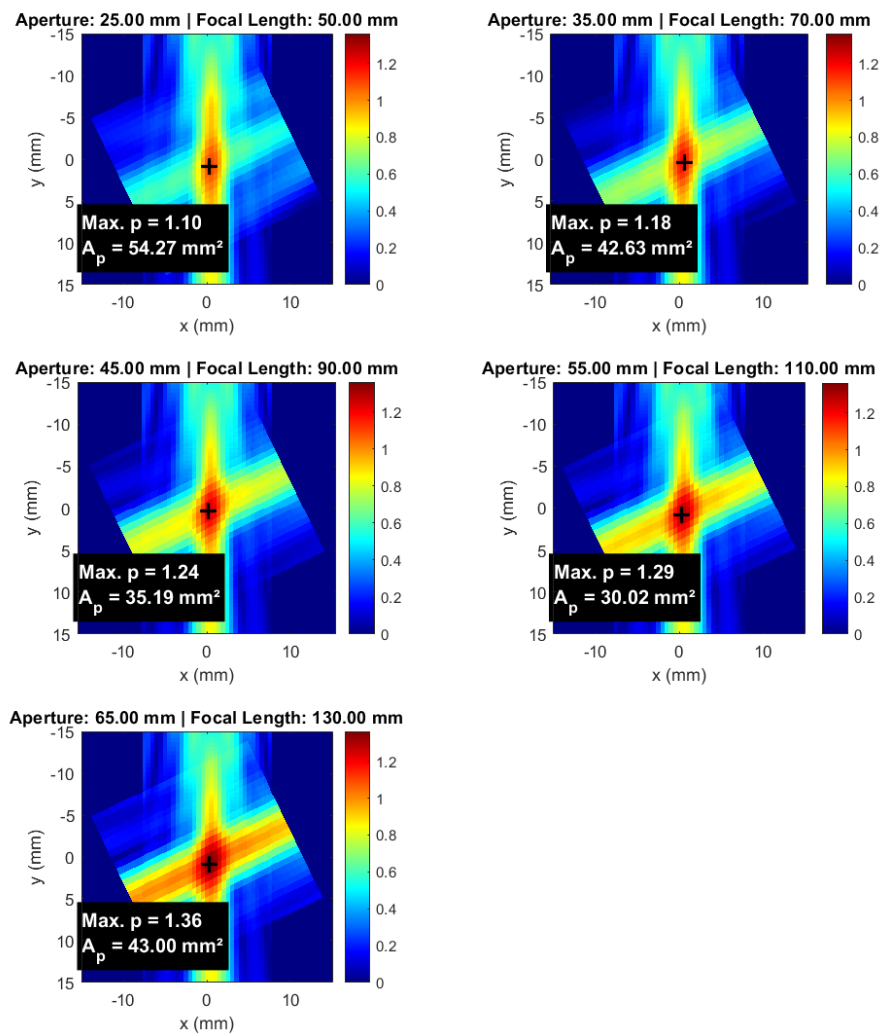


Figure C.1: Fixed transducer frequency: 750 kHz, varying transducer aperture

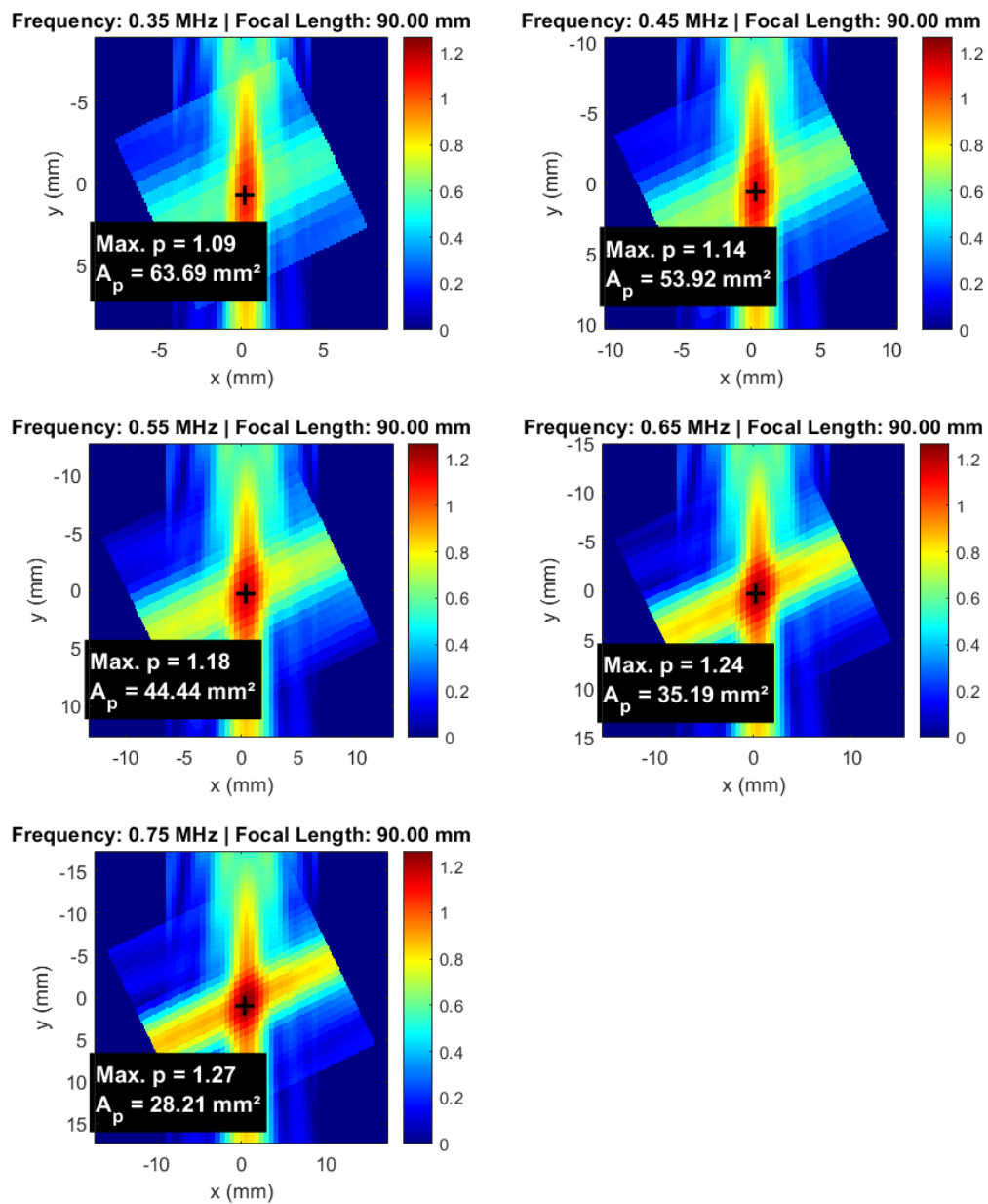


Figure C.2: Fixed Transducer Aperture: 45 mm, variable frequency